NAVAL POSTGRADUATE SCHOOL

MONTEREY, CALIFORNIA

THESIS

DOWNSTREAM IMPACTS DUE TO THE EXTRATROPICAL TRANSITION OF TROPICAL CYCLONES OVER THE WESTERN NORTH PACIFIC

by

Jonathan M. Dea

March 2007

Thesis Advisor:	Patrick Harr
Second Reader:	Russell Elsberry

Approved for public release; distribution is unlimited

THIS PAGE INTENTIONALLY LEFT BLANK

REPORT DOCUMENTATION PAGE		Form Approved OMB No. 0704-0188

Public reporting burden for this collection of information is estimated to average 1 hour per response, including the time for reviewing instruction, searching existing data sources, gathering and maintaining the data needed, and completing and reviewing the collection of information. Send comments regarding this burden estimate or any other aspect of this collection of information, including suggestions for reducing this burden, to Washington headquarters Services, Directorate for Information Operations and Reports, 1215 Jefferson Davis Highway, Suite 1204, Arlington, VA 22202-4302, and to the Office of Management and Budget, Paperwork Reduction Project (0704-0188) Washington DC 20503.

1. AGENCY USE ONLY *(Leave blank)*	2. REPORT DATE	3. REPORT TYPE AND DATES COVERED
	March 2007	Master's Thesis

4. TITLE AND SUBTITLE Downstream Impacts Due to the Extratropical Transition of Tropical Cyclones Over the Western North Pacific	5. FUNDING NUMBERS
6. AUTHOR(S) Jonathan M. Dea	
7. PERFORMING ORGANIZATION NAME(S) AND ADDRESS(ES) Naval Postgraduate School Monterey, CA 93943-5000	8. PERFORMING ORGANIZATION REPORT NUMBER
9. SPONSORING /MONITORING AGENCY NAME(S) AND ADDRESS(ES) N/A	10. SPONSORING/MONITORING AGENCY REPORT NUMBER

11. SUPPLEMENTARY NOTES The views expressed in this thesis are those of the author and do not reflect the official policy or position of the Department of Defense or the U.S. Government.

12a. DISTRIBUTION / AVAILABILITY STATEMENT	12b. DISTRIBUTION CODE
Approved for public release; Distribution is unlimited	

13. ABSTRACT (maximum 200 words)

Analysis of the eddy kinetic energy budget for four cases of extratropical transition (ET) with North Pacific tropical cyclones (TCs) is conducted. The cases compare varying ET and midlatitude flow characteristics. Each case was examined to determine the impacts of eddy kinetic energy generation and/or transfer on downstream development in the midlatitude circulation. Typhoon Tokage (October 2004) was a large TC that moved into a high-amplitude midlatitude circulation. Energetics analysis revealed that the ET of Tokage influenced the development of a deep trough over the central North Pacific before Tokage moved poleward and weakened transfer. Typhoon Banyan (July 2005) was a mid-summer case that influenced downstream development ultimately over the Aleutian Islands. Typhoon Guchol (August 2005) was a small TC that was dominated by midlatitude flow. However, the merger of Guchol with a midlatitude trough enabled development downstream of a separate trough. Typhoon Nabi was an intense TC that injected significant EKE into the midlatitude circulation during ET. Through downstream development, Nabi changed a zonal pattern over the North Pacific into an amplified pattern. These cases indicate that the ET process over the western North Pacific impacts the midlatitude circulation across the entire North Pacific basin.

14. SUBJECT TERMS Tropical Cyclones, Extratropical Transition, Downstream Development, Eddy Kinetic Energy Budget Analysis, Energetics Analysis, Baroclinic Conversion, Ageostrophic Geopotential Flux, Dynamic Tropopause, Potential Vorticity	15. NUMBER OF PAGES 119
	16. PRICE CODE

17. SECURITY CLASSIFICATION OF REPORT	18. SECURITY CLASSIFICATION OF THIS PAGE	19. SECURITY CLASSIFICATION OF ABSTRACT	20. LIMITATION OF ABSTRACT
Unclassified	Unclassified	Unclassified	UL

NSN 7540-01-280-5500

Standard Form 298 (Rev. 2-89)
Prescribed by ANSI Std. 239-18

THIS PAGE INTENTIONALLY LEFT BLANK

Approved for public release; distribution is unlimited

DOWNSTREAM IMPACTS DUE TO THE EXTRATROPICAL TRANSITION OF TROPICAL CYCLONES OVER THE WESTERN NORTH PACIFIC

Jonathan M. Dea
Captain, United States Air Force
B.S., Iowa State University, 2000

Submitted in partial fulfillment of the
requirements for the degree of

MASTER OF SCIENCE IN METEOROLOGY

from the

NAVAL POSTGRADUATE SCHOOL
March 2007

Author: Jonathan M. Dea

Approved by: Patrick Harr
Thesis Advisor

Russell Elsberry
Second Reader

Philip A. Durkee
Chairman, Department of Meteorology

THIS PAGE INTENTIONALLY LEFT BLANK

ABSTRACT

Analysis of the eddy kinetic energy budget for four cases of extratropical transition (ET) with North Pacific tropical cyclones (TCs) is conducted. The cases compare varying ET and midlatitude flow characteristics. Each case was examined to determine the impacts of eddy kinetic energy generation and/or transfer on downstream development in the midlatitude circulation.

Typhoon Tokage (October 2004) was a large TC that moved into a high-amplitude midlatitude circulation. Energetics analysis revealed that the ET of Tokage influenced the development of a deep trough over the central North Pacific before Tokage moved poleward and weakened transfer. Typhoon Banyan (July 2005) was a mid-summer case that influenced downstream development ultimately over the Aleutian Islands. Typhoon Guchol (August 2005) was a small TC that was dominated by midlatitude flow. However, the merger of Guchol with a midlatitude trough enabled development downstream of a separate trough. Typhoon Nabi was an intense TC that injected significant EKE into the midlatitude circulation during ET. Through downstream development, Nabi changed a zonal pattern over the North Pacific into an amplified pattern. These cases indicate that the ET process over the western North Pacific impacts the midlatitude circulation across the entire North Pacific basin.

THIS PAGE INTENTIONALLY LEFT BLANK

TABLE OF CONTENTS

I. INTRODUCTION 1
A. BACKGROUND 1
1. Extratropical Transition Climatology 2
2. Characteristics of the Extratropical Transition Process 4
B. MOTIVATION 6

II. DATA AND METHODOLOGY 9
A. DATA SOURCE 9
B. EDDY KINETIC ENERGY AND FLUX BUDGETS 9
1. The Eddy Kinetic Energy Equation and Ageostrophic Geopotential Flux 11
2. Lifecycle Stages in a Downstream Baroclinic System 14

III. ANALYSIS 17
A. TY TOKAGE 18
1. Synoptic Evolution 18
2. EKE Budget 22
a. Vertically Averaged EKE and Total EKE Flux Vectors 22
b. Components of Total EKE 28
3. Summary 36
B. TY BANYAN 37
1. Synoptic Evolution 37
2. EKE Budget 42
a. Vertically Averaged EKE and Total EKE Flux Vectors 42
b. Components of Total EKE 45
3. Summary 51
C. TY GUCHOL 52
1. Synoptic Evolution 52
2. EKE Budget 57
a. Vertically Averaged EKE and Total EKE Flux Vectors 57
b. Components of Total EKE 60
3. Summary 67
D. TY NABI 68
1. Synoptic Evolution 68
2. EKE Budget 72
a. Vertically Averaged EKE and Total EKE Flux Vectors 72
b. Components of Total EKE 80
3. Summary 91

IV. SUMMARY, CONCLUSIONS, AND RECOMMENDATIONS 93

A. SUMMARY 93
B. CONCLUSIONS 94
C. RECOMMENDATIONS FOR FUTURE RESEARCH 95
LIST OF REFERENCES 97
INITIAL DISTRIBUTION LIST 101

LIST OF FIGURES

Figure 1. Tracks of all TCs that experienced ET during 1970-99: (a) Western North Pacific with tracks of TCs defined to be extratropical in Joint Typhoon Warning Center best-track data; (b) Southwest Pacific with data source as in (a) and southeast Indian Ocean with tracks of TCs that accelerated toward the southeast under the influence of a midlatitude frontal system and maintained gales into midlatitudes, which are the so-called captured cyclones in Foley and Hanstrum (1994), best-track data taken from http://www.australiasevereweather.com/cyclones/history.htm and (c) North Atlantic with tracks of TCs defined to be extratropical in National Hurricane Center best-track data (after Jones et al. 2003)..... 3

Figure 2. Monthly total numbers of tropical cyclones (open bars) in each basin during 1970-99 and the number of TCs that experienced ET (shaded bars) based on the data sources described in Fig. 1 (after Jones et al. 2003). 4

Figure 3. The three stages in the evolution of a baroclinic wave (Orlanski and Sheldon 1995). Symbols are as given in the inset. *Stage 1:* Upstream system decays and downstream EKE center is generated (denoted by the script *W*) west of a new trough via geopotential fluxes. *Stage 2:* EKE fluxes radiate from a mature energy center (denoted by the script *W*) and fosters the growth of a new energy center (denoted by the script *E*) east of the trough. *Stage 3:* The new energy center matures, while the older energy center decays (after Orlanski and Sheldon 1995). 15

Figure 4. Illustration of the relationship between baroclinic wave components. The upper-level geopotential field is indicated by Φ_1 and Φ_2, and the geopotential anomaly ϕ' relative to the time mean is positive (negative) in the ridge (trough). Airflow relative to the wave is indicated by the heavy solid arrows and the ageostrophic wind is indicated by the open arrows. Centers of maximum vertically integrated EKE are shown as ellipses. An incipient disturbance is forming on the east side of the ridge at the center of the figure (after Orlanski and Sheldon 1995). 16

Figure 5. North Pacific Ocean synoptic environment at 1200 UTC 17 October 2004 including (a) mean sea-level pressure (grayscale shading and contours below 1000 hPa, 4 hPa interval) and 500 hPa heights (contours, 60 meter interval), and (b) potential temperature (shading and contours, 10 Kelvin interval) on the dynamic tropopause (2 PVU surface). 19

Figure 6. As in Fig. 5, except for 1200 UTC 18 October. 20

Figure 7. As in Fig. 5, except for 1200 UTC 19 October. 20

Figure 8. As in Fig. 5, except for 1200 UTC 20 October. 21

Figure 9. As in Fig. 5, except for 1200 UTC 21 October. 22
Figure 10. Vertically averaged EKE [color shading, refer to legend for values (units: MJ m^{-2})], total EKE flux vectors [arrows, refer to reference vector (units: MW m^{-1})], and 500 hPa heights [contours, 60 m intervals]. Total EKE flux vectors less than 20 MW m^{-1} are not plotted. The time period 1200 UTC 17 October through 0000 UTC 22 October 2004 is represented in panels (a) through (j). 24
Figure 11. Distribution of EKE components at 0000 UTC 19 October 2004 for (a) vertically averaged horizontal EKEFC [color shading (units: MW m^{-2}), refer to legend for values], horizontal EKE flux vectors [arrows (units: MW m^{-1}), refer to reference vector], and 500 hPa heights [contours, 60 m intervals]; and (b) vertically averaged EKE generation term [color shading (units: MW m^{-2}), refer to legend for values], AGF vectors [arrows (units: MW m^{-2}), refer to reference vector], and 500 hPa heights [contours, 60 m intervals]. 31
Figure 12. Distribution of vertically averaged EKE term components at 0000 UTC 19 October 2004 for (a) vertically averaged AGFC [color shading (units: MW m^{-2}), refer to legend for values], AGF vectors [arrows (units: MW m^{-2}), refer to reference vector], and 500 hPa heights [contours, 60 m intervals]; and (b) vertically averaged BC [color shading (units: MW m^{-2}), refer to legend for values] and 500 hPa heights [contours, 60 m intervals]..... 32
Figure 13. As in Fig. 11, except for 0000 UTC 20 October. 33
Figure 14. As in Fig. 12, except for 0000 UTC 20 October. 34
Figure 15. As in Fig. 11, except for 0000 UTC 21 October. 35
Figure 16. As in Fig. 12, except for 0000 UTC 21 October. 36
Figure 17. As in Fig. 5, except for 0000 UTC 25 July 2005. 38
Figure 18. As in Fig. 5, except for 0000 UTC 26 July 2005. 39
Figure 19. As in Fig. 5, except for 0000 UTC 27 July 2005. 40
Figure 20. As in Fig. 5, except for 0000 UTC 28 July 2005 41
Figure 21. As in Fig. 5, except for 0000 UTC 29 July 2005. 41
Figure 22. As in Fig.10, except that the time period 0000 UTC 26 July 2005 through 0000 UTC 29 July 2005 is represented in panels (a) through (e). 43
Figure 23. As in Fig. 11, except for 0000 UTC 26 July 2005. 46
Figure 24. As in Fig. 12, except for 0000 UTC 26 July 2005. 47
Figure 25. As in Fig. 11, except for 0000 UTC 27 July 2005. 48
Figure 26. As in Fig. 12, except for 0000 UTC 27 July 2005. 49
Figure 27. As in Fig. 11, except for 1200 UTC 28 July 2005. 50
Figure 28. As in Fig. 12, except for 1200 UTC 28 July 2005. 51
Figure 29. As in Fig. 5, except for 1200 UTC 22 August 2005. Red arrow in a) denotes the position of Guchol. 54
Figure 30. As in Fig. 29, except for 1200 UTC 23 August 2005..... 55
Figure 31. As in Fig. 29, except for 1200 UTC 24 August 2005..... 55
Figure 32. As in Fig. 29, except for 1200 UTC 25 August 2005..... 56

Figure 33. As in Fig. 29, except for 1200 UTC 26 August 2005..... 56
Figure 34. As in Fig.10, except that the time period 1200 UTC 22 August 2005 through 1200 UTC 26 August 2005 is represented in panels (a) through (e). Red arrows denote the positions of Guchol. 59
Figure 35. As in Fig. 11, except for 1200 UTC 24 August 2005. Red arrows denote positions of Guchol. 62
Figure 36. As in Fig. 12, except for 1200 UTC 24 August 2005. Red arrow denotes position of Guchol. 63
Figure 37. As in Fig. 35, except for 1200 UTC 25 August 2005..... 64
Figure 38. As in Fig. 36, except for 1200 UTC 25 August 2005..... 65
Figure 39. As in Fig. 35, except for 1200 UTC 26 August 2005..... 66
Figure 40. As in Fig. 36, except for 1200 UTC 26 August 2005..... 67
Figure 41. As in Fig. 5, except for 0000 UTC 5 September 2005. 69
Figure 42. As in Fig. 5, except for 0000 UTC 6 September 2005. 70
Figure 43. As in Fig. 5, except for 0000 UTC 7 September 2005. 70
Figure 44. As in Fig. 5, except for 0000 UTC 8 September 2005. 71
Figure 45. As in Fig. 5, except for 0000 UTC 9 September 2005. 71
Figure 46. As in Fig. 10, except that the time period 0000 UTC 3 September 2005 through 0000 UTC 9 September 2005 is represented in panels (a) through (m). 74
Figure 47. As in Fig. 11, except for 1200 UTC 3 September 2005. 82
Figure 48. As in Fig. 12, except for 1200 UTC 3 September 2005. 83
Figure 49. As in Fig. 11, except for 1200 UTC 4 September 2005. 84
Figure 50. As in Fig. 12, except for 1200 UTC 4 September 2005. 85
Figure 51. As in Fig. 11, except for 1200 UTC 6 September 2005. 86
Figure 52. As in Fig. 12, except for 1200 UTC 6 September 2005. 87
Figure 53. As in Fig. 11, except for 0000 UTC 7 September 2005. 88
Figure 54. As in Fig. 12, except for 0000 UTC 7 September 2005. 89
Figure 55. As in Fig. 11, except for 1200 UTC 8 September 2005. 90
Figure 56. As in Fig. 12, except for 1200 UTC 8 September 2005. 91

THIS PAGE INTENTIONALLY LEFT BLANK

LIST OF TABLES

Table 1. Selected basic information relevant to each TC analyzed in this thesis. [Compiled from Digital Typhoon (2007): http://agor.ex.nii.ac.jp/digital-typhoon/index.html.en] 8
Table 2. Tropical cyclones examined in this study with their associated times/dates of ET completion and their "center time" used to compute mean quantities. [ET times and dates compiled from Digital Typhoon (2007): http://agora.ex.nii.ac.jp/digital-typhoon/index.html.en] 10
Table 3. Descriptive names of terms in the EKE tendency equation and components (terms) of $-(\mathbf{v}\cdot\nabla\phi)$ 13

THIS PAGE INTENTIONALLY LEFT BLANK

ACKNOWLEDGMENTS

I would like to thank my thesis advisor, Professor Patrick Harr, for his role in the completion of this thesis and its associated presentation. Neither would have been possible without his outstanding guidance and hours of coding and editing efforts.

I also thank my second reader, Professor Russell Elsberry, as his tropical meteorology classes kindled a previously unexplored personal interest of mine. His teaching talents led me to choose a thesis topic in the discipline that I did.

I feel fortunate that I've always had support from my parents and friends as I was growing up. Their encouragement has enabled me to open countless avenues of opportunity that would have remained closed otherwise.

Most importantly, I thank my wife, Kerstin, for her support and understanding through the thesis process. This explains it best: ***Ich liebe dich!***

THIS PAGE INTENTIONALLY LEFT BLANK

I. INTRODUCTION

A. BACKGROUND

The extremely active and devastating 2005 Atlantic hurricane season has caused a dramatic increase in public interest of tropical cyclones (TCs). The recovery process from Hurricane Katrina in Louisiana, Mississippi, and Alabama has made global leaders and disaster management officials realize the dangers and reality of intense TCs making landfall near populated areas. Hopefully these US-landfalling events in 2005 have brought forth a new sense of awareness toward TCs, but many in the public today do not realize that given the right circumstances TCs can weaken over the ocean, experience extratropical transition (ET), and re-intensify as severe extratropical cyclones. As its name implies, extratropical transition is the process in which a TC loses tropical characteristics and becomes more extratropical in nature (Jones et al. 2003).

These cyclones present a danger to the poleward periphery of the global TC-affected basins, endangering shipping lanes, aviation interests, and the general public and property near the re-intensifying storm (Harr and Elsberry 2000). Tropical cyclones that undergo ET as a deeply intensified extratropical cyclone and propagate to the eastern side of the ocean basin bring strong winds and heavy rains to places not normally accustomed to TC-related impacts [Hurricane Floyd in 1993 (Rabier et al. 1996); Hurricane Lili in 1996 (Browning et al. 1998)].

Moreover, the poleward movement and ET of a TC may induce downstream development of cyclonic extratropical circulations through the import of kinetic energy (KE) into the midlatitude circulation. Orlanski and Sheldon (1993) developed an eddy KE (EKE) budget analysis process and showed that downstream development occurred in idealized simulations of baroclinic waves. Later, Orlanski and Sheldon (1995) defined a model of downstream development based on local KE budgets.

1. Extratropical Transition Climatology

Extratropical transition occurs in nearly every ocean basin that experiences TCs (Fig. 1), with a temporal distribution of ET events that is similar to, but always fewer than, the total TC distribution (Fig. 2) (Jones et al. 2003). While western North Pacific has the largest number of ET events (Fig. 2b), the Atlantic basin has the largest percentage of TCs that undergo ET (Fig. 2a), as 45% of all TCs experience ET based on the 30-year dataset examined by Jones et al. (2003). A strong, persistent subtropical ridge north of the eastern North Pacific basin makes this region unfavorable for ET (Jones et al. 2003). More detailed climatologies of ET are available for the west coast of Australia (Foley and Hanstrum 1994), the western North Pacific (Klein et al. 2000), the North Atlantic (Hart and Evans 2001), and the western South Pacific (Sinclair 2002).

Extratropical transition has a significant impact on Australia and New Zealand in the western South Pacific basin, since ET becomes likely when a midlatitude trough approaches a poleward-moving TC from the west (Sinclair 2002). Because of the limited time period examined, and the lack of a comprehensive definition of ET, the threat posed by ET to eastern Australia is underestimated in Fig. 1b (Jones et al. 2003).

In the eastern South Indian Ocean, few TCs experience ET (Figs. 1b and 2d). In this basin, conditions only become favorable for ET when a large-amplitude cold front approaches within a distance of 1700 km of a TC. These conditions result in a significant ET event roughly every 20 years (Jones et al. 2003). They occur usually during late summer or autumn (Jones et al. 2003).

Extratropical transition in the Atlantic basin was found to occur at lower latitudes in the early and late portions of the hurricane season, and at higher latitudes during the peak season (Hart and Evans 2001). September and October have the highest percentage of Atlantic basin ET events, which is due to

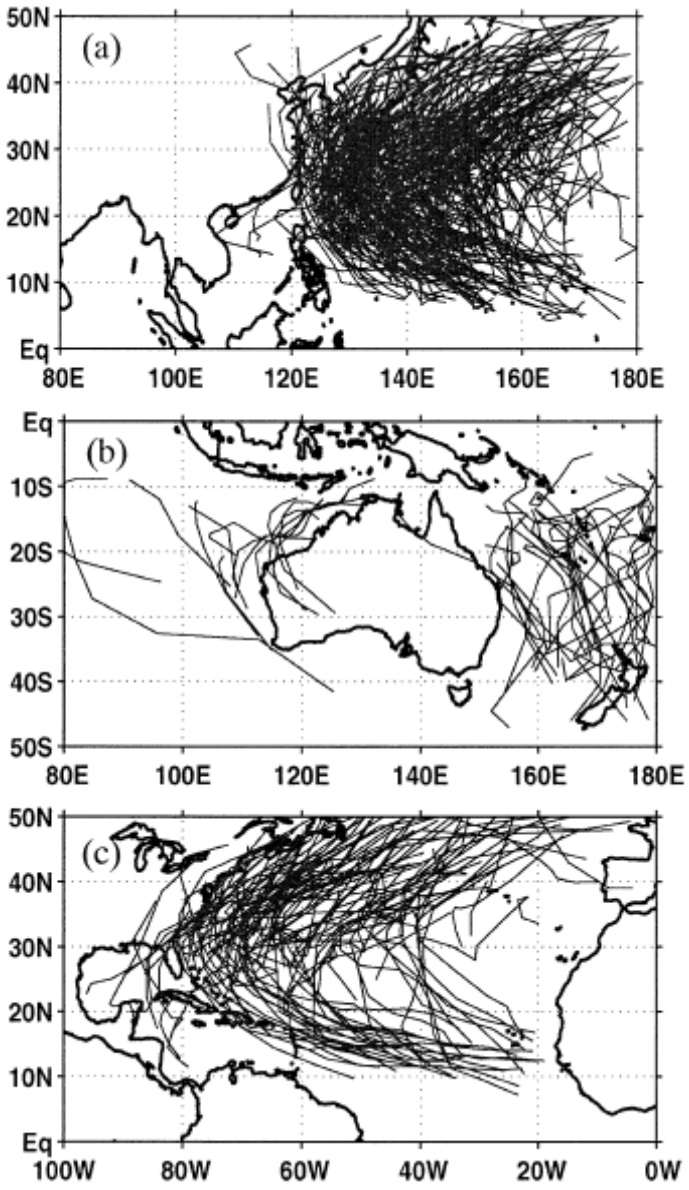

Figure 1. Tracks of all TCs that experienced ET during 1970-99: (a) Western North Pacific with tracks of TCs defined to be extratropical in Joint Typhoon Warning Center best-track data; (b) Southwest Pacific with data source as in (a) and southeast Indian Ocean with tracks of TCs that accelerated toward the southeast under the influence of a midlatitude frontal system and maintained gales into midlatitudes, which are the so-called captured cyclones in Foley and Hanstrum (1994), best-track data taken from http://www.australiasevereweather.com/cyclones/history.htm and (c) North Atlantic with tracks of TCs defined to be extratropical in National Hurricane Center best-track data (after Jones et al. 2003).

the close proximity of the regions that support TC development and the regions that support ET relative to the rest of the hurricane season (Hart and Evans 2001). Most of the Atlantic TCs that intensify after ET form in the deep tropics, and a large number of these are Cape Verde cyclones (Hart and Evans 2001).

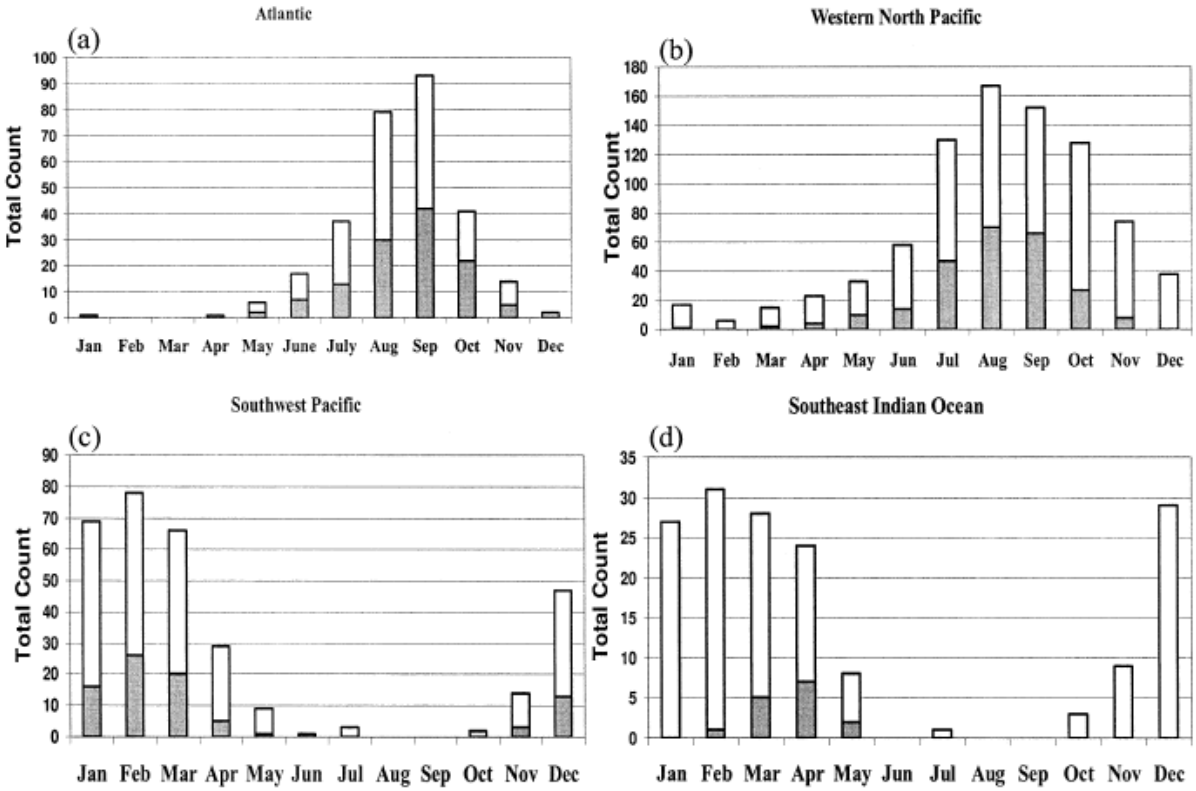

Figure 2. Monthly total numbers of tropical cyclones (open bars) in each basin during 1970-99 and the number of TCs that experienced ET (shaded bars) based on the data sources described in Fig. 1 (after Jones et al. 2003).

2. Characteristics of the Extratropical Transition Process

Using data from the western North Pacific basin, Klein et al. (2000) developed a conceptual model of ET that involved two stages, a transformation stage and a re-intensification stage. The transformation stage is defined by an interaction between a recurving TC and a pre-existing, lower-tropospheric baroclinic zone and the associated vertical wind shear (Klein et al. 2000). During the transformation stage, lower-tropospheric temperature advection,

frontogenesis, and a vertical motion dipole become established, the TC warm core disperses, and isentropic ascent/decent define interactions between the midlatitude baroclinic zone and the TC (Klein et al. 2000). On satellite imagery, the transformation stage has an asymmetric pattern in cloud and precipitation structure due to inflow of colder, drier (warmer, more moist) environmental air in the western (eastern) section of the outer TC circulation (Harr et al. 2000).

The deepening of the ex-TC as a baroclinic cyclone is defined as the re-intensification stage of ET. It concludes when a minimum sea-level pressure (SLP) is attained prior to a period of observed steady or rising SLP (Klein et al. 2000). At the beginning of re-intensification, the wind and precipitation are already asymmetric due to processes mentioned in the transformation stage (Klein et al. 2000; Harr et al. 2000). In addition, this stage is marked by the evolution of extratropical features such as fronts and extratropical-type wind, cloud and precipitation patterns (Harr et al. 2000). In several prior ET studies (DiMego and Bosart 1982; Sinclair 1993; Foley and Hanstrum 1994; Harr and Elsberry 2000; Harr et al. 2000), re-intensification of the TC remnants is described as being similar to Petterssen-Smebye type-B extratropical cyclogenesis (Petterssen and Smebye 1971). In this condition, low-level cyclone development occurs when an area of upper-level positive vorticity advection becomes superposed upon a low-level frontal zone (Petterssen 1955, and Sutcliffe and Forsdyke 1950). Klein et al. (2002) found that if Petterssen-Smebye type-B extratropical cyclogenesis is to be the method by which the TC remnants deepen in the re-intensification stage, the TC must translate poleward to phase with upper-level positive vorticity advection (PVA) that exist in midlatitude circulation patterns.

During the transformation and re-intensification stages, a nearly barotropic tropical cyclone evolves into a baroclinic extratropical cyclone. Therefore, it is natural that frontogenesis should be involved in this process. Vector-frontogenesis diagnostics are useful for the examination of changes in the

magnitude (scalar frontogenesis) and direction (rotational frontogenesis) of the horizontal θ gradient (Keyser et al. 1988). Harr and Elsberry (2000) noted that the rotational frontogenesis parameter does seem to represent the evolution of the ET process, but does not seem to provide a detailed measure for characteristics that would be involved in ET. Harr and Elsberry (2000) suggest that it would be easier to use rotational frontogenesis as a detector of ET, rather than trying to detect changes in the inner core of the TC.

B. MOTIVATION

Often, the accuracy of numerical weather prediction models is reduced following an ET event, which may be related to the complex thermodynamics and dynamic processes involved in ET. Downstream from an ET event, the midlatitude circulation often becomes perturbed due to movement of the decaying TC. These perturbations may impact downstream development of the extratropical circulation. Because of uncertainties in representing the ET process, forecasts of the downstream development may not be accurate. Therefore, the influence on downstream development by ET events will be examined here in terms of the transport of EKE from the decaying TC to the midlatitude circulation.

The availability of high-resolution, gridded datasets provided by model initializations and reanalysis projects spurred maturation of local EKE budget analyses (Orlanski and Katzfey 1991; Orlanski and Chang 1993; Chang and Orlanski 1993; Orlanski and Sheldon 1993). Application of this EKE budget method confirmed that, in certain cases, energy transfers between distinct midlatitude synoptic-scale disturbances are often involved when an upstream wave dissipates and a downstream development occurs.

Orlanski and Katzfey (1991) applied EKE budget analysis to diagnose a cyclone over the eastern South Pacific. They concluded that ageostrophic geopotential fluxes (AGF) from an upstream circulation comprised the major *source* of the cyclone EKE during its developmental stage, and the radiation of

ageostrophic geopotential fluxes downstream was the major *sink* of the cyclone EKE during its decay stage. Orlanski and Chang (1993) examined the energetics of downstream-developing waves and found that while the initial perturbation grows by baroclinic conversion, development of downstream perturbations is triggered by the convergence of AGFs radiating from existing upstream perturbations.

Decker and Martin (2005) compared EKE budgets for two consecutive explosively deepening extratropical cyclones over North America in April 2001. They found that significantly different cyclolysis rates occurred in each event that resulted from differences in the onset of the downstream radiation of AGFs, and the positioning of the surface cyclone center relative to the associated EKE center.

Chang (1993) applied a regression method to the EKE budget and determined that eastern (western) North Pacific basin cyclones experienced more EKE generation through ageostrophic geopotential flux (baroclinic conversion). Chang's findings on the western (eastern) North Pacific basin agrees with intuition, considering the warm (cold) poleward (equatorward) ocean currents along the eastern Asian (western American) coast and the often (rare) occurrences of cold continental air masses migrating over the warmer western (colder eastern) North Pacific, which contribute to frequent (infrequent) baroclinity.

Orlanski and Sheldon (1993) defined the process of dispersion and spreading of energy in a growing unstable system that is characteristic of high-frequency baroclinic waves as "downstream baroclinic development." In this framework, downstream baroclinic development may be involved in the generation of observed disturbances that may not be anticipated based solely on an examination of local available baroclinicity. Orlanski and Sheldon (1993) noted that on some occasions an intense ridge-trough system develops over the eastern Pacific Ocean and the west coast of North America that draws frigid air

southward over the coastal regions. They calculated an EKE budget on one such an event that occurred in December 1990 and which brought the first freeze to California since the 1936-1937 growing season. This budget showed that the early growth of the EKE center associated with this event mainly developed from the convergence of AGFs (Orlanski and Sheldon 1993).

In this thesis, EKE budget analyses are conducted for several ET events (Table 1) that occurred over the western North Pacific. The purpose is to identify the contributions of the ET process to downstream development for several events with contributions from varying TC and ET characteristics.

Table 1. Selected basic information relevant to each TC analyzed in this thesis. [Compiled from Digital Typhoon (2007): http://agor.ex.nii.ac.jp/digital-typhoon/index.html.en]

TC Name	Minimum Pressure	Maximum Wind	Average Forward Speed	Lifetime
Tokage	940 hPa	85 kt (43.7 m s^{-1})	23.2 km/h (6.4 m s^{-1})	186 h
Banyan	975 hPa	55 kt (28.3 m s^{-1})	25.6 km/h (7.1 m s^{-1})	150 h
Guchol	980 hPa	55 kt (28.3 m s^{-1})	30.0 km/h (8.3 m s^{-1})	102 h
Nabi	925 hPa	95 kt (48.9 m s^{-1})	24.6 km/h (6.8 m s^{-1})	234 h

In Chapter II, the data and method of analysis are defined. Chapter III contains a synoptic description of each case that is then followed by the results of the kinetic energy analyses. Results, conclusions, and future work topics are presented in Chapter IV.

II. DATA AND METHODOLOGY

A. DATA SOURCE

Standard meteorological observations do not contain enough information to calculate the terms of the EKE budget. As such, the datasets used to calculate these terms here are from the National Centers for Environmental Prediction (NCEP) Final "FNL" Global Data Assimilation System analyses. The FNL analyses data are collected by the Naval Postgraduate School Department of Meteorology on a regular basis to support educational and research activities. The FNL analysis incorporates observations with a cutoff period of five hours past synoptic time, and utilizes them to make a global analysis and 3-, 6-, and 9-hour forecasts four times per day (Iredell 2007). This FNL analysis is distinguished from the operational GFS analysis, which only incorporates those observations received within two hours and 45 minutes after synoptic time (CISL 2007).

The FNL analyses data have a horizontal resolution of 1 deg. lat./long., a temporal resolution of six hours and 26 vertical levels from 1000 hPa to 10 hPa. Also, surface variables, sea-level variables, and many other miscellaneous atmospheric and surface observations are contained in the FNL dataset. This study utilizes the 0000 UTC and 1200 UTC analyses at vertical levels from 1000 hPa to 100 hPa in 50 hPa increments of heights, relative humidities, vertical velocities, temperatures, zonal and meridional wind components, mean sea-level pressures, and potential temperature on the 2.0 potential vorticity unit (PVU) surface.

B. EDDY KINETIC ENERGY AND FLUX BUDGETS

The EKE budget that is used in this downstream development diagnosis is computed by defining the 'eddies' as perturbations from a 'mean' flow as represented by the following equations:

$$\mathbf{V}_{total} = \mathbf{V}_{mean} + \mathbf{v}_{eddy} \qquad \text{[for any vector; here, the horizontal wind]} \qquad (2.1)$$

$$Q_{total} = Q_{mean} + q_{eddy} \quad \text{[for any scalar, including vertical velocity } \omega\text{]} \qquad (2.2)$$

The mean flow quantities in (2.1) and (2.2) are either a time or a zonal mean. Although computation of the time mean is the preferred method, Orlanski and Sheldon (1993) utilized a zonal mean over 116° of longitude as a time mean was not practical with their dataset.

This study will consider four TCs in the western North Pacific. The time and date that each TC completed ET was generally utilized as the representative center time on which 30-day means were calculated (Table 2). The strategy was to designate the date with the nearest 0000 UTC time relative to the ET completion time as the "center time" used in the mean calculations. In the cases of Guchol and Saola, which both completed ET at 1200 UTC, 0000 UTC on the same day was chosen as the common center time to sample more of the storms' tropical characteristics. Furthermore, choosing 0000 UTC simplified dataset retrieval and assures diurnal model consistency among the TCs.

Table 2. Tropical cyclones examined in this study with their associated times/dates of ET completion and their "center time" used to compute mean quantities. [ET times and dates compiled from Digital Typhoon (2007): http://agora.ex.nii.ac.jp/digital-typhoon/index.html.en]

TC Name	**ET Completion Time and Date**	**"Center Time" for 30-day Mean Calculation**
Tokage	1800 UTC 20 October 2004	0000 UTC 21 October 2004
Banyan	0000 UTC 28 July 2005	0000 UTC 28 July 2005
Guchol	1200 UTC 25 August 2005	0000 UTC 25 August 2005
Nabi	0600 UTC 8 September 2005	0000 UTC 8 September 2005

For each TC, 30-day time averages were computed for zonal and meridional wind components, vertical velocities, heights, relative humidities, and temperatures, which produce the mean values for each of the variables at each grid point. These averages represented the mean field terms in (2.1) and (2.2).

The "eddy" values in (2.1) and (2.2) are found by subtracting 30-day mean values for each variable from the analyzed values from the FNL dataset at the 0000 and 1200 UTC times. Values in the time window starting three to four days before ET through one day after were the focus in this study. These eddy variables were used to calculate the EKE budget analysis.

1. The Eddy Kinetic Energy Equation and Ageostrophic Geopotential Flux

From Orlanski and Sheldon (1993), the EKE equation in pressure coordinates is given by:

$$\frac{\partial K_e}{\partial t} = -(\mathbf{v}\cdot\nabla\phi) - [\nabla\cdot(\mathbf{V}K_e)] - \frac{\partial(\omega K_e)}{\partial p} + residue\,, \tag{2.3}$$

where $K_e = (1/2)|\mathbf{v}|^2$. The term on the left side of (2.3) is the tendency of EKE, and the first three terms on the right side of (2.3) are the advection of eddy geopotential heights by the eddy velocity, and the horizontal and vertical divergence of the EKE fluxes (Orlanski and Sheldon 1993). Two other terms $\mathbf{v}\cdot(\mathbf{v}\cdot\nabla\mathbf{v})_m$ and $\mathbf{v}\cdot(\mathbf{v}\cdot\nabla\mathbf{V}_m)$ and the dissipation are included in the *residue* term (Orlanski and Sheldon 1993).

Orlanski and Katzfey (1991) showed that the first term on the right side of (2.3) can be written as:

$$-\mathbf{v}\cdot\nabla\phi = -\nabla\cdot(\mathbf{v}_{a0}\phi) - \omega\alpha - \frac{\partial(\omega\phi)}{\partial p}\,. \tag{2.4}$$

Because the eddy geostrophic wind $\mathbf{v}_{g0}$ (defined using a constant f_0) is nondivergent (Orlanski and Sheldon 1993), the flux defined by the ageostrophic velocity $\mathbf{v}_{a0}$ is:

$$\mathbf{v}_{a0}\phi = \mathbf{v}\phi - \frac{\mathbf{k}}{f_0}\times\frac{\nabla\phi^2}{2}\,. \tag{2.5}$$

The last term in (2.5) is the geopotential field multiplied by the geostrophic velocity (geostrophic geopotential flux), which is nondivergent (Orlanski and Sheldon 1993). Geopotential fluxes defined using the ageostrophic velocity $\mathbf{v}_{a0}$ retain the entire divergent component of the total flux $\mathbf{v}\phi$ (Orlanski and Sheldon 1993).

The first term on the right side of (2.4) is the divergence of the AGFs, which represents the dispersion of energy by nonadvective processes (Orlanski and Sheldon 1993). The term $-(\omega\alpha)$ represents the conversion of available eddy potential to kinetic energy (Orlanski and Sheldon 1993). The term $\frac{\partial(\omega\phi)}{\partial p}$ represents the vertical flux divergence that redistributes energy vertically via work done by pressure forces (Orlanski and Sheldon 1993). Orlanski and Sheldon (1993) found that the vertical integral of the third term over the entire atmosphere is usually very small.

When the latitudinal extent of the domain becomes large, the ageostrophic velocity $\mathbf{v}_{a0}$ will contain a large portion of the geostrophically balanced flow for latitudes different from that selected for defining the constant Coriolis parameter f_0 in (2.5). Because only the convergence and divergence of fluxes have importance for energy balance, the flux vector becomes less useful as an indicator of the direction of energy flow (Orlanski and Sheldon 1993). To overcome this shortcoming, Orlanski and Chang (1993) presented a modification that redefined the nondivergent component of the geopotential fluxes (2.5) in cases of a variable Coriolis parameter:

$$(\mathbf{v}\phi)_a = \mathbf{v}\phi - \mathbf{k}\times\nabla\frac{\phi^2}{2f(y)}. \tag{2.6}$$

In (2.6), the removed flux is still nondivergent and reduces to (2.5) when f is constant (Orlanski and Sheldon 1993).

Decker and Martin (2005) noted that the various EKE tendency equation terms can be calculated at each vertical level and grid point, and a vertical average can be extracted for each grid point with losing much information about the energetics of the analyzed situation. This approach would eliminate the need to examine cross sections or multiple levels in many instances. With *A* referring to any variable and ρ defined as density, the vertical average is defined as:

$$\tilde{A} = \frac{1}{z_{top} - z_{bottom}} \int_{z_{bottom}}^{z_{top}} \rho A dz \, . \tag{2.7}$$

In this thesis, geopotential fluxes serve as a diagnostic tool, and flux vectors as generated by (2.6) are utilized in the EKE budget analyses. Table 3 is a summary of the descriptive names of the terms in the EKE tendency equation and the components of the advection of eddy geopotential heights by eddy velocity. In addition, vertically averaged quantities as calculated in (2.7) were used for the EKE budget analyses.

Table 3. Descriptive names of terms in the EKE tendency equation and components (terms) of $-(\mathbf{v}\cdot\nabla\phi)$.

EKE Terms	**Descriptive Name**
$-(\mathbf{v}\cdot\nabla\phi)$	Advection of eddy geopotential heights by eddy velocity
$-[\nabla\cdot(\mathbf{V}K_e)]$	Horizontal EKE flux convergence **(EKEFC)**
$\frac{\partial(\omega K_e)}{\partial p}$	Vertical divergence of EKE fluxes
$-(\mathbf{v}\cdot\nabla\phi)$ **Terms**	**Descriptive Name**
$-\nabla\cdot(\mathbf{v}_{a0}\phi)$	Convergence of ageostrophic geopotential fluxes **(AGFC)**
$-\omega\alpha$	Baroclinic conversion of available potential energy to KE **(BC)**
$-\frac{\partial(\omega\phi)}{\partial p}$	Vertical geopotential flux convergence

2. Lifecycle Stages in a Downstream Baroclinic System

Orlanski and Sheldon (1995) formulated a three-stage model of downstream development (Fig. 3). In the first stage, an existing EKE center radiates EKE downstream via AGF fluxes. This EKE passes through a ridge immediately downstream and a new EKE center (denoted by a script *W* in Fig. 3) develops downstream of this ridge. In the second stage, this new energy center grows vigorously, at first due to the convergence of AGF and then later as a result of BC. As this new EKE center matures, it begins radiating EKE through the next ridge downstream as a result of AGF divergence. A new energy center (denoted by a script *E* in Fig. 3) then starts developing farther downstream as a result of AGF convergence in that new location. In the third stage, the old EKE center (script *W*) is decaying through AGF divergence. The new energy center (script *E*) is nearing maximum intensity with the aid of baroclinic conversion and is starting to radiate EKE downstream via AGF divergence.

The first stage can occur again and the cycle potentially can iterate multiple times and produce a coherent wave train of ridges and troughs limited in zonal extent. Lee and Held (1993) dubbed these structures as a “wave packet”, and provided observational and idealized modeling evidence of their existence. Chang and Yu (1999) and Chang (1999) provided basic characteristics of observed wave packets, e.g., that the group velocity of a wave packet is greater than the phase speed of the individual ridges and troughs within the wave packet. Also, consistent with the phase speed characteristic, ridges and troughs develop on the leading (downstream) side of the wave packet and eventually move to the trailing (upstream) side of the wave packet and decay.

Orlanski and Sheldon (1995) also described why geopotential fluxes are predominantly directed downstream (Fig. 4). In a trough, negative eddy ageostrophic wind components coincide with negative eddy geopotential values such that this product is positive. In a ridge, positive eddy ageostrophic wind

components coincide with positive eddy geopotential such that their product is also positive. Therefore, fluxes of eddy geopotential by the ageostrophic wind will be directed downstream.

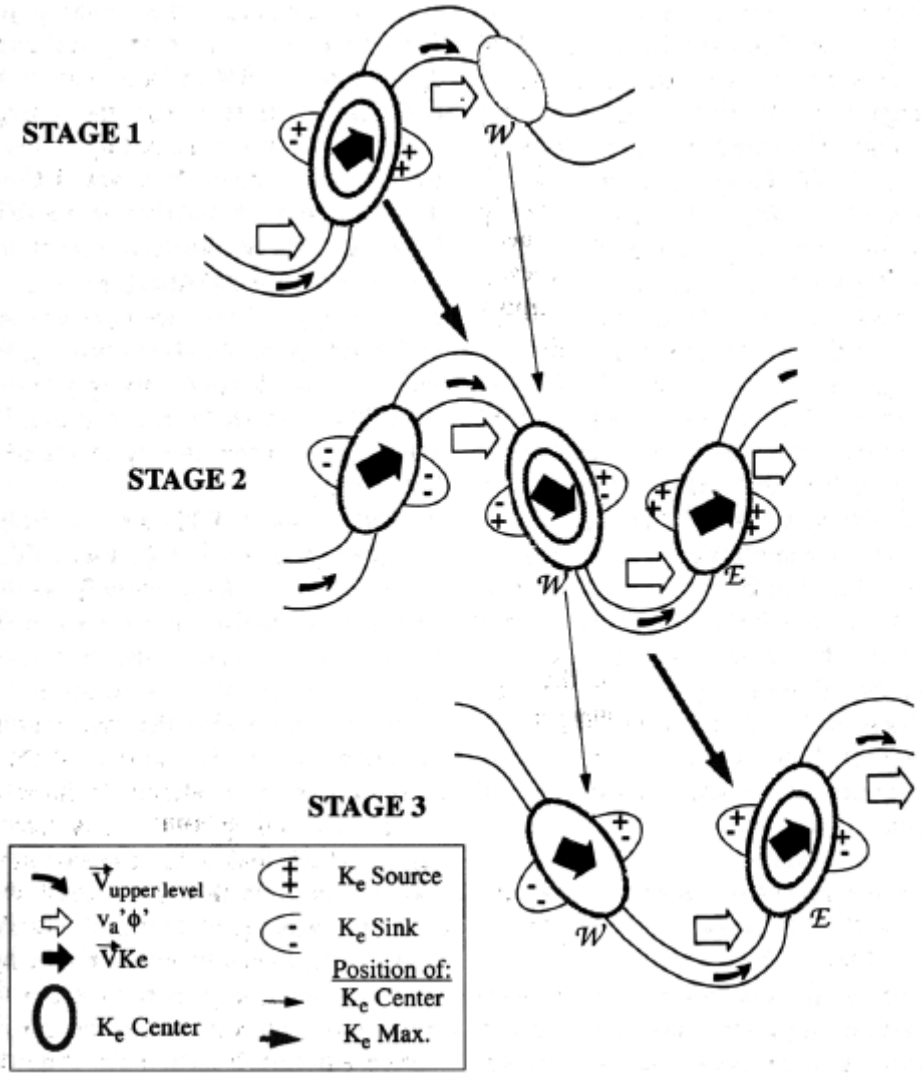

Figure 3. The three stages in the evolution of a baroclinic wave (Orlanski and Sheldon 1995). Symbols are as given in the inset. *Stage 1:* Upstream system decays and downstream EKE center is generated (denoted by the script *W*) west of a new trough via geopotential fluxes. *Stage 2:* EKE fluxes radiate from a mature energy center (denoted by the script *W*) and fosters the growth of a new energy center (denoted by the script *E*) east of the trough. *Stage 3:* The new energy center matures, while the older energy center decays (after Orlanski and Sheldon 1995).

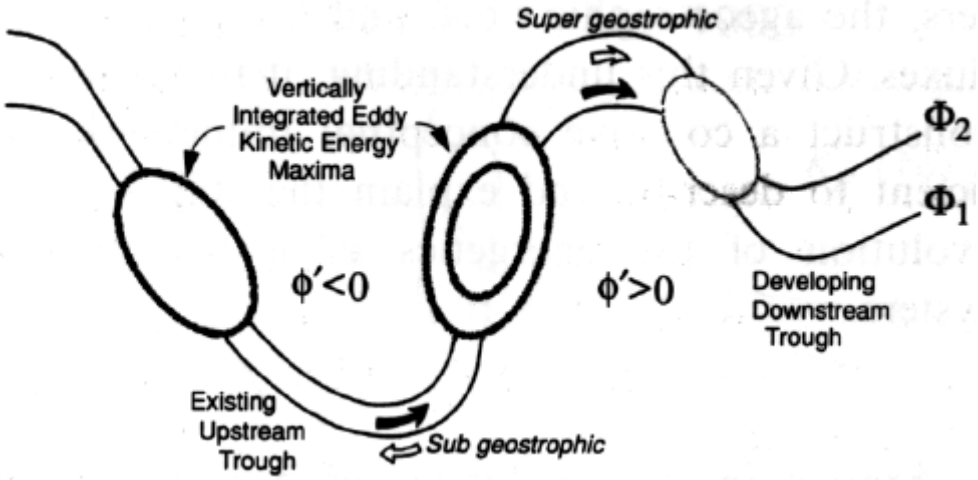

Figure 4. Illustration of the relationship between baroclinic wave components. The upper-level geopotential field is indicated by Φ_1 and Φ_2, and the geopotential anomaly ϕ' relative to the time mean is positive (negative) in the ridge (trough). Airflow relative to the wave is indicated by the heavy solid arrows and the ageostrophic wind is indicated by the open arrows. Centers of maximum vertically integrated EKE are shown as ellipses. An incipient disturbance is forming on the east side of the ridge at the center of the figure (after Orlanski and Sheldon 1995).

III. ANALYSIS

As indicated in Tables 1 and 2, four cases have been chosen from the 2004 and 2005 seasons to represent a variety of TC characteristics and midlatitude flow patterns. TY Tokage in October 2004 was a strong TC that moved into a midlatitude flow pattern that contained well-defined EKE centers associated with a high-amplitude ridge-trough pattern across the North Pacific. The high-amplitude pattern and EKE distribution weakened as Tokage began ET. The fluxes of EKE from Tokage influenced the development of a deep trough over the western North Pacific. However, the ET process sufficiently weakened Tokage and reduced the fluxes of EKE such that the connection to the developing trough was severed. The ET of TY Banyan in July 2005 represents a midsummer case in which an ET event significantly modified the circulation over the North Pacific. Although amplitudes of EKE parameters were small, a significant downstream development across the North Pacific was associated with the flux of energy from Banyan during the transformation and re-intensification stages of ET. By contrast, no direct impact on the downstream circulation occurred from the ET of TY Guchol, which was a small TC. However, the merger of TY Guchol with a developing midlatitude trough increased the generation of EKE in the trough and also increased the downstream dispersion of the energy. Finally, the case of TY Nabi is one in which a significant impact to downstream development was made by the ET of the TC as it re-intensified into a deep extratropical cyclone.

For each case, the synoptic evolution associated with the TC and downstream circulation prior to and during the ET period is defined. Then, the evolution of total EKE is described for key time periods. Finally, the components of the total EKE tendency are described during these time periods.

A. TY TOKAGE

With maximum sustained 10-minute wind speeds of 85 knots (43.7 m s^{-1}) and a minimum central pressure of 940 hPa (Table 1), Tokage represents a case involving an international class 5 TC (from Digital Typhoon (2007): http://agora.ex.nii.ac.jp/digital-typhoon/summary/wnp/s/200423.html.en). The time of ET was defined as 1800 UTC 20 October 2004 (Table 2).

1. Synoptic Evolution

At 1200 UTC 17 October 2004, Typhoon Tokage was at 20.3° N, 130.1° E (Fig. 5a). A midlatitude 500 hPa ridge was north of Tokage over the Japan Sea (Fig. 5a). Downstream across the North Pacific, a rather high amplitude height pattern existed, with a strong ridge over the central North Pacific and a trough over the west coast of North America. A longwave trough northeast of Tokage had an associated extratropical cyclone east of the Kamchatka Peninsula. The high amplitude height pattern is consistent with the distribution of PV on the dynamic tropopause (Fig. 5b).

Over the next 24 h, Tokage moved northwestward to 23.0° N, 126.9°E (Fig. 6a). At 500 hPa, the axis of the upper-level ridge north of Tokage had moved over Japan. On the dynamic tropopause, a noticeable increase in amplitude of the ridge had occurred over the previous 24 h (Fig. 6b), as well as an increase in amplitude in the trough immediately downstream of this ridge.

By 1200 UTC 19 October 2004, Tokage moved north-northeastward to 27.4° N, 128.9° E. At 500 hPa (Fig. 7a), the ridge over Japan had continued to drift to the east. On the dynamic tropopause, the ridge had increased in amplitude during the previous 24 h, as had the trough immediately downstream (Fig. 7b).

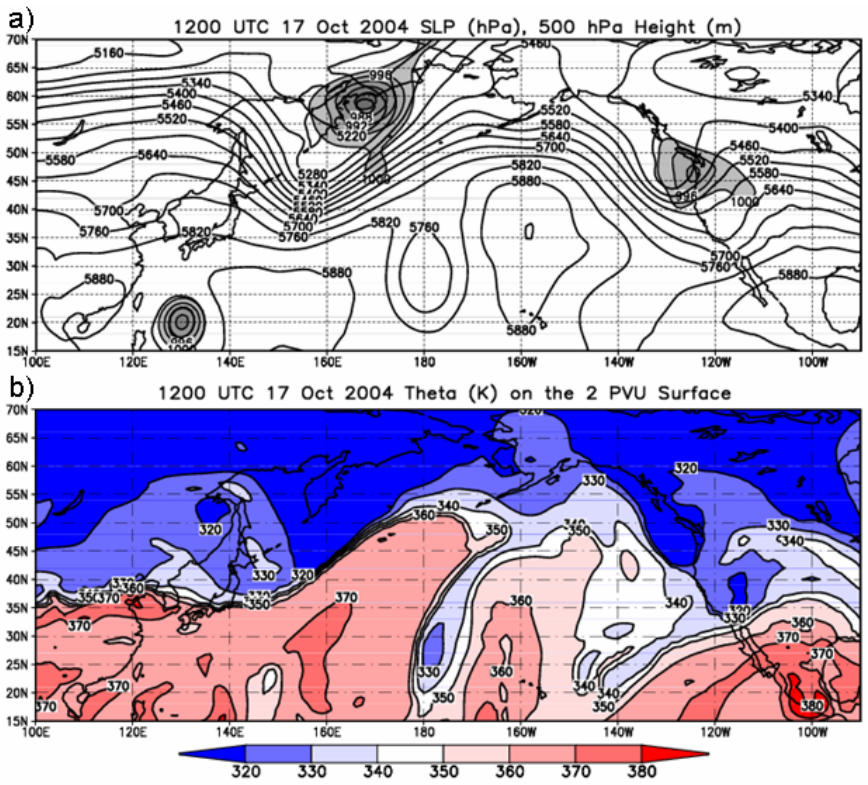

Figure 5. North Pacific Ocean synoptic environment at 1200 UTC 17 October 2004 including (a) mean sea-level pressure (grayscale shading and contours below 1000 hPa, 4 hPa interval) and 500 hPa heights (contours, 60 meter interval), and (b) potential temperature (shading and contours, 10 Kelvin interval) on the dynamic tropopause (2 PVU surface).

Tokage then moved more rapidly northeastward to 35.4° N, 138.3° E by 1200 UTC 20 October 2004 (Fig. 8a). At 500 hPa, the ridge (now to the east of Tokage) began to have a more southwest-northeast tilt. Over this 24 h period, the 500-hPa trough downstream of this ridge had deepened. On the dynamic tropopause, the downstream ridge now between 160° E and 170° W continued to amplify (Fig. 8b). At the same time, the trough downstream of the ridge extended farther south.

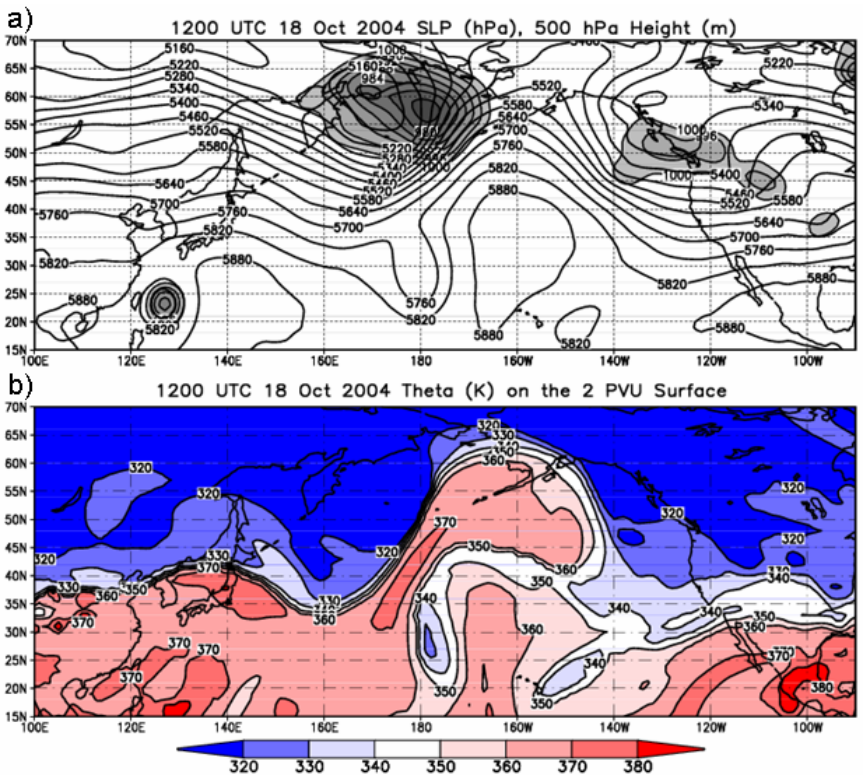

Figure 6. As in Fig. 5, except for 1200 UTC 18 October.

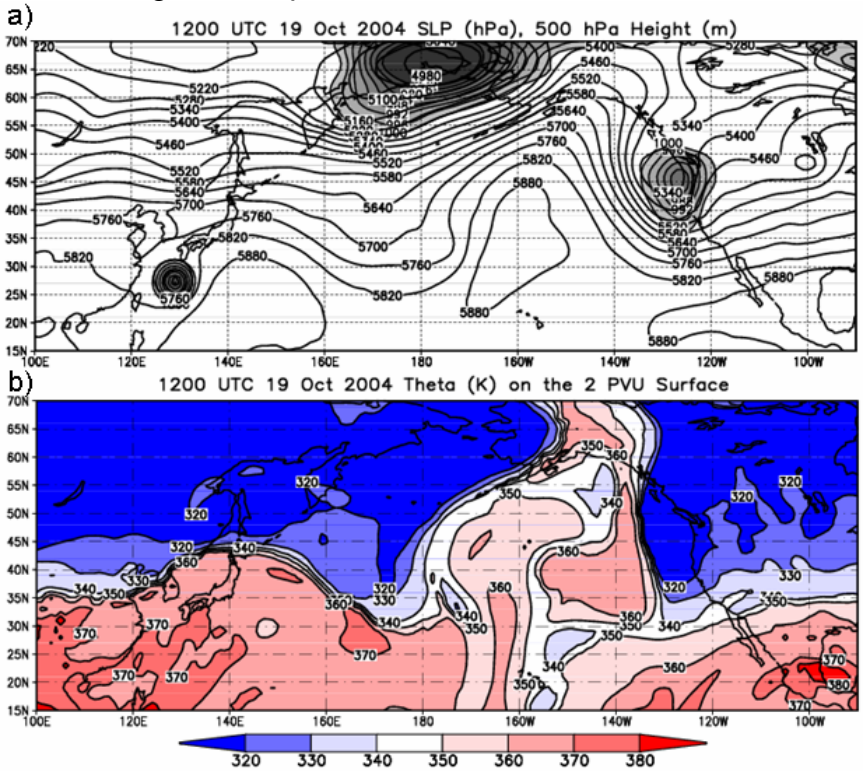

Figure 7. As in Fig. 5, except for 1200 UTC 19 October.

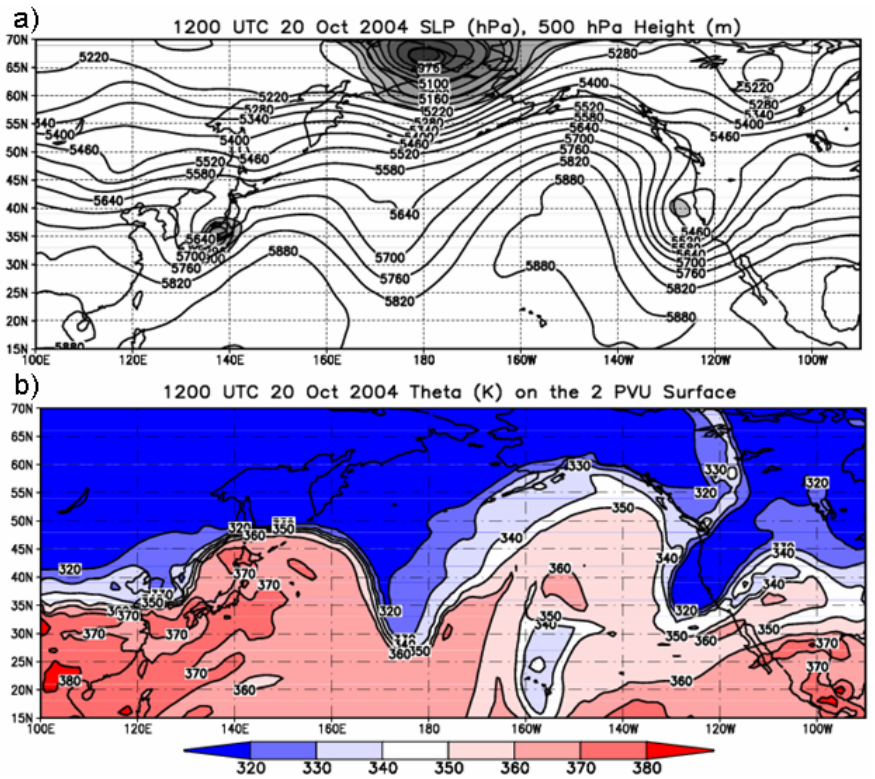

Figure 8. As in Fig. 5, except for 1200 UTC 20 October.

As Tokage moved into the midlatitude flow at 1200 UTC 21 October 2004, the 500-hPa ridge east of Tokage became even more positively tilted (Fig. 9a) and the trough downstream of this ridge began to cut-off. The positive tilt of this upper-tropospheric ridge was also evident on the dynamic tropopause. The trough immediately downstream of that ridge became very narrow as it extended into the subtropics (Fig. 9b).

As Tokage moved poleward, the flow across the North Pacific contained a series of high amplitude ridges and troughs. Over the western North Pacific, the longwave trough that was present prior to the recurvature of Tokage was replaced by a strong upper-level ridge. The original longwave trough over the western North Pacific then moved to the central North Pacific, extended southward, and eventually cut-off. The changes over the North Pacific during the ET of Tokage are clear by comparing Figs. 5b and 9b. The weak cut-off low over

the central North Pacific prior to the movement of Tokage into the midlatitudes was replaced by a stronger cut-off circulation that formed downstream of the ridge that amplified northeast of Tokage. Furthermore, the trough over western North America deepened and became sheared anticyclonically (Thorncroft et al. 1993). The impact of the ET of TY Tokage on this evolution is defined by examining the evolution of EKE throughout this period.

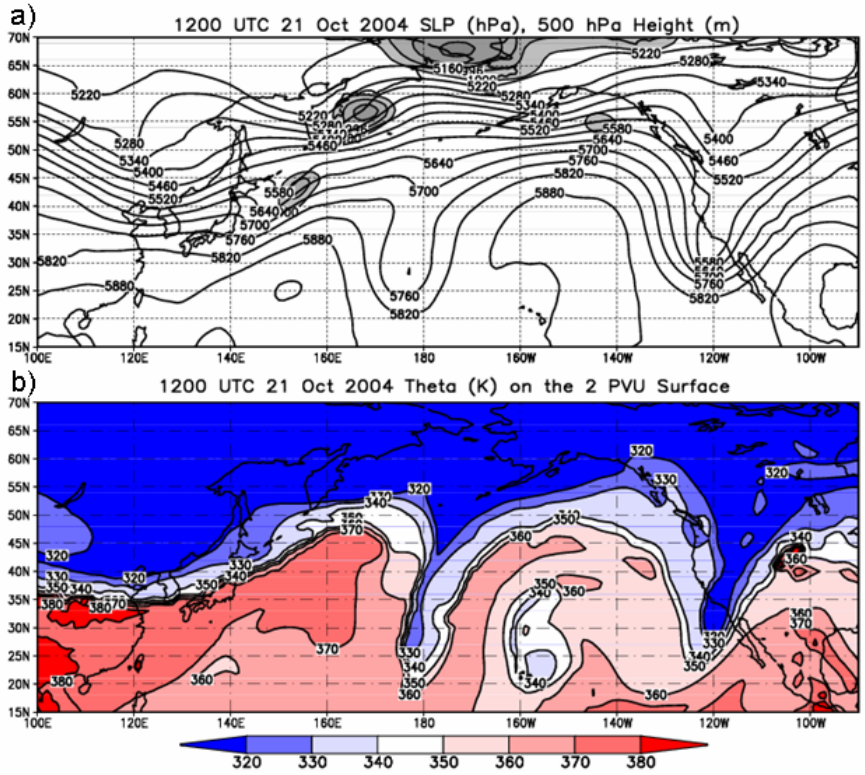

Figure 9. As in Fig. 5, except for 1200 UTC 21 October.

2. EKE Budget

a. Vertically Averaged EKE and Total EKE Flux Vectors

At 1200 UTC 17 October 2004, a significant amount of EKE was contained in the midlatitude circulation over the North Pacific (Fig. 10a). A midlatitude trough in the western North Pacific contained EKE centers on both its upstream and downstream sides, and a subtropical mid-tropospheric low near 180° E contained a lesser amount of EKE (Fig. 10a). Tokage was associated with an even smaller amount of EKE at this time. Twelve hours later (Fig. 10b),

the midlatitude trough approaching the central North Pacific experienced a sizeable EKE increase in its downstream EKE center and a loss of EKE in its upstream EKE center. Eddy kinetic energy increased on the downstream side of the subtropical mid-tropospheric low centered near 180° E (Fig. 10b), and a new EKE center developed just south of Alaska.

Although the upstream EKE center associated with the central North Pacific trough almost completely disappeared by 1200 UTC 18 October 2004 (Fig. 10c), the large downstream EKE center associated with this trough maintained its intensity. Equatorward of this large midlatitude EKE center, energy was being transferred from the subtropical EKE center into the larger midlatitude EKE center. Over eastern North Pacific, the midlatitude EKE center intensified downstream of an amplifying subtropical ridge centered along 160° W (Fig. 10c).

By 0000 UTC 19 October 2004 (Fig. 10d), the large EKE center over the central North Pacific had elongated and partially merged with the EKE center formerly in the subtropics. A small amount of EKE was transferring from this EKE center into the EKE center in the eastern North Pacific through the strong ridge near 155° W (Fig. 10d). The circulation associated with Tokage had not yet connected with the midlatitude circulation (Fig. 10d). The large EKE center in the central North Pacific weakened over the next 12 h (Fig. 10e), and EKE transfer to the eastern North Pacific EKE center diminished as EKE encircled the mid-tropospheric low north of the Bering Sea. At this time, a weak connection between Tokage and the midlatitude circulation became evident (Fig. 10e).

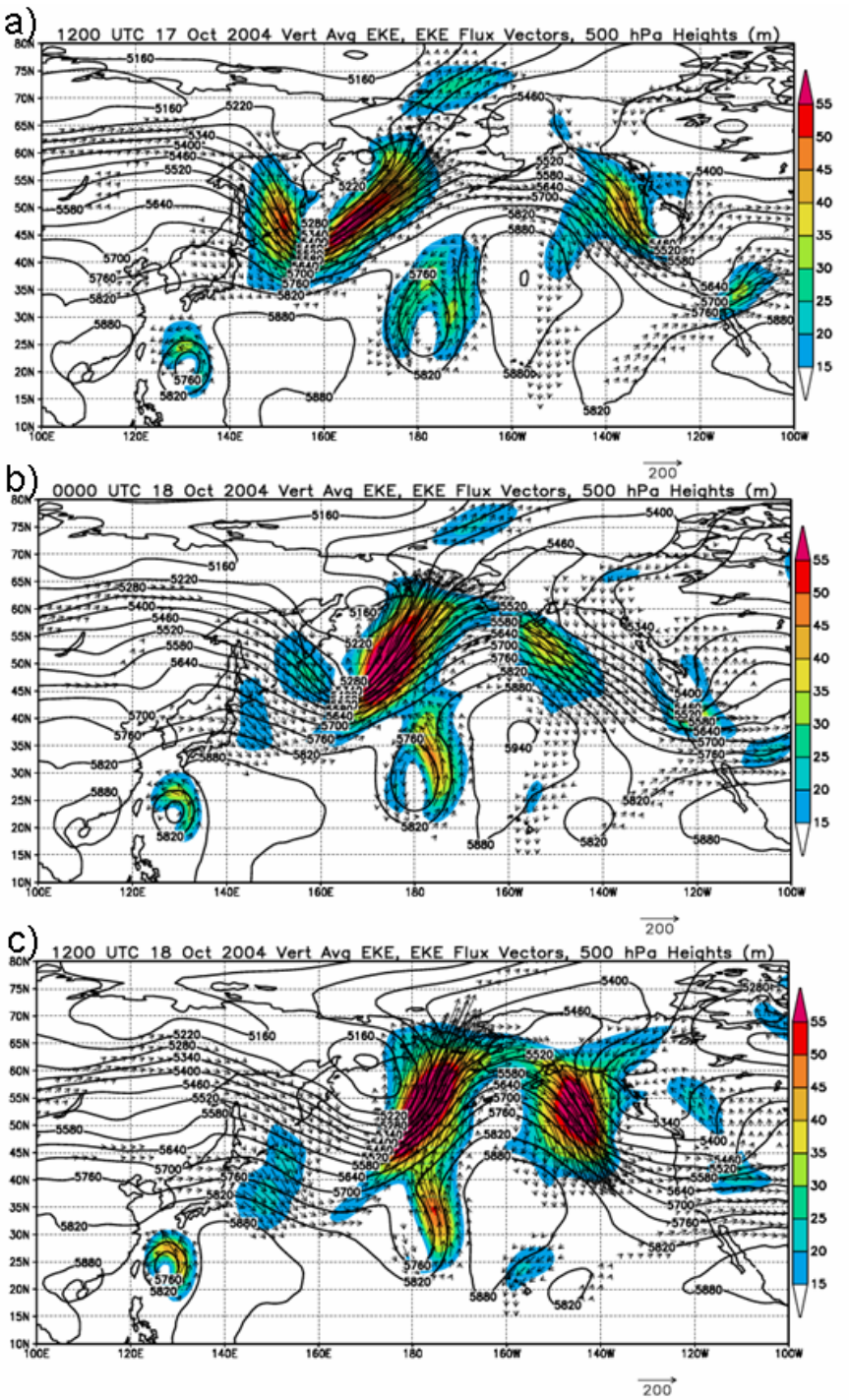

Figure 10. Vertically averaged EKE [color shading, refer to legend for values (units: MJ m^{-2})], total EKE flux vectors [arrows, refer to reference vector (units: MW m^{-1})], and 500 hPa heights [contours, 60 m intervals]. Total EKE flux vectors less than 20 MW m^{-1} are not plotted. The time period 1200 UTC 17 October through 0000 UTC 22 October 2004 is represented in panels (a) through (j).

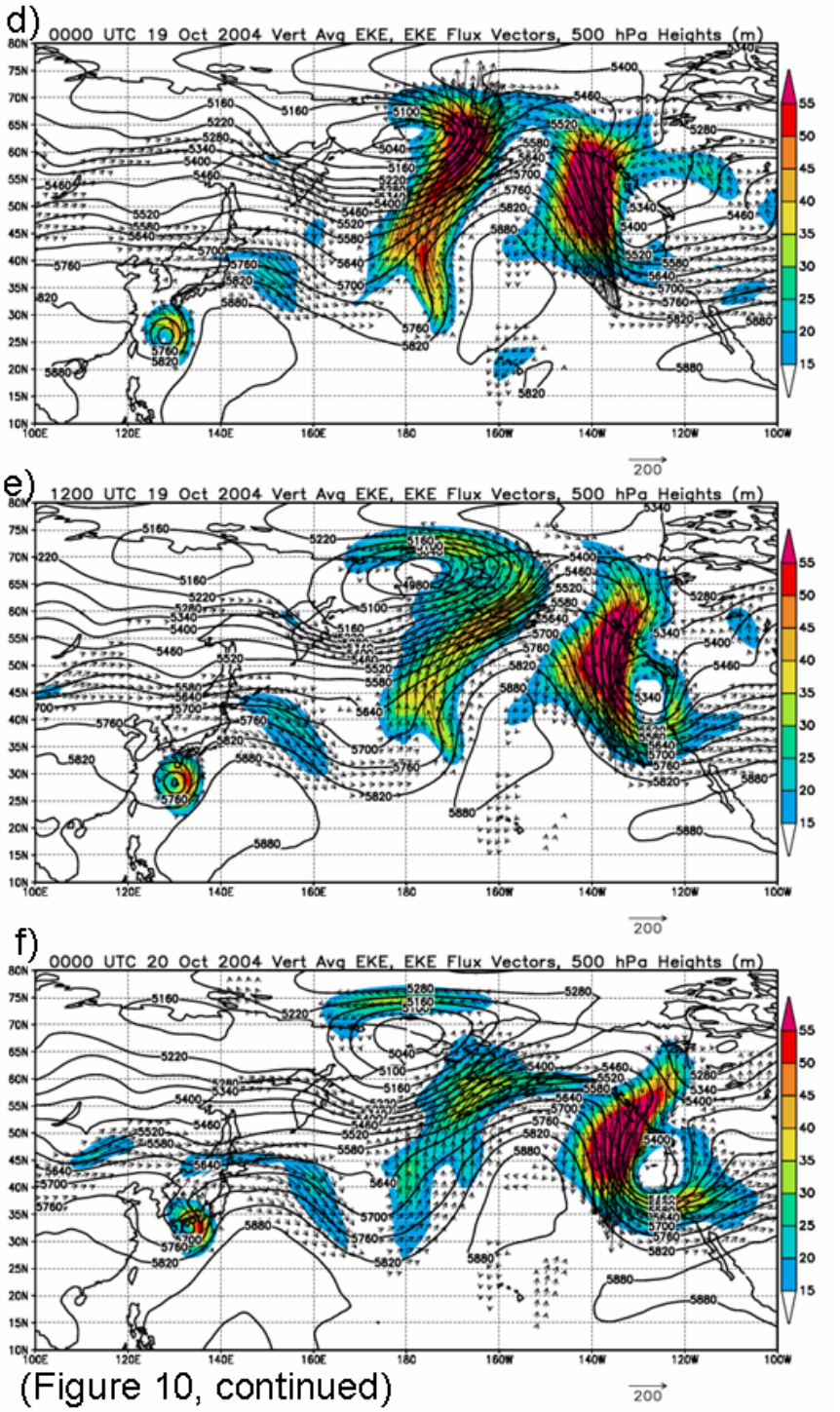

(Figure 10, continued)

An EKE center developed north of Tokage along 140° E by 0000 UTC 20 October 2004 (Fig. 10f). This EKE center resulted from fluxes of EKE from a midlatitude EKE center near 45° N, 115° E and from Tokage. The EKE

center north of Tokage was also connected to a center that was on the upstream side of a new trough developing along 170° E (Fig. 10f). On the eastern side of the trough, there was a connection to the downstream EKE centers over the eastern North Pacific (Fig. 10f). The flux of EKE into the midlatitude circulation from Tokage increased over the following 12 h (Fig. 10g). This energy flow was directed toward the center on the western side of the central North Pacific trough. This EKE center increased in intensity from the previous 12 h. Although the eastern portion of the central North Pacific trough continued to transfer EKE downstream towards the EKE center over southwestern Alaska and the large EKE center off the west coast of North America (Fig. 10g), the entire EKE distribution over the eastern North Pacific weakened.

By 0000 UTC 21 October 2004, the EKE contribution from Tokage to the western EKE center near 35° N, 170° E diminished as Tokage weakened through the ET process (Fig. 10h). The EKE center on the eastern side of the central North Pacific trough increased in intensity slightly and continued to radiate EKE fluxes to both the EKE center in southern Alaska and the weakening centers near the west coast of North America (Fig. 10h). Eddy kinetic energy centers diminished in intensity on both sides of the trough in the central North Pacific as EKE fluxes from the remnants of Tokage diminished over the next 12 h (Fig. 10i). As the remnants of Tokage underwent a weak re-intensification as an extratropical cyclone, the EKE center east of the Kamchatka Peninsula intensified (Fig. 10i).

After another 12 h, an EKE center intensified in association with the re-intensification of Tokage's remnants near 45° N, 165° E (Fig. 10j). This EKE center transferred EKE into the larger center over the Bering Sea. The subtropical mid-tropospheric low in the central North Pacific became isolated from midlatitude EKE fluxes and its eastern EKE center intensified (Fig. 10j).

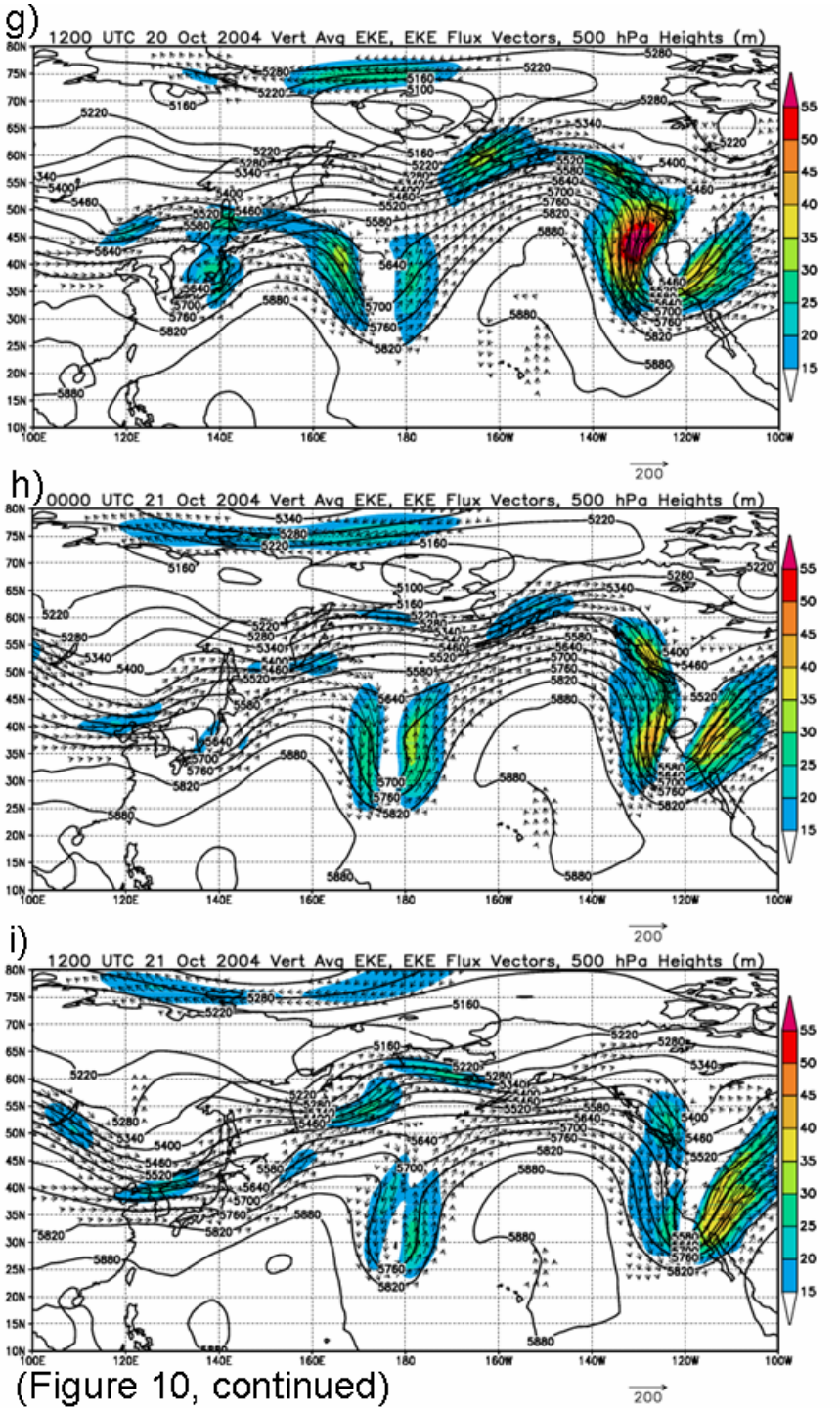

(Figure 10, continued)

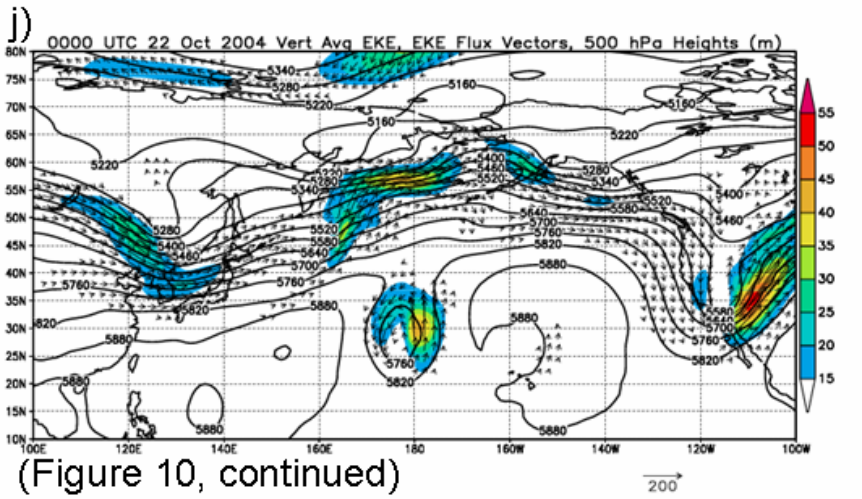

(Figure 10, continued)

This was a case in which large amounts of EKE in the midlatitude circulation existed prior to the movement of the TC into the midlatitudes. Once the high-EKE, high-amplitude midlatitude weather system moved downstream, a lower-EKE, less-amplified midlatitude pattern remained over the western North Pacific. As Tokage moved poleward and began ET, an increase in the flux of EKE occurred downstream that contributed to an intensifying trough over the central North Pacific. As EKE increased in this trough, it extended into the subtropics to be cut off from the midlatitude flow. Since Tokage only weakly re-intensified as an extratropical cyclone, further transfer of energy from Tokage was minimal and limited to the higher latitudes. Therefore, Tokage had an initial impact on the development of a downstream trough, but this did not continue as Tokage weakened and moved farther poleward before weakly re-intensifying as an extratropical cyclone. In the following section, the flux convergence of EKE and contributions to EKE generation are investigated for key periods associated with Tokage moving into the midlatitudes.

b. Components of Total EKE

As Tokage was starting to inject EKE into the midlatitudes around 0000 UTC 19 October 2004 (Fig. 10d), a strong positive/negative EKEFC couplet was located north of Tokage and also over the downstream EKE center near 40°

N, 145° E (Fig. 11a). The pattern of EKEFC is such that convergence occurs downstream of the EKE center and divergence upstream of the EKE center. Therefore, the depletion of EKE to the rear of the center is balanced by accumulation of EKE ahead of the center. Furthermore, this region is one of large EKE generation (Fig. 11b).

While the total flux of EKE between Tokage and the midlatitude circulation (Fig. 10d) is weak, the flux due to ageostrophic flow from Tokage is well-defined (Fig. 12a). The flow associated with Tokage is producing EKE via BC (Fig.12b) and a large region of flux divergence (Fig. 12a) between 130° E and 140° E indicates that this energy is being dispersed into the midlatitudes. Therefore, the developing EKE center near 150° E (Fig. 10d) is due to a combination of sources that include Tokage and the shortwave trough west of the Kamchatka Peninsula. However, the pattern of EKEFC indicates that the majority of the horizontal flux of energy is being advected into the developing center at 150° E from directly upstream, which is due to the flux from Tokage.

Twenty-four hours later, distinct EKEFC couplets and EKE generation were still found about the EKE center downstream of Tokage near 40° N, 165° E (Fig. 13a). Ageostrophic geopotential fluxes from Tokage were contributing to EKE generation in the downstream EKE center near 40° N, 160° E (Fig. 13b). However, a larger contribution to EKE generation was due to the recirculation of energy from the downstream side of the trough as the trough amplified. The contributions to EKE generation (Fig. 14a,b) indicated that the circulation of Tokage continued to be a source of EKE through BC (Fig. 14b) and the energy was being dispersed into the midlatitude flow (Fig. 14a).

By 0000 UTC on 21 October 2004 (Fig. 15), EKE fluxes originating from Tokage had less contribution to the EKE center on the western side of the central North Pacific trough as the trough extended southward. The AGFs emanating from Tokage were now primarily directed toward the shortwave trough west of the Kamchatka Peninsula (Fig. 15b).

As ex-Tokage began re-intensification, BC of EKE continued and expanded as the remnants of Tokage interacted with the shortwave trough (Fig. 16b). The pattern of the AGF divergence indicated that this energy was being dispersed into the shortwave over the Sea of Okhotsk (Fig. 16a). Tokage moved poleward as a weaker extratropical cyclone (Fig. 10h,j) in association with the EKE distribution.

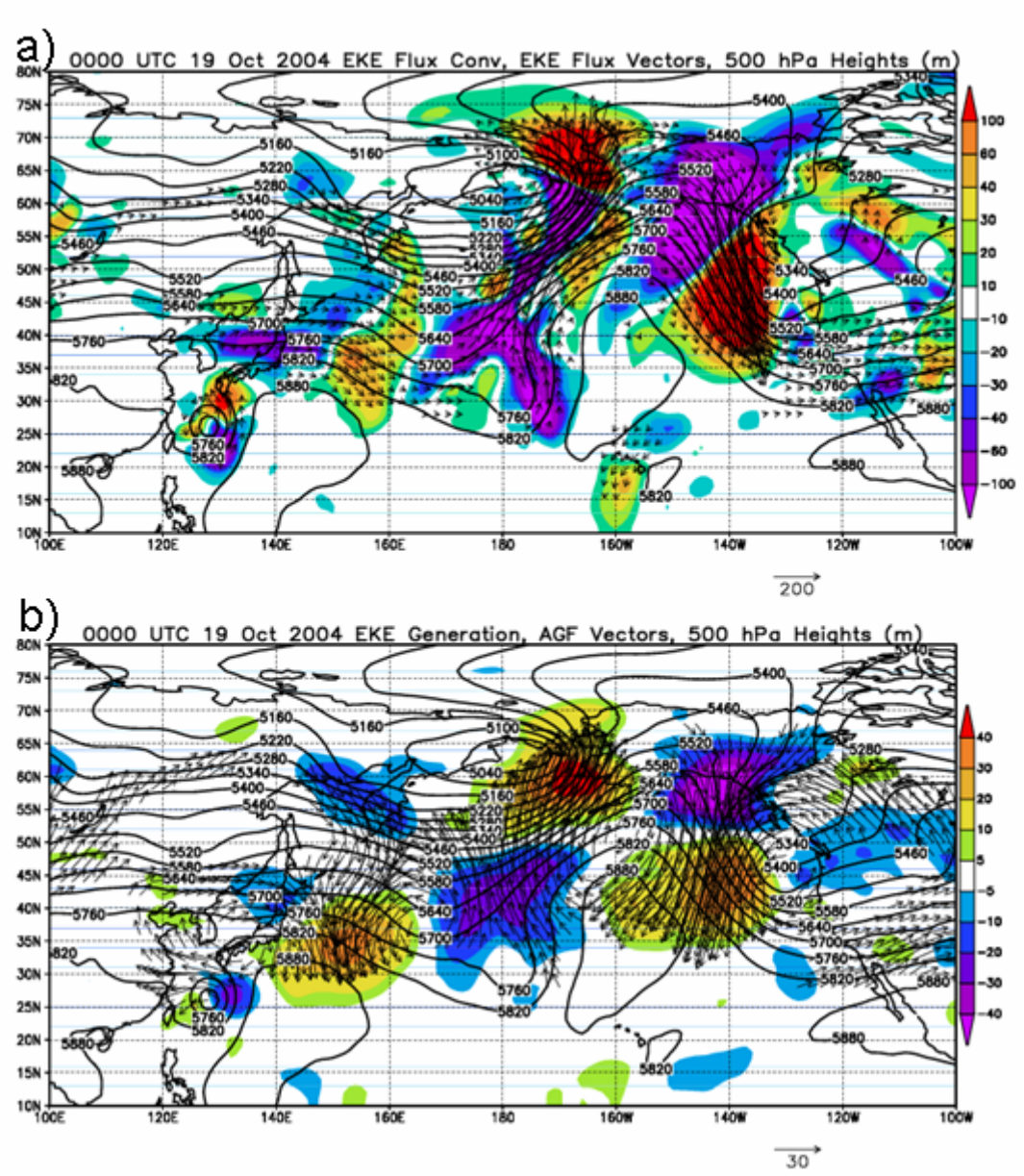

Figure 11. Distribution of EKE components at 0000 UTC 19 October 2004 for (a) vertically averaged horizontal EKEFC [color shading (units: MW m^{-2}), refer to legend for values], horizontal EKE flux vectors [arrows (units: MW m^{-1}), refer to reference vector], and 500 hPa heights [contours, 60 m intervals]; and (b) vertically averaged EKE generation term [color shading (units: MW m^{-2}), refer to legend for values], AGF vectors [arrows (units: MW m^{-2}), refer to reference vector], and 500 hPa heights [contours, 60 m intervals].

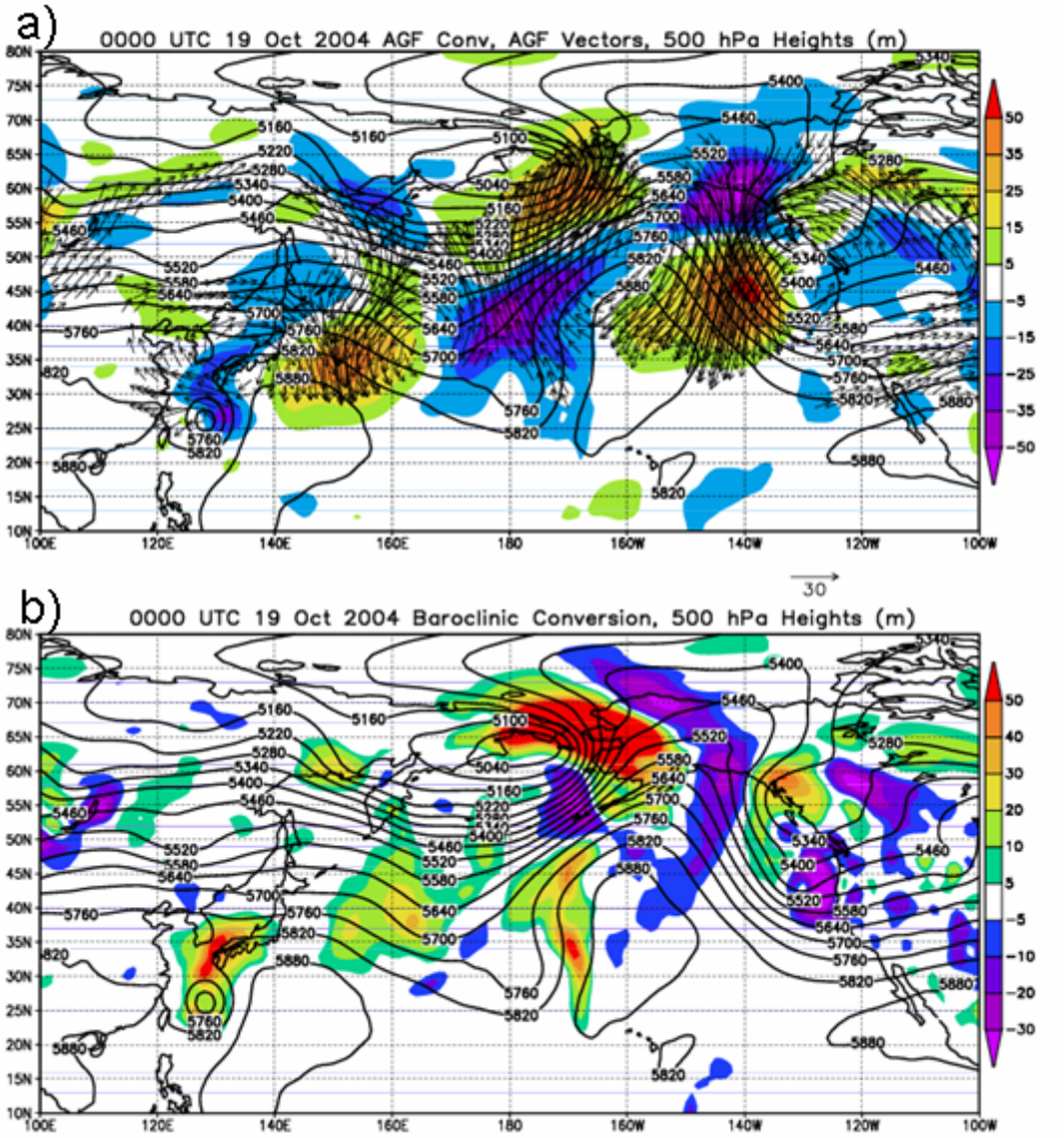

Figure 12. Distribution of vertically averaged EKE term components at 0000 UTC 19 October 2004 for (a) vertically averaged AGFC [color shading (units: MW m^{-2}), refer to legend for values], AGF vectors [arrows (units: MW m^{-2}), refer to reference vector], and 500 hPa heights [contours, 60 m intervals]; and (b) vertically averaged BC [color shading (units: MW m^{-2}), refer to legend for values] and 500 hPa heights [contours, 60 m intervals].

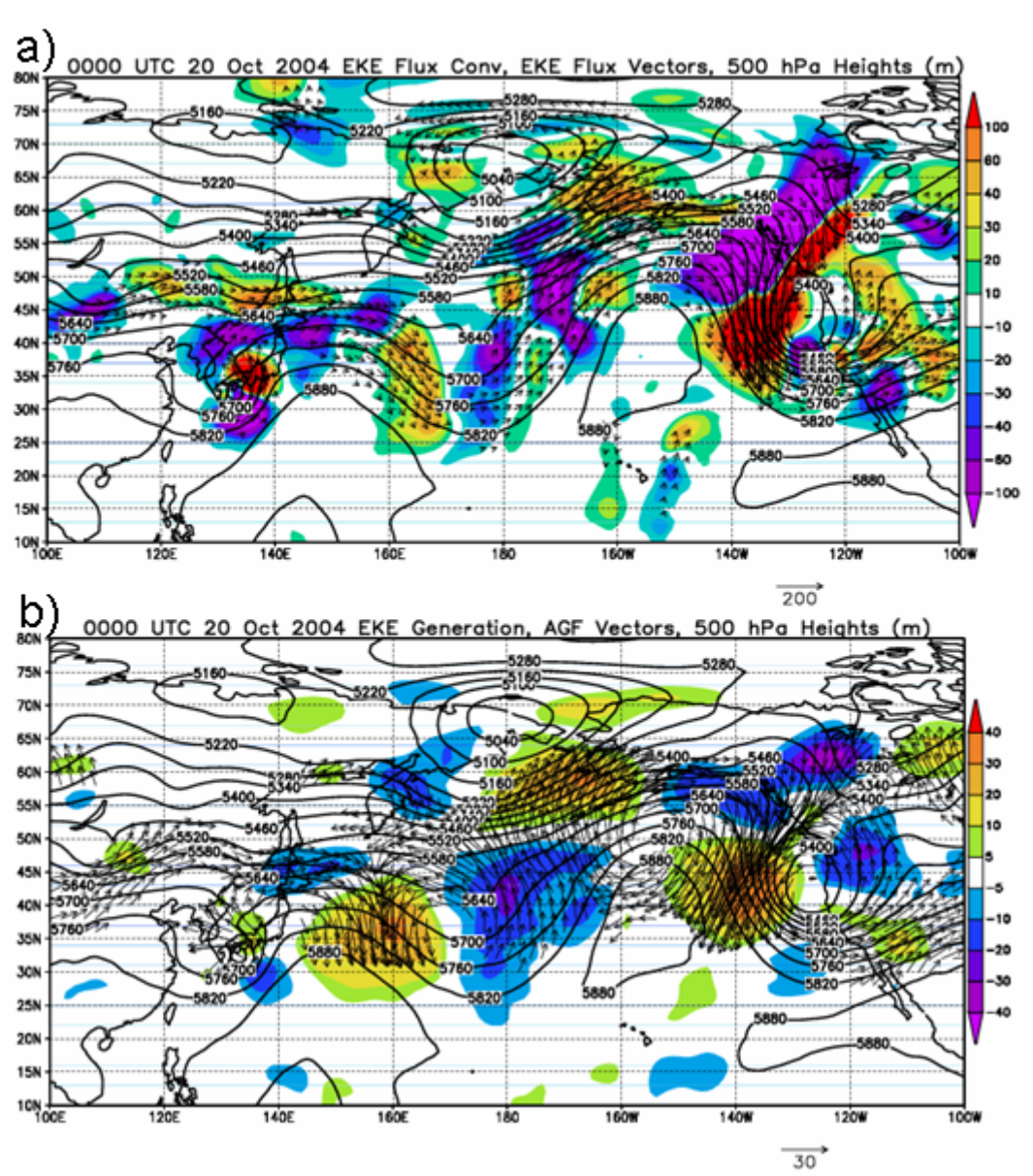

Figure 13. As in Fig. 11, except for 0000 UTC 20 October.

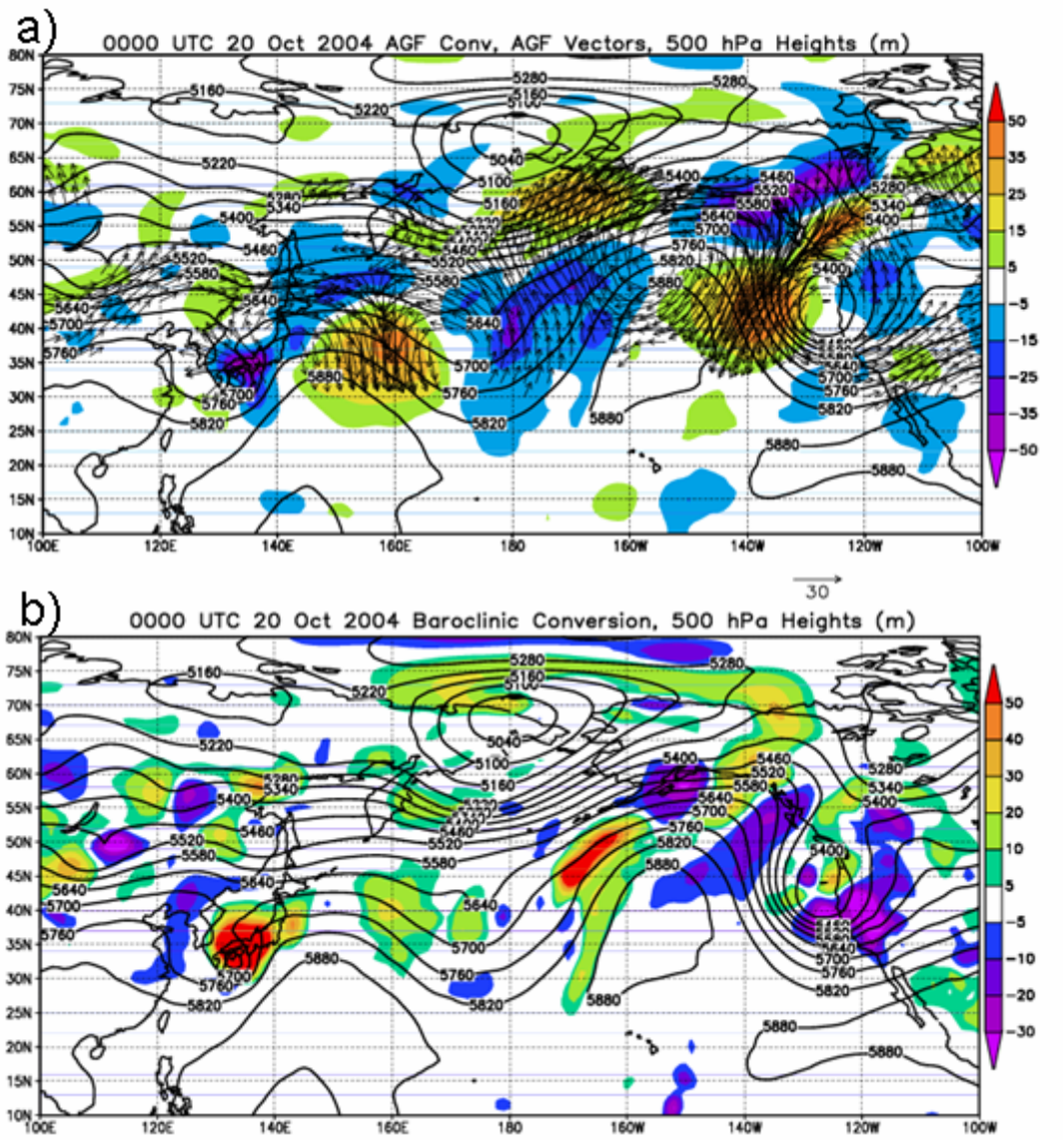

Figure 14. As in Fig. 12, except for 0000 UTC 20 October.

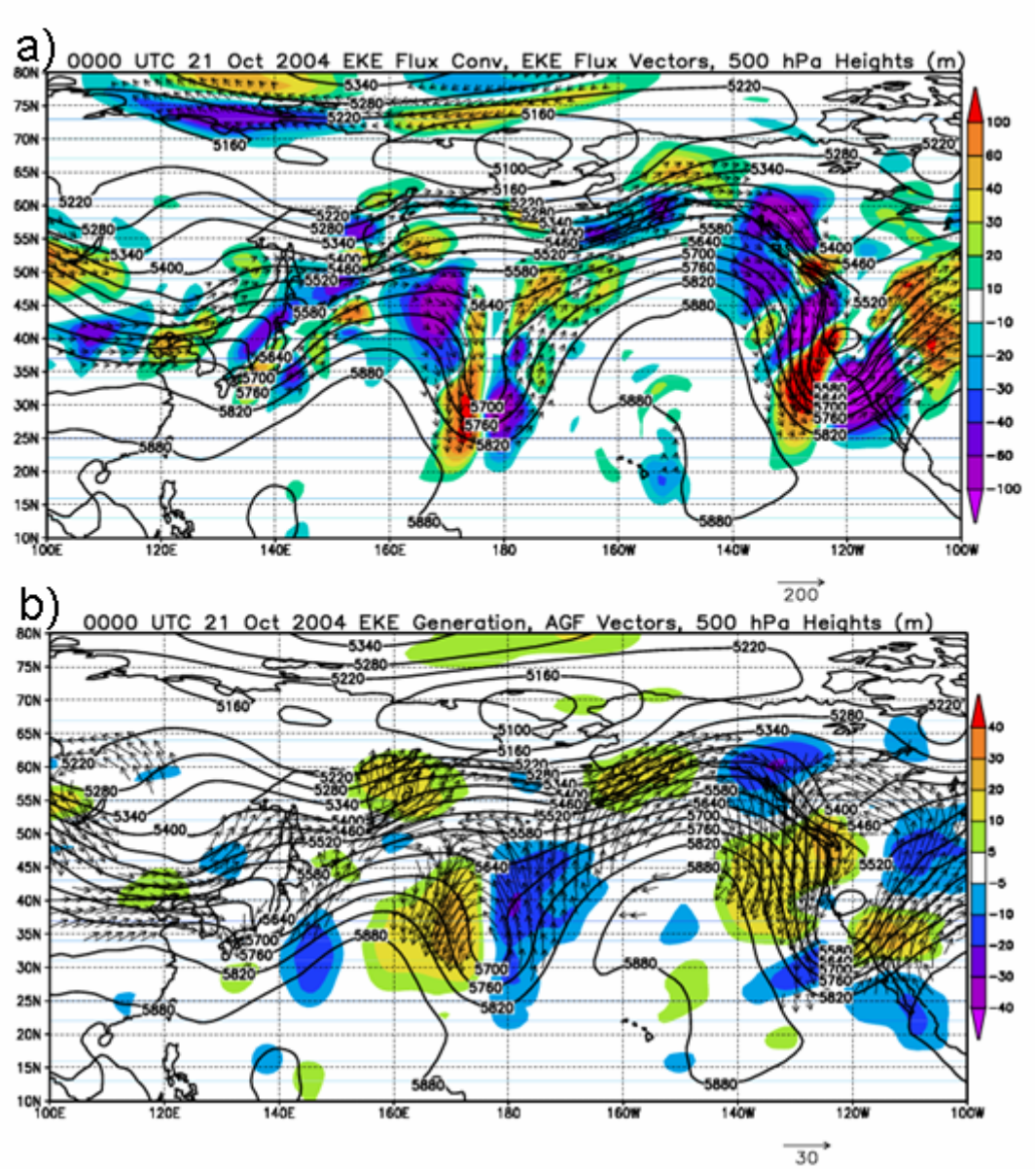

Figure 15. As in Fig. 11, except for 0000 UTC 21 October.

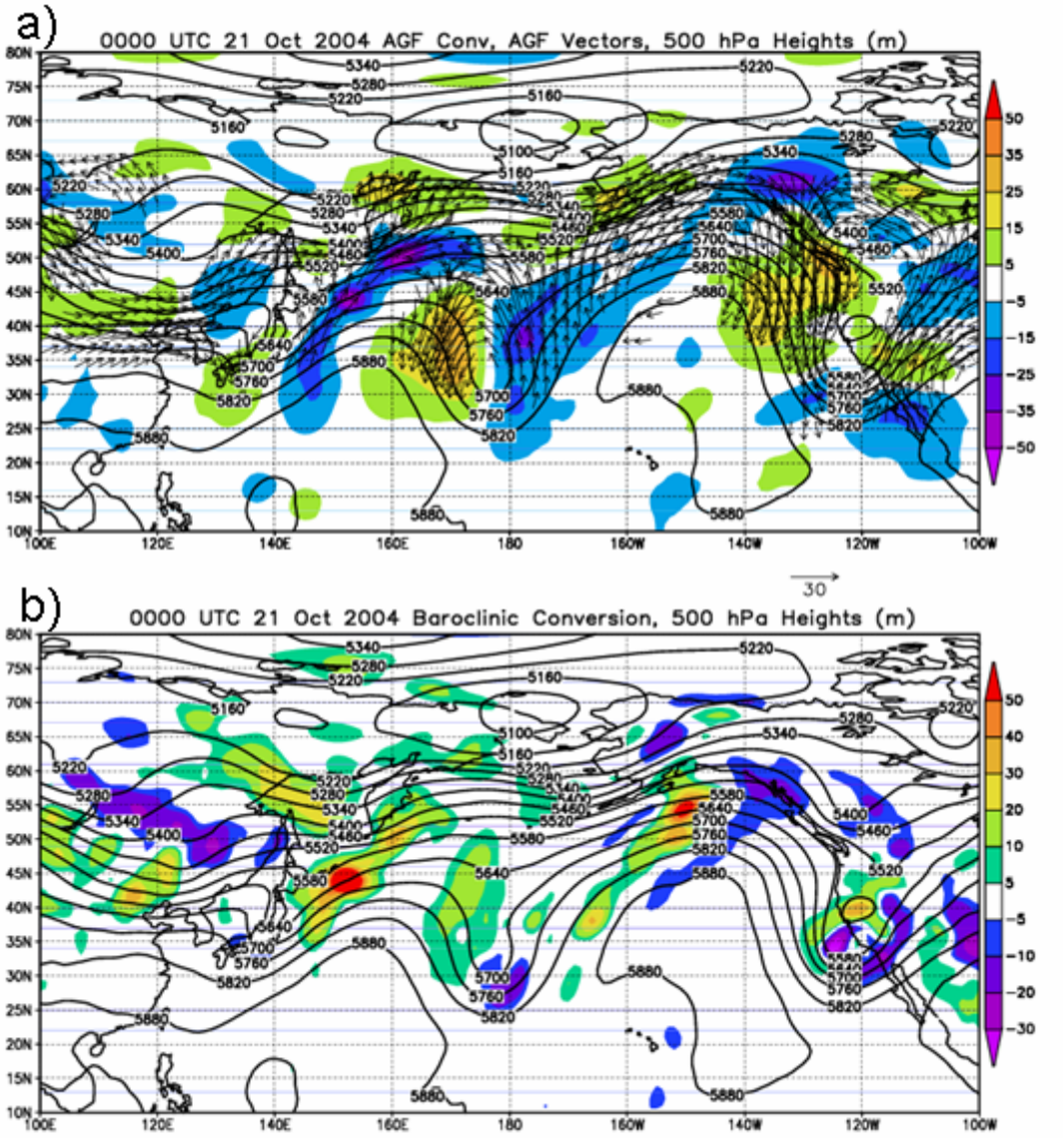

Figure 16. As in Fig. 12, except for 0000 UTC 21 October.

3. Summary

Just prior to the ET of Tokage, the distribution of EKE across the North Pacific weakened. The movement of TY Tokage into the midlatitudes contributed to an increase in EKE over the western North Pacific and the development of a deep trough downstream. Baroclinic processes due to the circulation of Tokage contributed to EKE generation, which was dispersed to the midlatitudes via ageostrophic fluxes. This energy was then transported downstream into a developing trough over the western North Pacific. However, this trough extended

rapidly equatorward, which resulted in it being cut off from further energy transport as the Tokage remnants moved poleward to merge with a separate shortwave trough over the Sea of Okhotsk.

B. TY BANYAN

Banyan, with a maximum 10-minute sustained wind speed of 55 knots (28.3 m s^{-1}), represented a case involving an international class 4 TC (Table 1) (from Digital Typhoon (2007): http://agora.ex.nii.ac.jp/digital-typhoon/summary/wnp/s/200507.html.en). This mid-summer case completed ET 0000 UTC 28 July 2005 in a relatively weak midlatitude flow.

1. Synoptic Evolution

At 0000 UTC 25 July 2005, Typhoon Banyan was at 26.8° N, 137.0° E (Fig. 17a). A weak 500 hPa midlatitude trough was over eastern China and a weak subtropical ridge was directly east of Banyan. A weak 500 hPa low was also directly northeast of Banyan (Fig. 17a). The subtropical ridge and a small upper-level low east of Japan were clearly defined on the dynamical tropopause (Fig. 17b).

Banyan then moved north-northeastward to 32.3° N, 137.6° E by 0000 UTC 26 July 2005 (Fig. 18a). The weak midlatitude trough upstream of Banyan the previous day had extended southeastward and encompassed Banyan. The weak subtropical 500 hPa ridge began to amplify northward directly east of Banyan (Fig. 18a). The 500 hPa low immediately downstream of the subtropical ridge east of Banyan moved southeastward and merged with another weak 500 hPa low. On the dynamic tropopause, the amplification of the ridge immediately downstream of Banyan was clearly identifiable by the northward extension of the elevated tropopause over Japan (Fig. 18b).

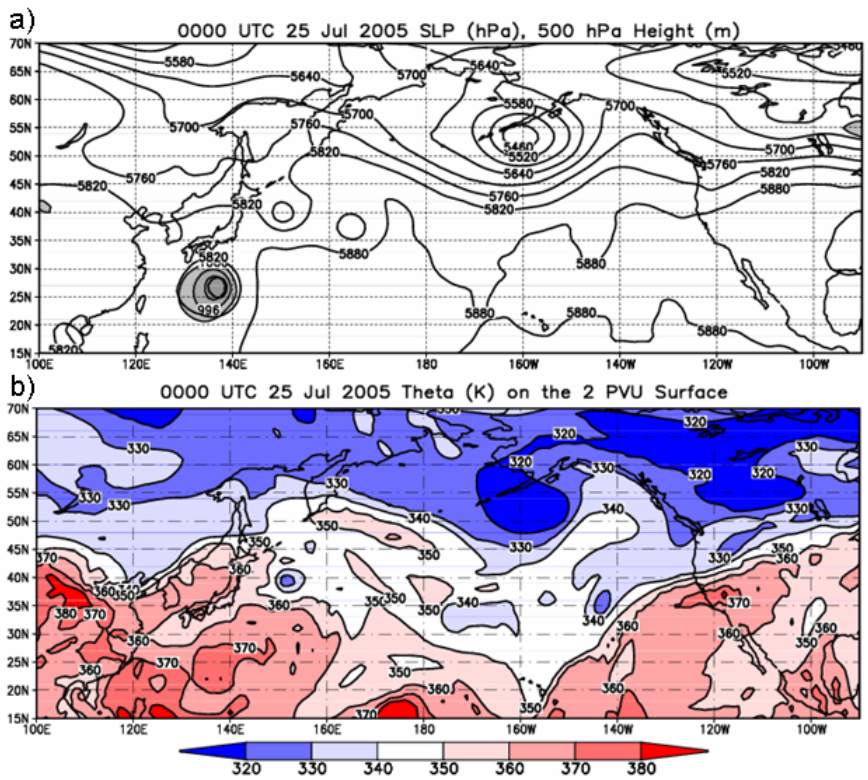

Figure 17. As in Fig. 5, except for 0000 UTC 25 July 2005.

By 0000 UTC 27 July 2005 (Fig. 19a), Banyan had moved northeast to 39.0° N, 144.8° E. At 500 hPa, the subtropical ridge downstream of Banyan had amplified slightly, while the closed low downstream had continued to move southeastward (Fig. 19a). Banyan also remained embedded in a weak trough. Strong ridge amplification on the dynamic tropopause occurred downstream of Banyan during this time period (Fig. 19b).

Banyan then moved rapidly northeastward to 46.2° N, 149.9° E on 0000 UTC 28 July 2005 (Fig. 20a). The 500 hPa subtropical ridge east of Banyan was pushed southward by the small closed low that continued to move southeastward and fill (Fig. 20a). A 500 hPa closed low was analyzed above Banyan. The ridge on the dynamic tropopause east of Banyan significantly amplified and continued to move downstream (Fig. 20b).

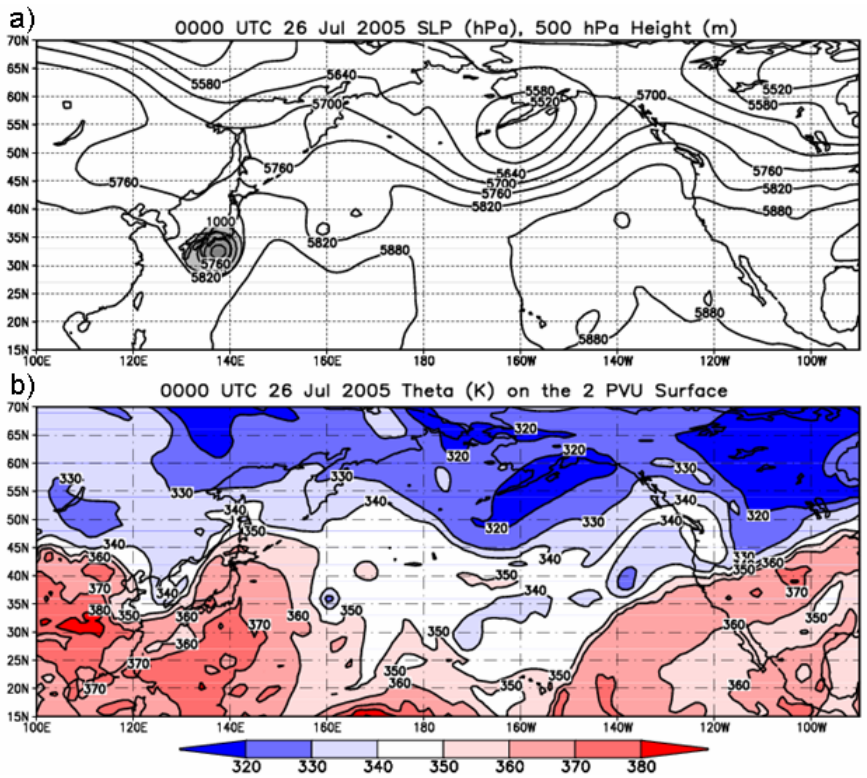

Figure 18. As in Fig. 5, except for 0000 UTC 26 July 2005.

By 0000 UTC 29 July 2005 (Fig. 21a), the extratropical cyclone that had developed from the remnants of Banyan had moved east-northeast to 49.1° N, 156.3° E. A 500 hPa low moved with the surface low to the northeast, and the midlatitude ridge downstream intensified (Fig. 21a). The ridge on the dynamic tropopause continued to surge northeastward downstream of Banyan as it had done over the previous 72 h (Fig. 21b).

The ridge on the dynamic tropopause downstream of Banyan amplified greatly as Banyan underwent ET, which is displayed clearly by the elevated tropopause (represented by the 370 K closed contour) east of Banyan. At 0000 UTC 27 July 2005, the 370 K closed contour was east of Japan (Fig. 19b). Over successive 24-h periods, the 370 K closed center was south of the Kamchatka Peninsula (Fig. 20b), and then east of the Kamchatka Peninsula (Fig. 21b). Therefore, the movement of Banyan into the midlatitudes was associated with a strong amplification of a ridge immediately downstream of the decaying tropical

cyclone. Downstream of the ridge circulation directly linked to Banyan, the primary North Pacific low pressure center moved eastward throughout the period. As this low moved into the Gulf of Alaska, a slight southward amplification occurred as defined by the 330K contour on the dynamic tropopause (Fig. 21b). The role of the ET of Banyan on the downstream evolution is examined with the EKE distribution.

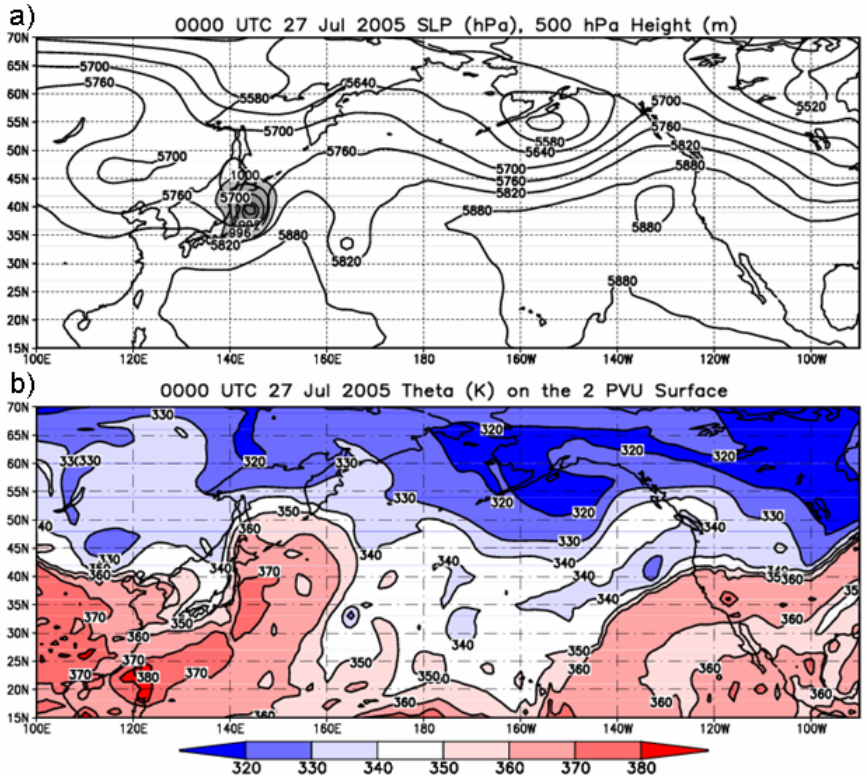

Figure 19. As in Fig. 5, except for 0000 UTC 27 July 2005.

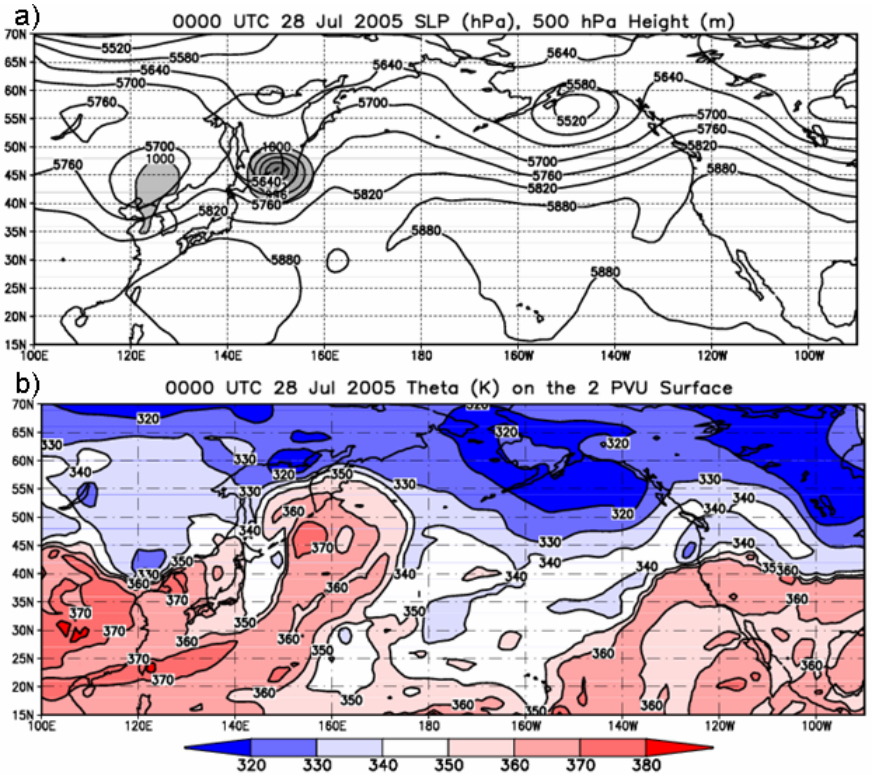

Figure 20. As in Fig. 5, except for 0000 UTC 28 July 2005

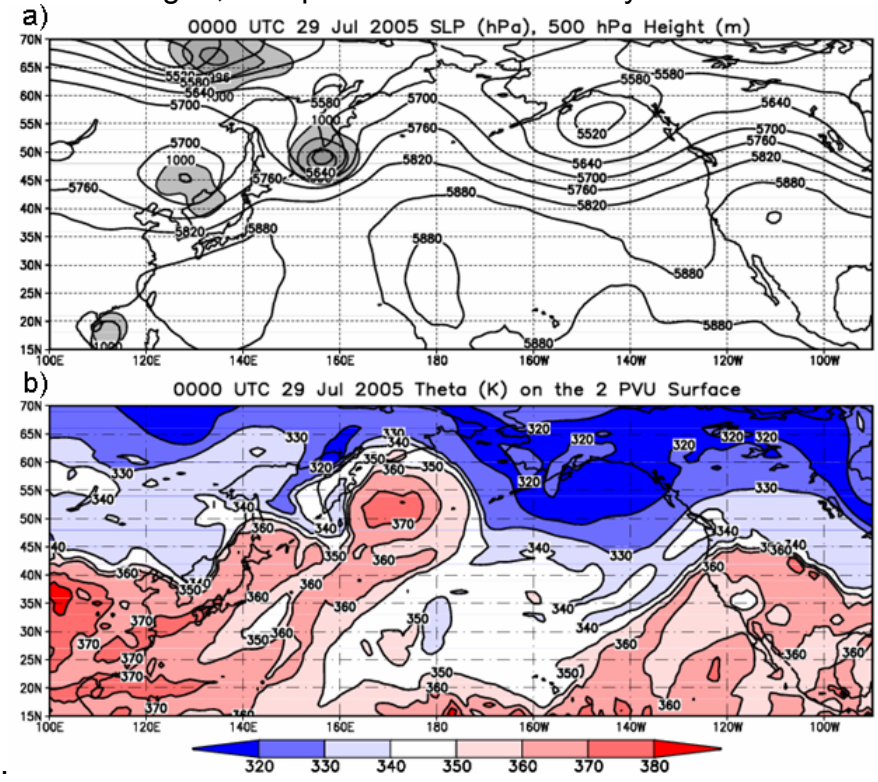

Figure 21. As in Fig. 5, except for 0000 UTC 29 July 2005.

2. EKE Budget

a. Vertically Averaged EKE and Total EKE Flux Vectors

Northerly EKE fluxes into weak midlatitude flow extended from the poleward side of Banyan by 0000 UTC 26 July 2005 (Fig. 22a). A small EKE center near 35°N, 160° E was associated with the mid-level low east of Banyan. Eddy kinetic energy transfer increased from Banyan into the EKE center near 35° N, 160° E by 0000 UTC 27 July 2005 (Fig. 22b). Eddy kinetic energy fluxes continued to stream out of Banyan's EKE center in an anticyclonic arc on 1200 UTC 27 July 2005 (Fig. 22c). However, at that time the majority of the EKE flux was directed into the shortwave trough north of Banyan.

Over the next 24 h, the remnants of Banyan reintensified and interacted with the trough to the north as an extratropical cyclone (Fig. 22d). The distribution of EKE increased substantially at that time. As the EKE center intensified, it continued to be a source for the anticyclonic arc of EKE fluxes toward the small midlatitude low (Fig. 22d).

By 0000 UTC 29 July 2005 (Fig. 22e), two EKE centers on the upstream and downstream sides of the mid-tropospheric trough were associated with remnants of Banyan (Fig. 22e). The anticyclonic arc of EKE fluxes originating from the downstream EKE center of Banyan's remnants were still observed (Fig. 22e), but EKE transfer along the extremity of this arc had diminished. A new EKE center intensified in the Bering Sea in association with downstream development due to the re-intensification of the remnants of Banyan (Fig. 22e).

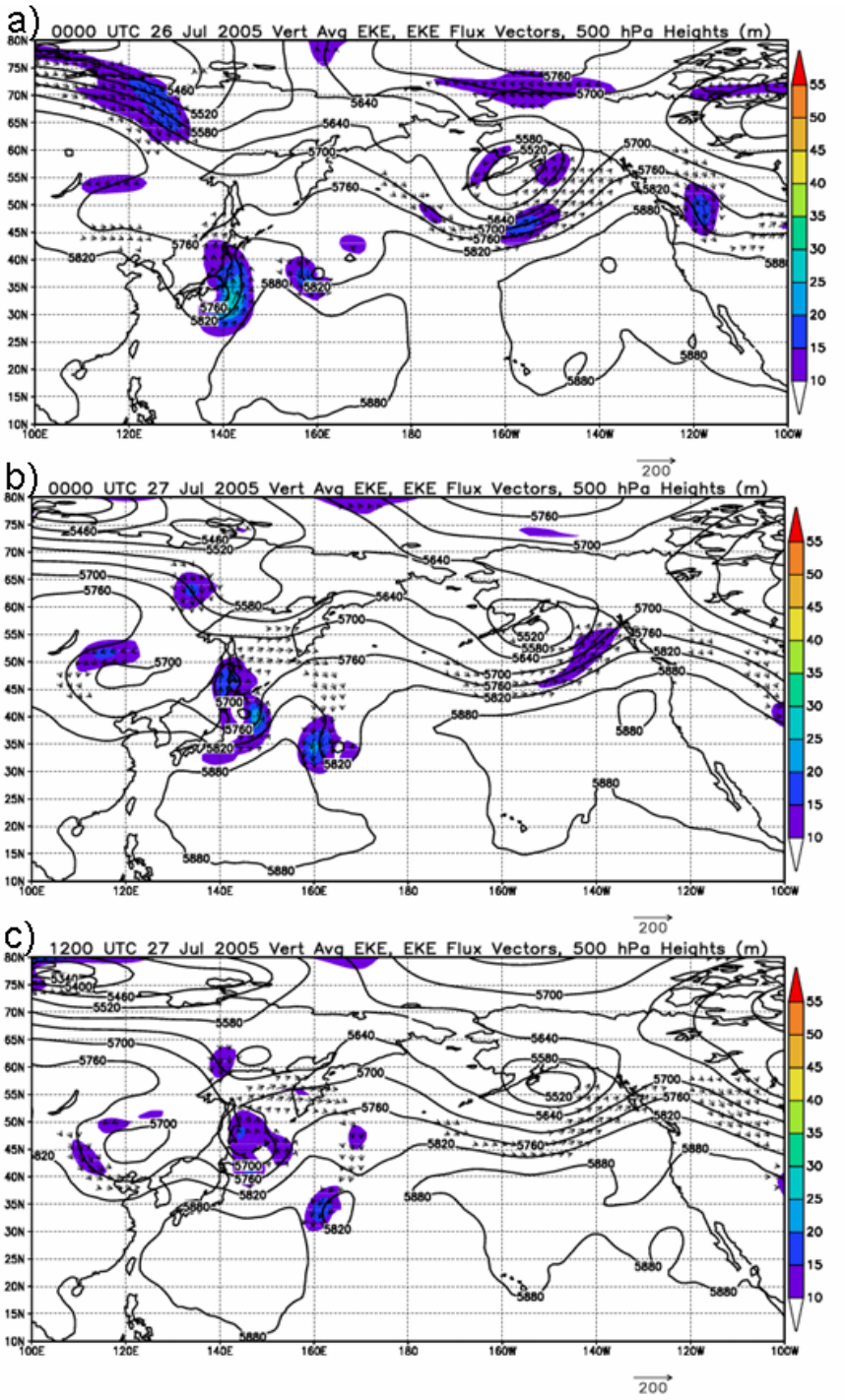

Figure 22. As in Fig.10, except that the time period 0000 UTC 26 July 2005 through 0000 UTC 29 July 2005 is represented in panels (a) through (e).

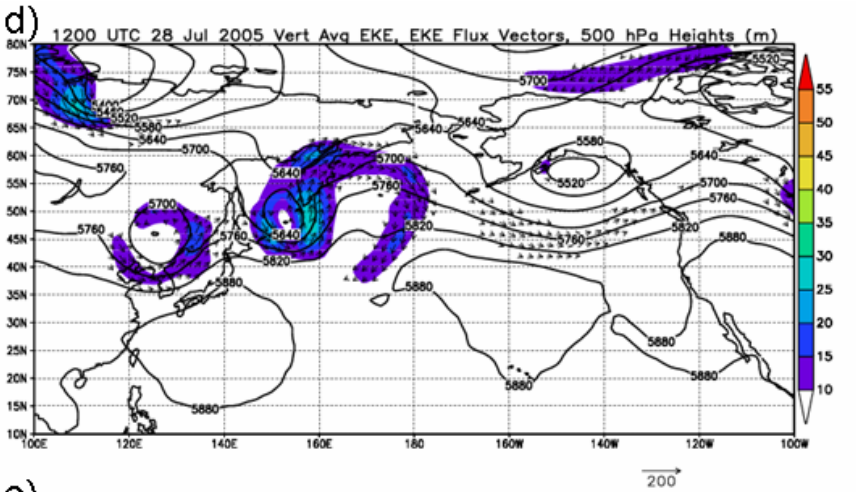

(Figure 22, continued)

The midlatitude circulation into which Banyan moved was weak. However, fluxes of EKE associated with Banyan contributed to a small cyclonic circulation near 35° N, 165° E, and then to a shortwave trough that would eventually strengthen during re-intensification of Banyan as an extratropical cyclone. Therefore, the re-intensification occurred in an environment in which EKE was not readily available from the midlatitude circulation. In the following section, the flux convergence of EKE and contributions to EKE generation are investigated for key periods associated with Banyan moving into the midlatitudes.

b. Components of Total EKE

At 0000 UTC 26 July 2005, Banyan was off the coast of southern Japan and an increase in EKE was occurring north of Banyan due to EKEFC (Fig. 23a). However, the generation terms associated with Banyan were negative (Fig. 23b). Although BC processes were generating EKE around Banyan (Fig. 24b), AGFs were also acting to disperse this EKE poleward (Fig. 24a). Twenty-four hours later, similar patterns of EKEFC (Fig. 25a) were evident and a net EKE loss was still occurring over Banyan (Fig. 25b) as AGFs continued to disperse (Fig. 26a) the increasing amounts of EKE generated through BC (Fig. 26b). Eddy kinetic energy flux vectors were connected to the downstream energy center near 35° N, 160° E at this time (Fig. 25a).

By 1200 UTC 28 July 2005 (Fig. 27a), the couplet of EKEFC clearly defined the translation of energy from Banyan to the shortwave to the north. Eddy kinetic eddy generation through BC (Fig. 28b) at this point was contributing to regions around the re-intensifying remnants of Banyan (Fig. 27b), and then energy was being dispersed by AGFC (Fig. 28a) into the trough that will contribute to the re-intensification of Banyan.

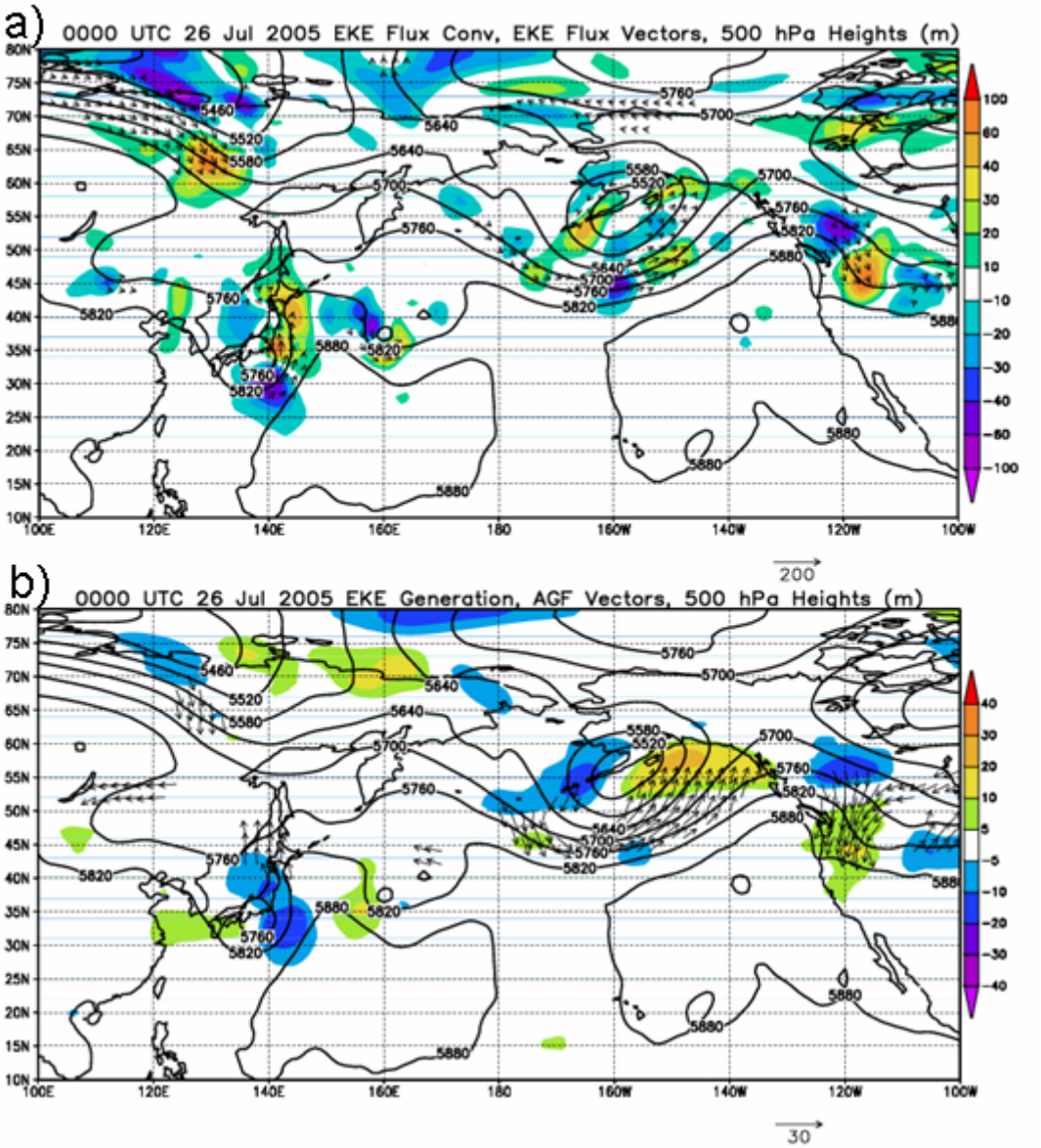

Figure 23. As in Fig. 11, except for 0000 UTC 26 July 2005.

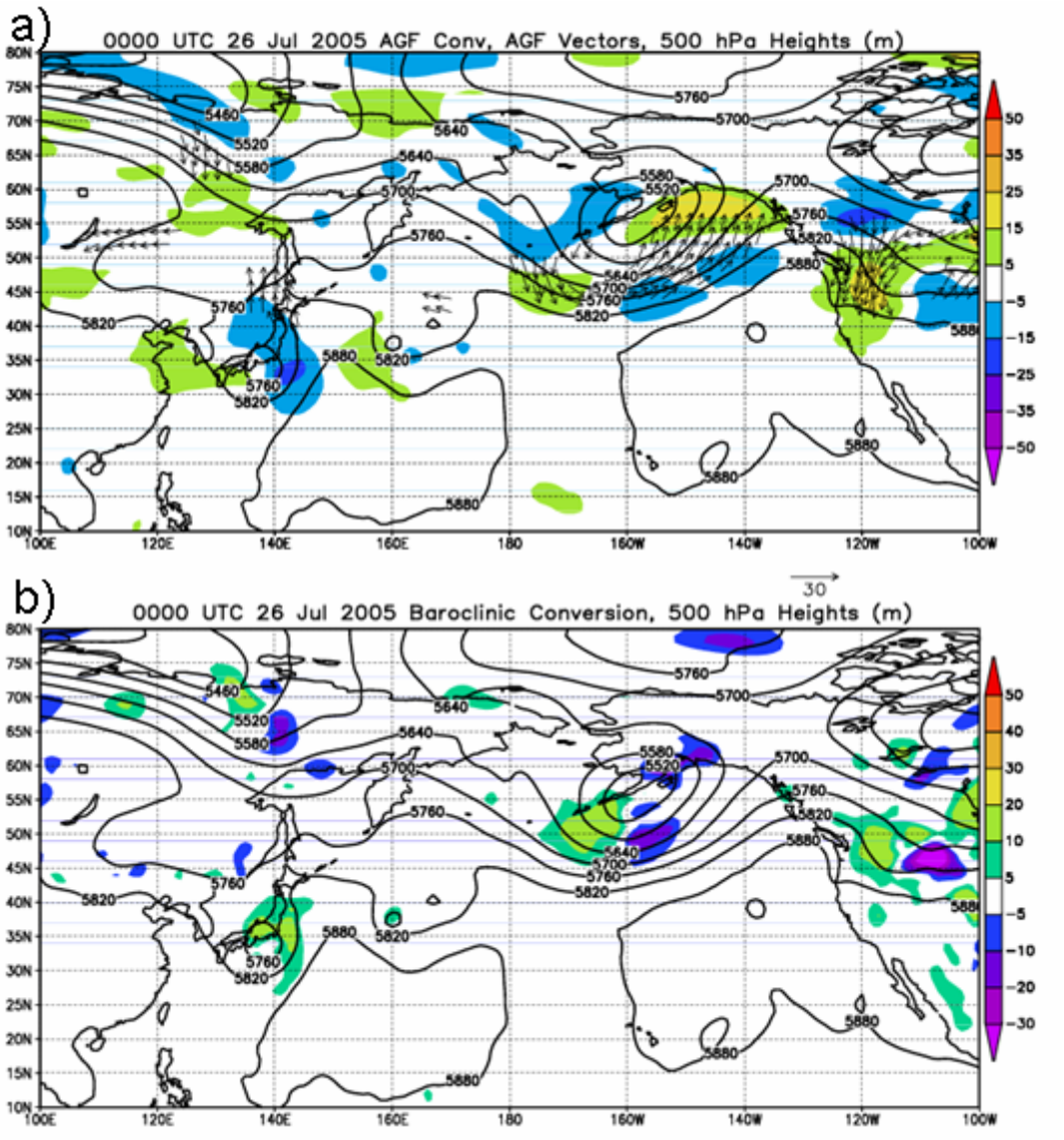

Figure 24. As in Fig. 12, except for 0000 UTC 26 July 2005.

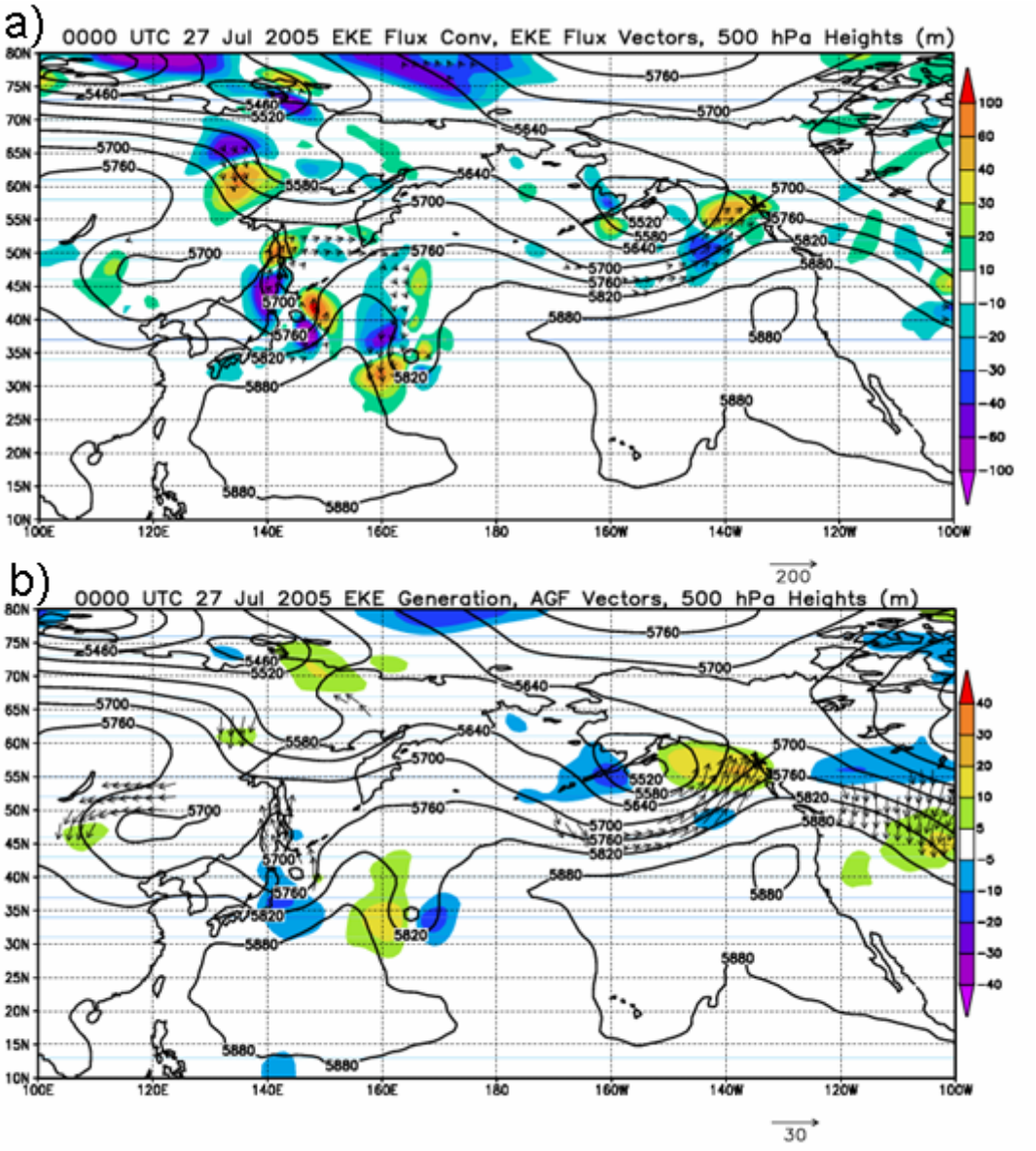

Figure 25. As in Fig. 11, except for 0000 UTC 27 July 2005.

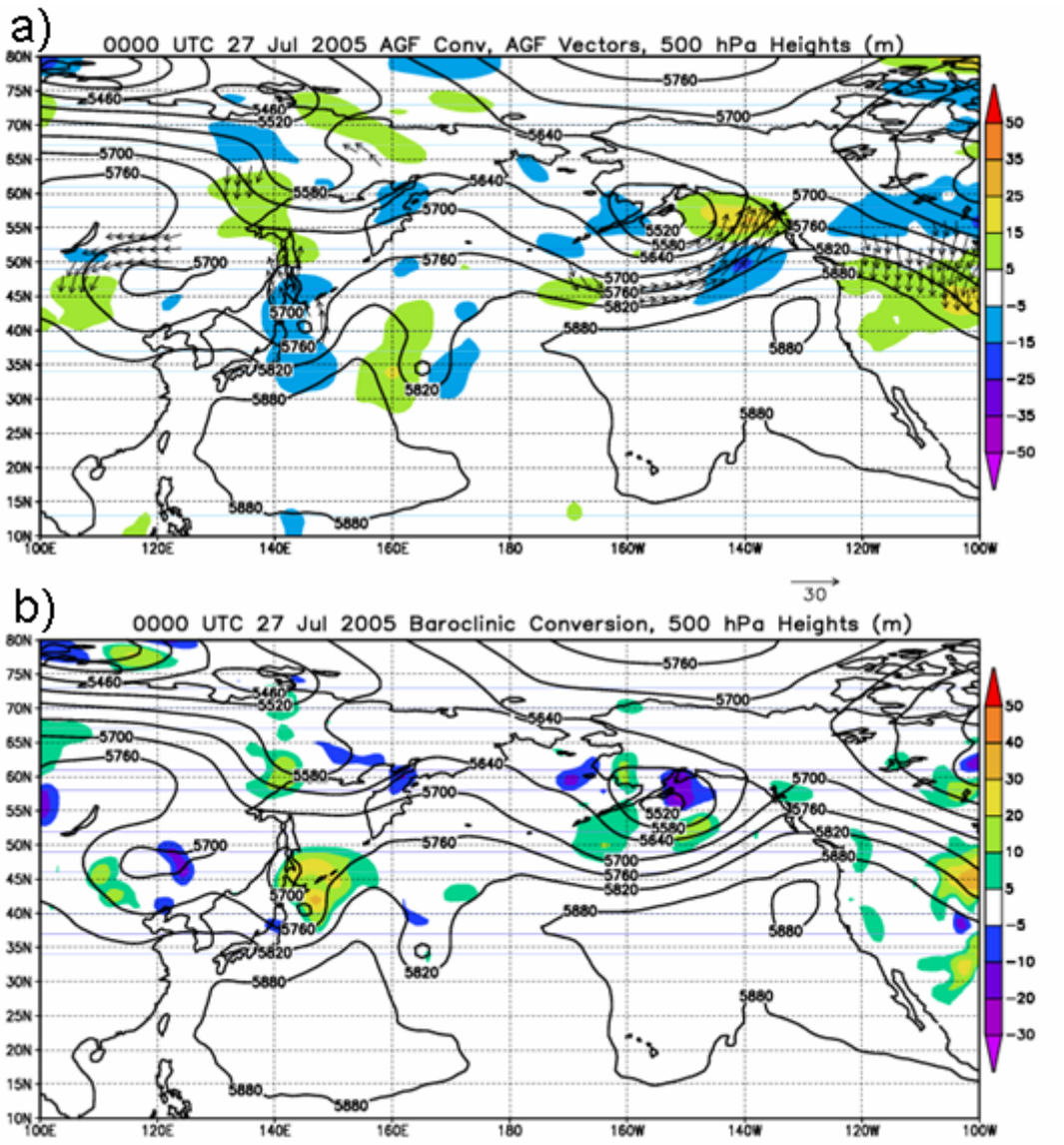

Figure 26. As in Fig. 12, except for 0000 UTC 27 July 2005.

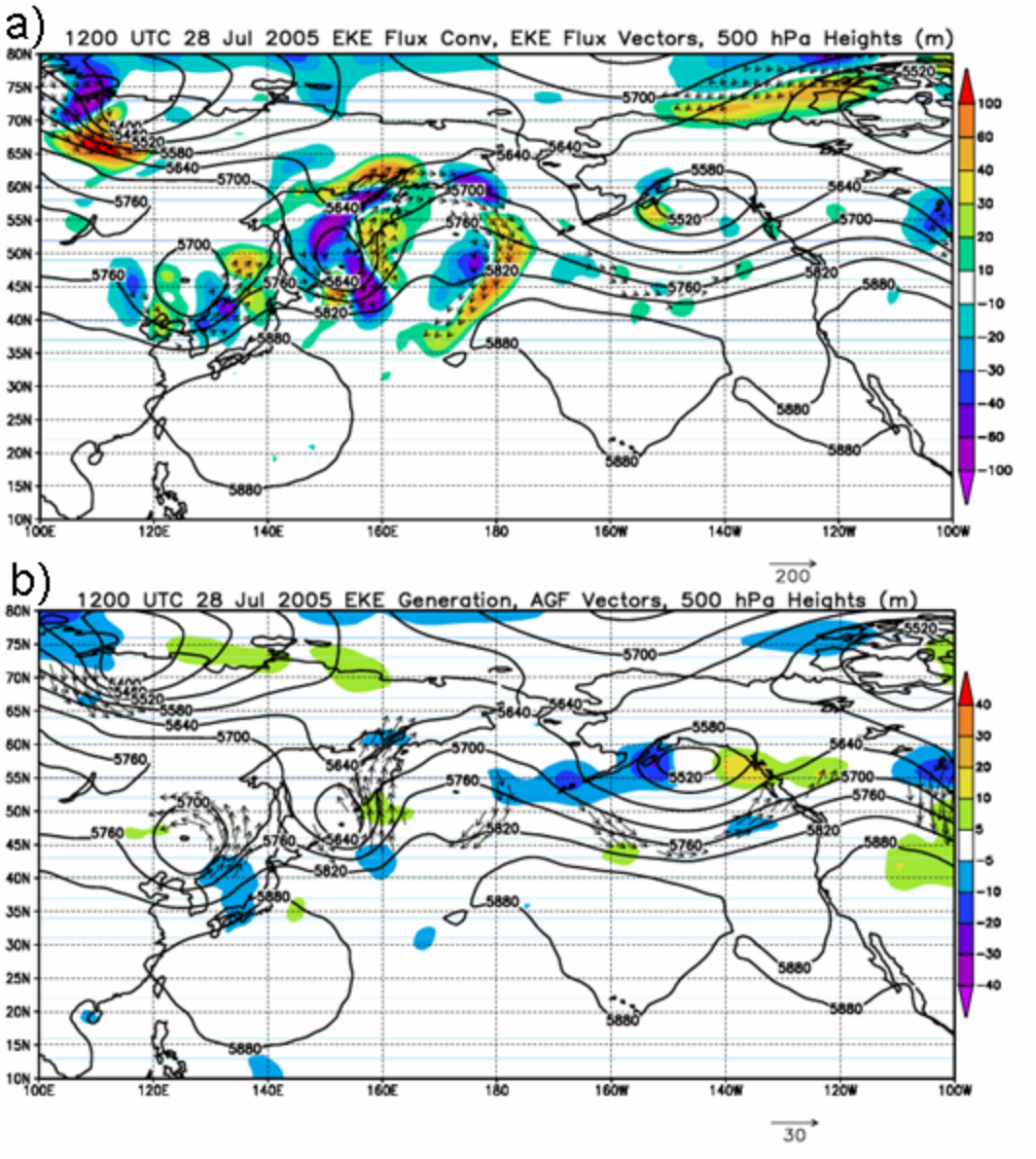

Figure 27. As in Fig. 11, except for 1200 UTC 28 July 2005.

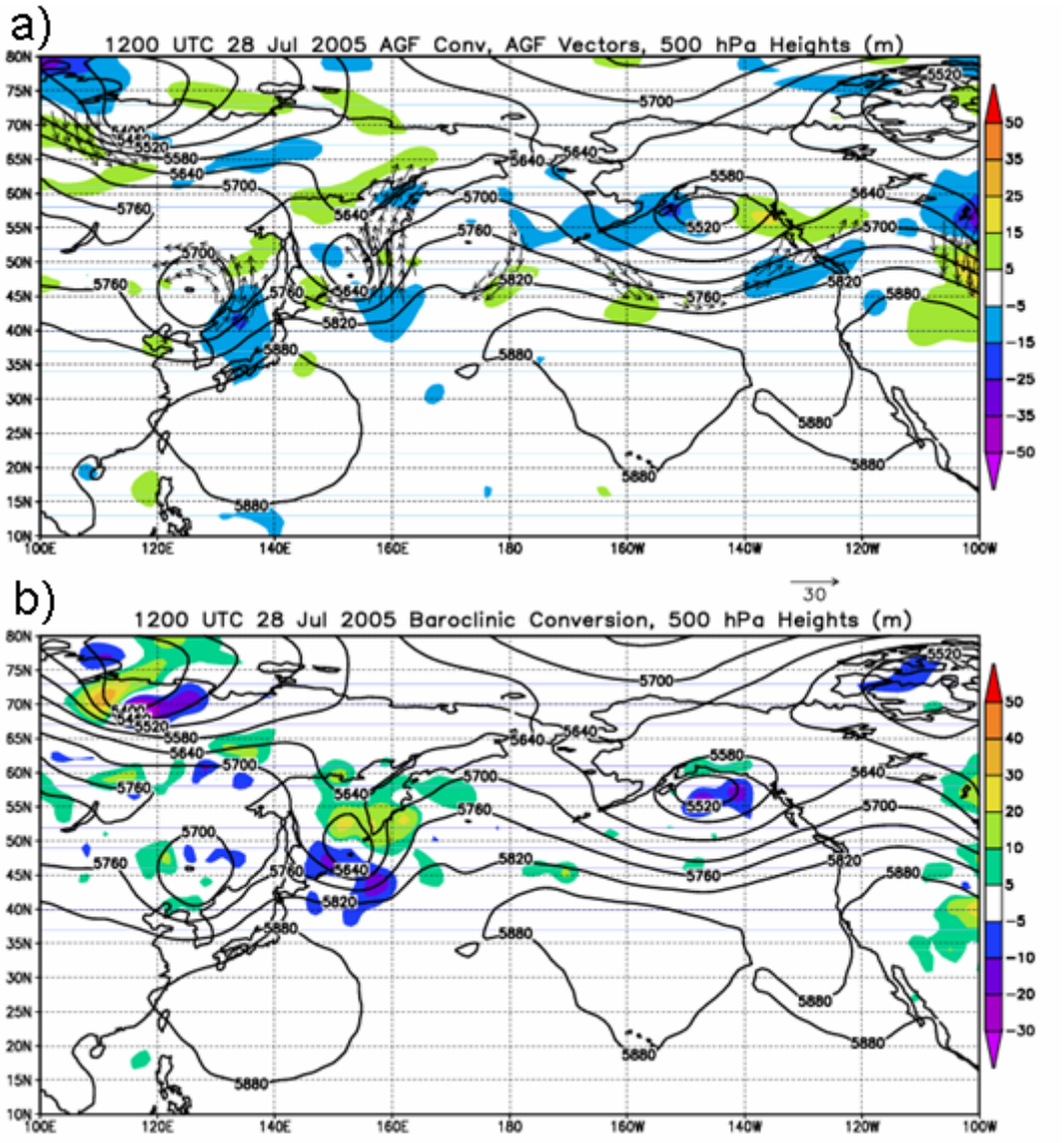

Figure 28. As in Fig. 12, except for 1200 UTC 28 July 2005.

3. Summary

This mid-summer case contained only weak midlatitude influences on the midlatitude circulation over the North Pacific. Energy was transferred from Banyan downstream through EKEFC and AGFs. The downstream flux of energy into the shortwave trough contributed to the re-intensification of Banyan as an extratropical cyclone. Consistent with the observation of the stronger EKEFC

couplet over the Bering Sea at 1200 UTC 28 July 2005 (Fig. 27a), a new EKE center was present 12 h later centered near 50° N, 170° W (Fig. 22e).

Following the re-intensification of ex-Banyan, energy was directed downstream toward the eastern North Pacific in association with a developing shortwave.

C. TY GUCHOL

Guchol, with a maximum 10-minute sustained wind speed of 55 knots (28.3 m s^{-1}), 105 h lifespan, and 30.0 km/h (8.3 m s^{-1}) average forward speed represented a case involving an international class 4 TC (Table 1) (from Digital Typhoon (2007): http://agora.ex.nii.ac.jp/digital-typhoon/summary/wnp/s/200512.html.en). Guchol was a late-summer TC that completed ET at 1200 UTC 25 August 2005 (Table 2) in a moderately strong midlatitude flow immediately downstream of an approaching midlatitude trough.

1. Synoptic Evolution

At 1200 UTC 22 August 2005, Typhoon Guchol was at 29.1° N, 146.3° E (Fig. 29a). As depicted in the NCEP GFS FNL analysis, a strong 500 hPa subtropical ridge was over Guchol (Fig. 29a). A midlatitude cyclone was near the Aleutian Islands north of the strong subtropical ridge, and a weak midlatitude trough between Korea and Japan extended northward along the eastern coast of Asia (Fig. 29a). A cut-off 500-hPa low was located east of the subtropical ridge in the eastern North Pacific. Upper-tropospheric ridges and troughs on the dynamic tropopause were consistent with the positions of these 500 hPa features (Fig. 29b). A large gradient of potential temperature was associated with the trough approaching Guchol from the northwest.

During the next 24 h, Guchol recurved and moved to 33.6° N, 148.3° E (Fig. 30a). The 500-hPa trough formerly over the Japan Sea had moved to the east coast of Japan and was now northwest of Guchol. The large southwest-northeast oriented 500-hPa ridge across the North Pacific became separated into two parts by the deepening midlatitude cyclone north of the Aleutians and the

eastern North Pacific cut-off low that drifted northwest (Fig. 30a). Key developments in the upper troposphere (Fig. 30b) are the circulation pattern over the western North Pacific increased in amplitude and the sharp gradient in potential temperature approached Guchol.

By 1200 UTC 24 August 2005, Guchol had moved northeast to 37.9° N, 155.2° E (Fig. 31a). The 500-hPa trough upstream of Guchol and the ridge downstream of Guchol maintained their position relative to Guchol as all three moved downstream. A 500-hPa trough moved out of the Bering Sea and into the Gulf of Alaska, amplified, and began linking with the pre-existing cut-off circulation near 40°N, 150°W (Fig. 31a). The upper-level ridges and troughs on the dynamic tropopause also indicated this evolution, except for the Gulf of Alaska trough linkage with the cut-off low in the eastern North Pac (Fig. 31b) and that the upper-tropospheric trough is closer to Guchol than the 500-hPa trough.

Guchol then moved northeast to 45.6° N, 164.7° E by 1200 UTC 25 August 2005 (Fig. 32a). The circulation of Guchol became absorbed in the 500-hPa trough over the western North Pacific, while a new trough developed in the Bering Sea, which led to a more zonal subtropical ridge downstream of Guchol. The upper-tropospheric trough immediately upstream of Guchol had the appearance of a cyclonically sheared extratropical cyclone (Fig. 32b), and the cut-off low in the eastern North Pacific became linked to the trough on the dynamic tropopause.

By 1200 UTC 26 August 2005 (Fig. 33a), the ex-Guchol cyclone had slowly moved north-northeastward to 48.2° N, 166.0° E. The 500-hPa closed circulation was over the surface low center (Fig. 33a), and the subtropical ridge downstream of Guchol increased in amplitude. Downstream of the ridge, a trough that was previously in the Bering Sea had moved over the Gulf of Alaska. The eastern North Pacific cut-off low downstream of this ridge had drifted farther southeast and became isolated from the midlatitude flow (Fig. 33a). The ridge over the central North Pacific on the dynamic tropopause increased in amplitude,

while a trough amplified and moved into the Gulf of Alaska (Fig. 33b). At this level, the cut-off low over the eastern North Pacific remained linked to the midlatitudes.

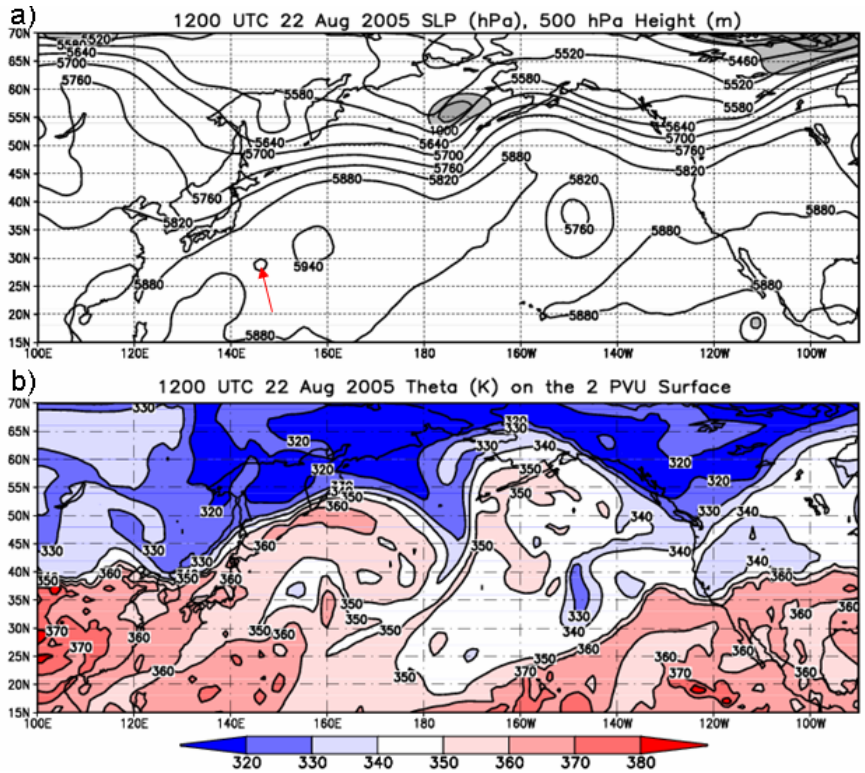

Figure 29. As in Fig. 5, except for 1200 UTC 22 August 2005. Red arrow in a) denotes the position of Guchol.

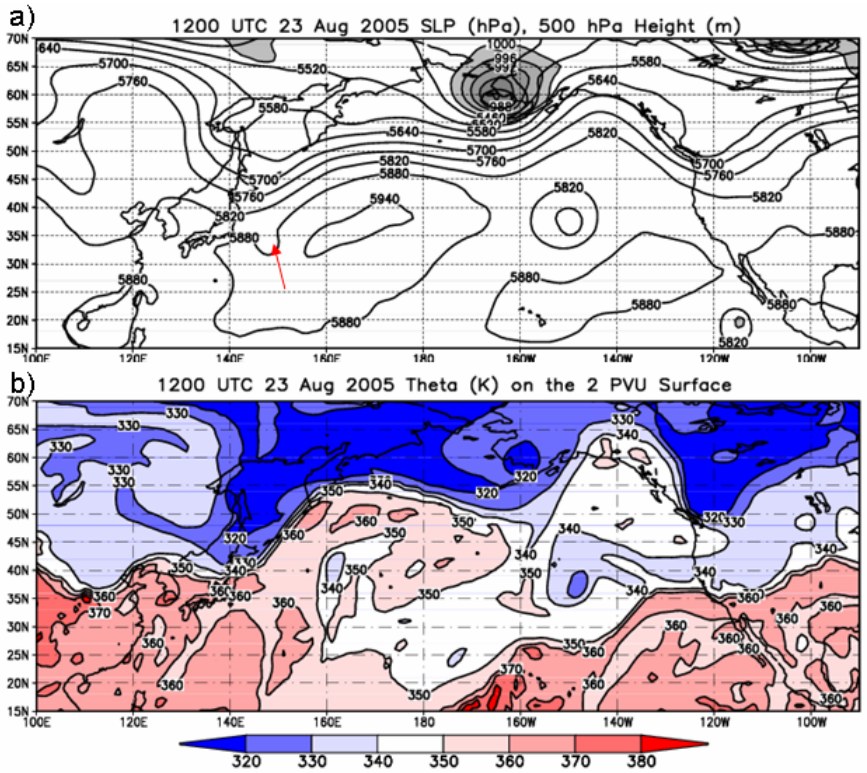

Figure 30. As in Fig. 29, except for 1200 UTC 23 August 2005.

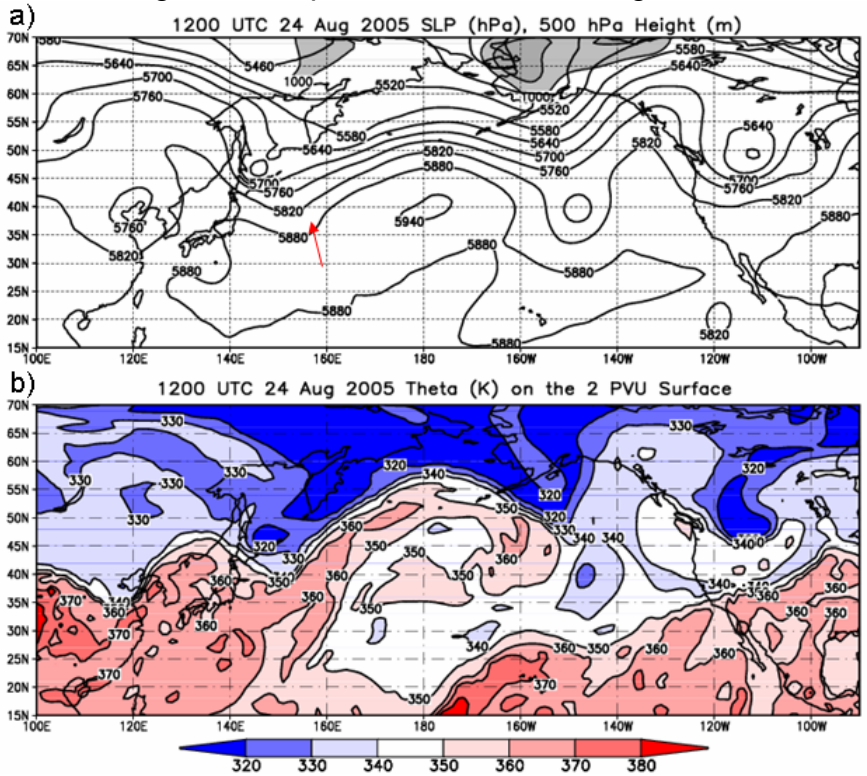

Figure 31. As in Fig. 29, except for 1200 UTC 24 August 2005.

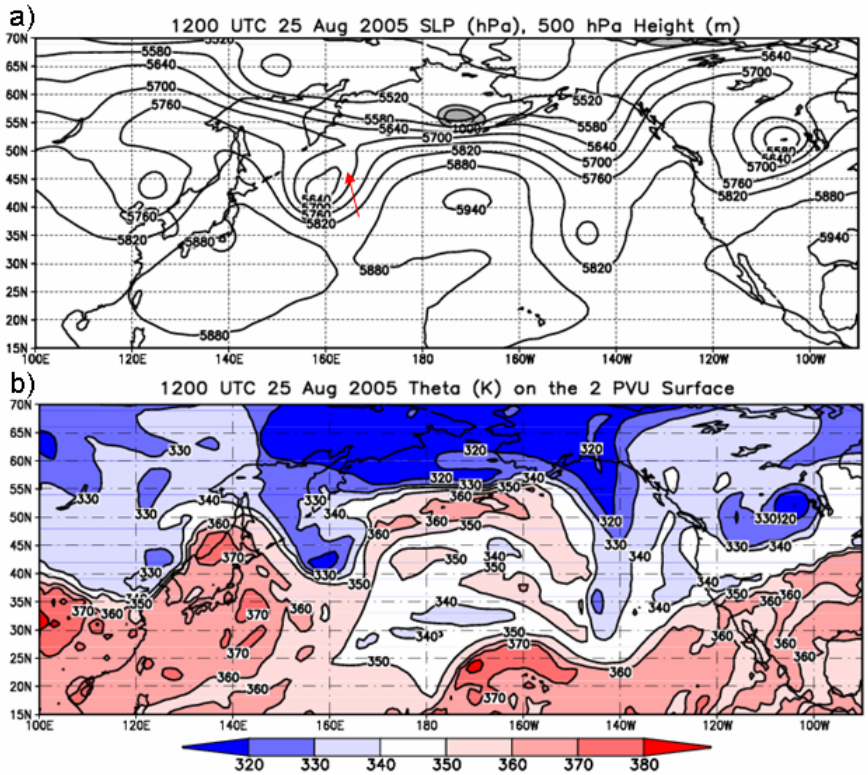

Figure 32. As in Fig. 29, except for 1200 UTC 25 August 2005.

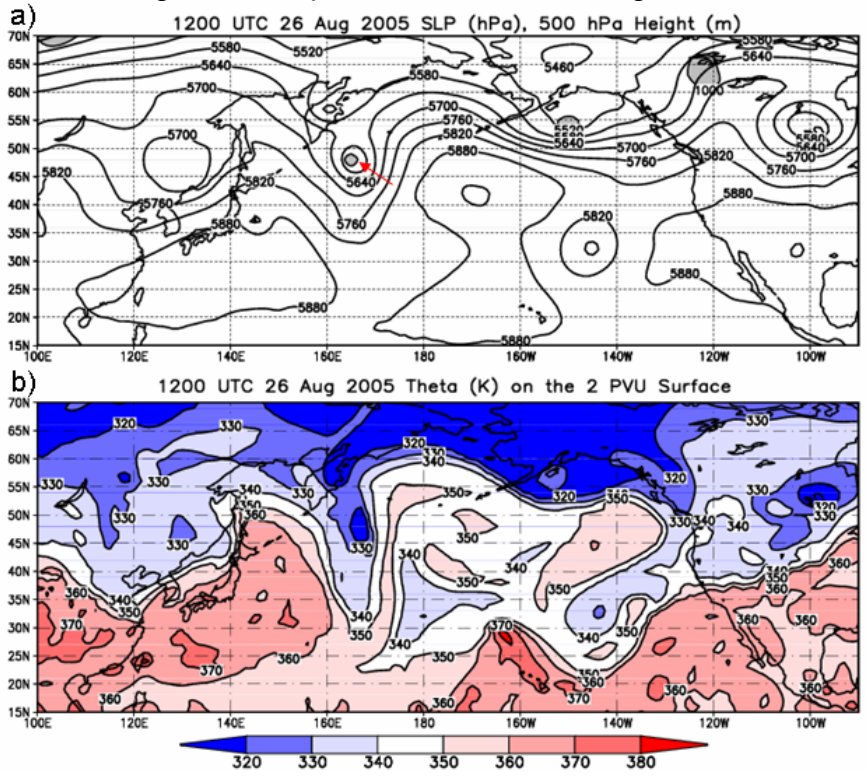

Figure 33. As in Fig. 29, except for 1200 UTC 26 August 2005.

The dynamic tropopause appeared to be influenced more by the combination of midlatitude features rather than by Guchol during the time of extratropical transition (Figs. 29b – 33b). The small circulation of Guchol did not seem to cause a direct impact in midlatitude flow as it became absorbed into a midlatitude trough, which was a pre-existing feature that had moved over the North Pacific from the Asian mainland (Figs. 29a – 33a). However, as Guchol merged with the midlatitude trough, strong ridge amplification occurred to the east along 170°W. Following this merger, a trough amplified downstream over the Gulf of Alaska and extended southward as defined by the change in the 330K contour on the dynamic tropopause (Figs. 29b – 33b).

2. EKE Budget

a. Vertically Averaged EKE and Total EKE Flux Vectors

At 1200 UTC 22 August 2005 (Fig. 34a), almost all of the significant vertically averaged EKE was found in the midlatitudes. The major EKE centers of concern at this time were associated with a shortwave trough near 65° N, 130° E, and along the mid-tropospheric jet across the North Pacific (Fig. 34a). Twenty-four hours later (Fig. 34b), the EKE center near 60° N, 135° E had increased in intensity as this center and an EKE center associated with the mid-tropospheric jet northeast of Japan straddled a wide trough over the Sea of Okhotsk.

Eddy kinetic energy centers associated with the trough over the western North Pacific continued to intensify as Guchol began to move into the midlatitude flow on the downstream side of this trough at 1200 UTC 24 August 2005 (Fig. 34c). As Guchol merged with the midlatitude trough at 1200 UTC 25 August 2005 (Fig. 34d), a closed mid-tropospheric cyclonic circulation developed with a large EKE center on the downstream side. This EKE center transferred EKE downstream over the Aleutian Islands and added energy to the center near 45° N, 155° E (Fig. 34d).

The EKE energy center near 45°N, 170° E intensified sharply by 1200 UTC 26 August 2005 (Fig. 34e). The flux of EKE to the EKE center on the upstream side of the western North Pacific trough was diminishing. However, the flux of EKE downstream of the western North Pacific trough increased to a ridge that was building into the Bering Sea and into another EKE center near southeastern mainland Alaska.

Prior to Guchol's interaction with the midlatitude circulation, the distribution of EKE across the North Pacific consisted of a near-continuous band associated with the jet stream. The combination of an EKE center on the upstream side of a trough moving from eastern Asia over the western Pacific Ocean and its interaction with Guchol appeared to increase the transfer of EKE downstream, which resulted in midlatitude trough amplification across the western and central North Pacific. Near the end of the analyzed sequence, downstream development of an additional EKE center occurred over southwestern Alaska as a ridge amplified over the Bering Sea. In the following section, the flux convergence of EKE and contributions to EKE generation are investigated for several key periods in this scenario.

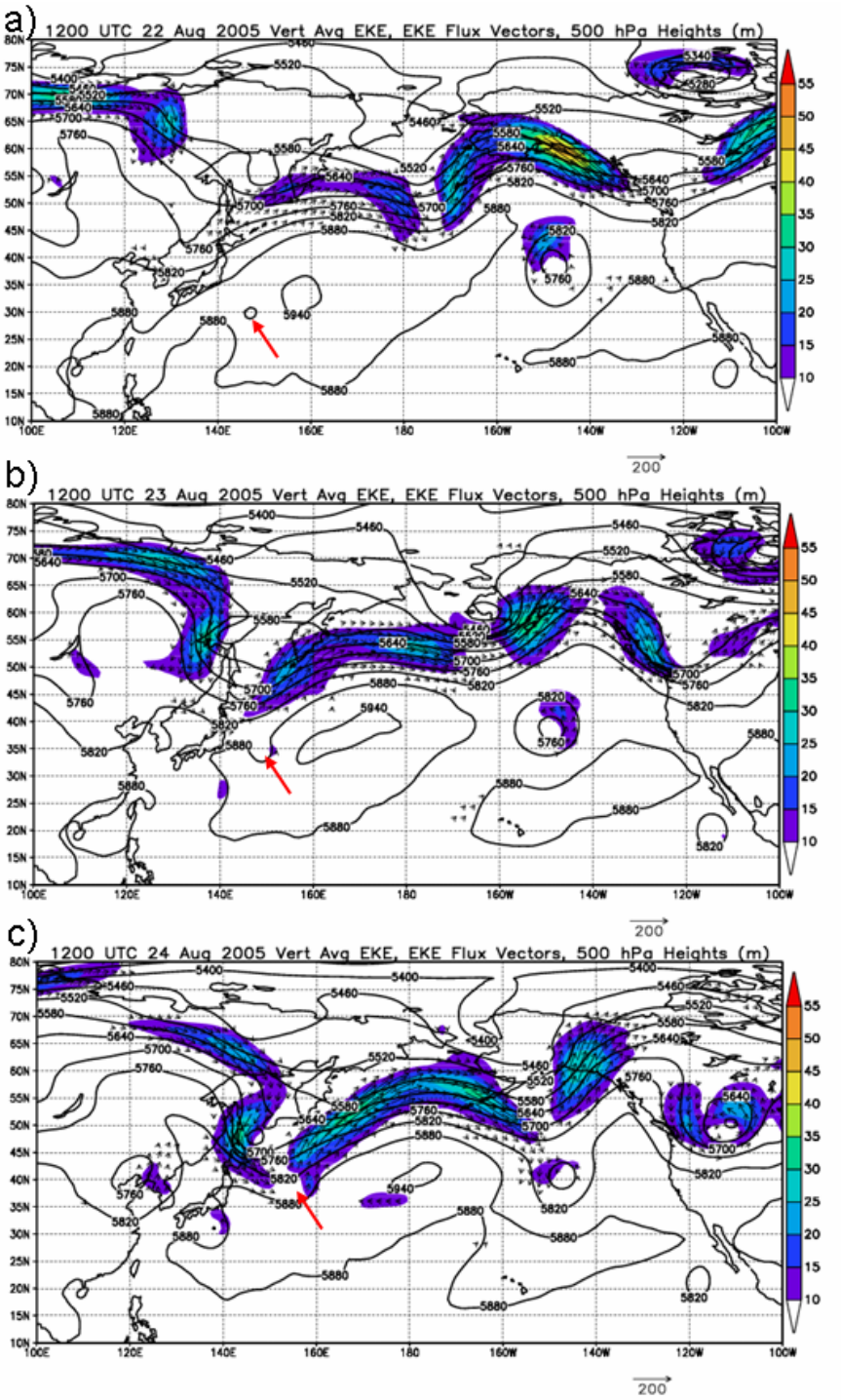

Figure 34. As in Fig.10, except that the time period 1200 UTC 22 August 2005 through 1200 UTC 26 August 2005 is represented in panels (a) through (e). Red arrows denote the positions of Guchol.

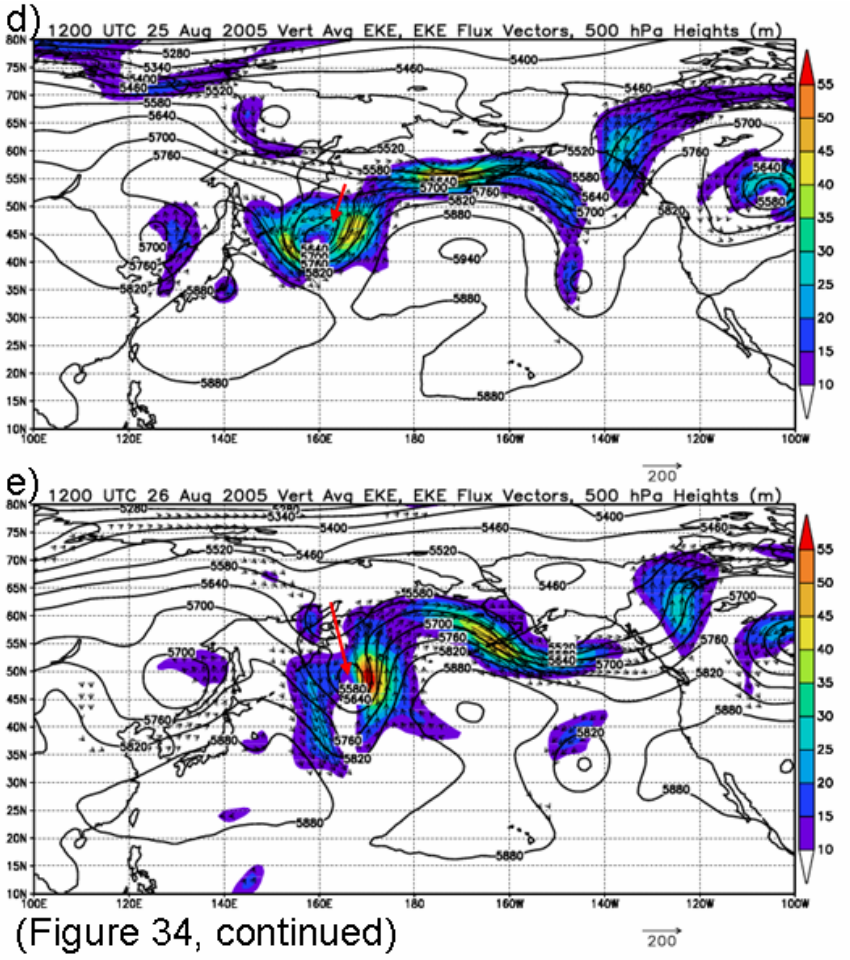

(Figure 34, continued)

b. Components of Total EKE

The contribution to the distribution of total EKE is examined for the period immediately surrounding the merger of Guchol and the midlatitude low on 1200 UTC 25 August 2005.

At 1200 UTC 24 August 2005, the transport of EKE into the trough over the western North Pacific (Fig. 35a) was nearly equal to the generation of EKE (Fig. 35b). Baroclinic conversion generated EKE in a band from the northern Japan Sea northeastward to just south of the Kamchatka Peninsula (Fig. 36b). This EKE generation was dispersed into the trough by AGFC (Fig. 36a) in roughly the same area, which contributed to the EKE center in the region south-southwest of the Kamchatka Peninsula (Fig. 35b).

By 1200 UTC 25 August 2005 (Fig. 37), EKE was being generated in the base of the trough (Fig. 37b) and being transferred downstream (Fig. 37a). It is clear that the ageostrophic fluxes (Fig. 37b) are responsible for the depletion of EKE in the downstream side of the trough near 47° N, 165° E. Part of this energy is being dispersed downstream and part is being recycled back into the trough. Although Guchol is being absorbed by the trough at this time, the primary source of EKE is BC in the base of the trough slightly upstream of Guchol (Fig. 38b). The large flux divergence due to the ageostrophic wind at 47° N, 165° E (Fig. 38a) is due to the merger of Guchol with the trough at this location. Therefore, it appears that cold air sinking (not shown) is responsible for EKE generation as air flows into the back side of the trough, and this energy is then dispersed on the front side of the trough. Although the dispersion is primarily downstream, some energy is recycling back to the trough.

Over the next 24 h (Fig. 39), the pattern of EKE generation (Fig. 39b) and translation (Fig. 39c) continues and intensifies. The dispersion of energy downstream toward the Bering Sea dominates over the recycling back to the trough (Fig. 39b). The generation of EKE continues through BC processes in the base of the trough (Fig. 40b) with maximum dispersion by the ageostrophic wind remaining downstream (Fig. 40a) of the BC region.

In this case, the distribution of EKE associated with the trough moving over the Sea of Okhotsk upstream of Guchol was primarily dominated by EKEFC. Once reaching the western North Pacific and encountering a recurving Guchol and another EKE center on the upstream side of a trough over the western North Pacific, the AGFC and BC terms become more important in the EKE distribution. This development allowed the EKE centers to grow and disperse energy downstream.

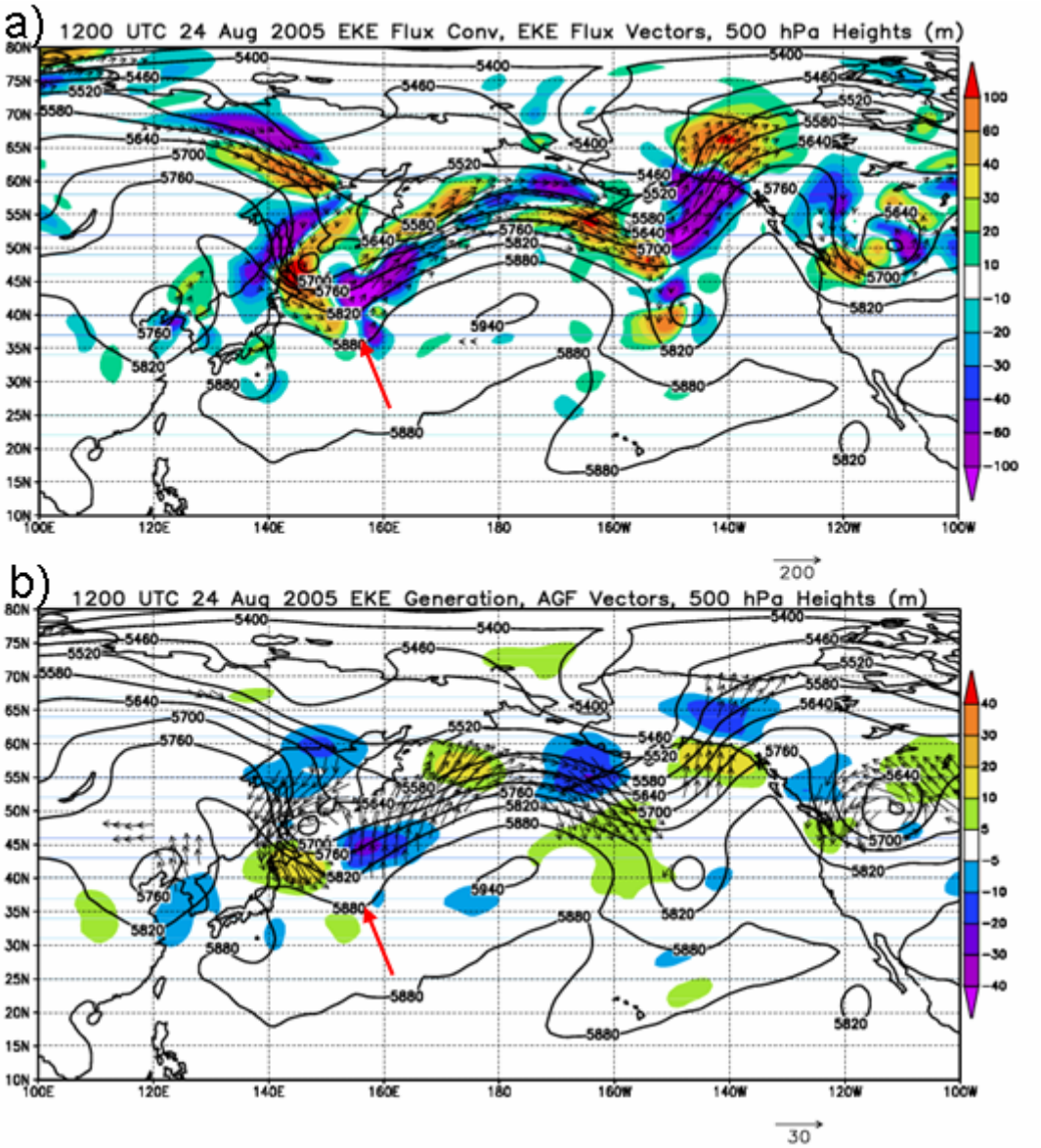

Figure 35. As in Fig. 11, except for 1200 UTC 24 August 2005. Red arrows denote positions of Guchol.

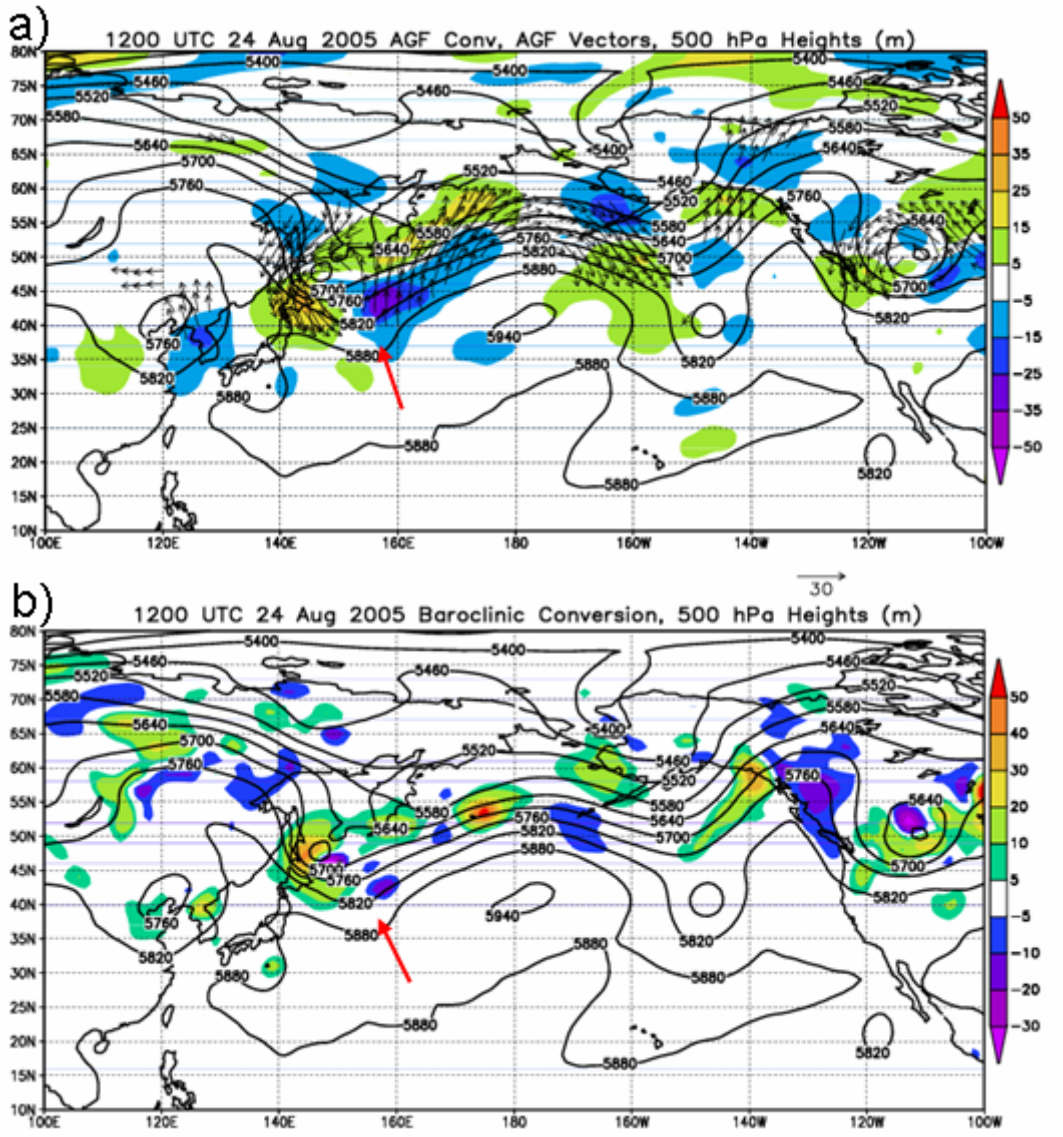

Figure 36. As in Fig. 12, except for 1200 UTC 24 August 2005. Red arrow denotes position of Guchol.

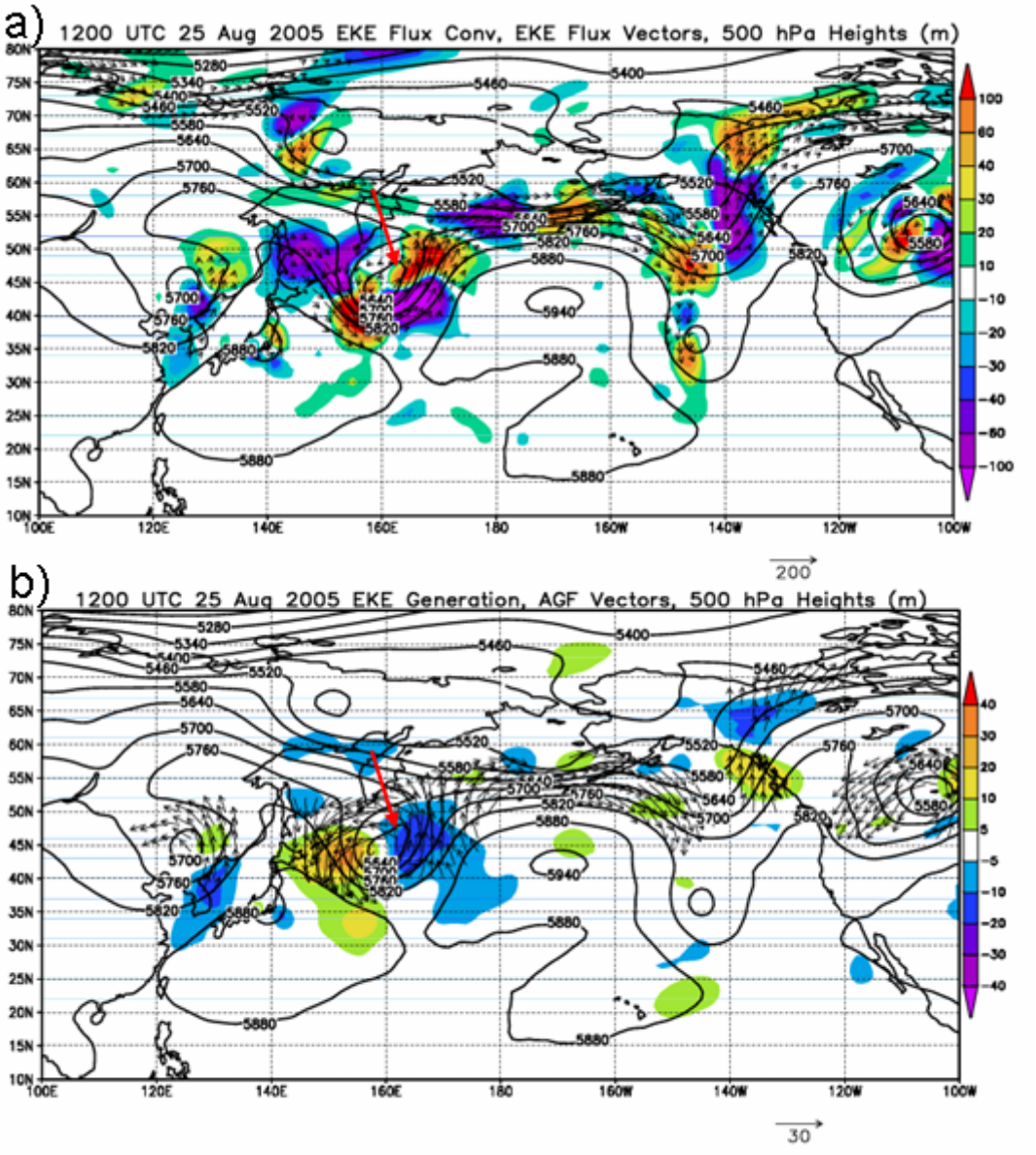

Figure 37. As in Fig. 35, except for 1200 UTC 25 August 2005.

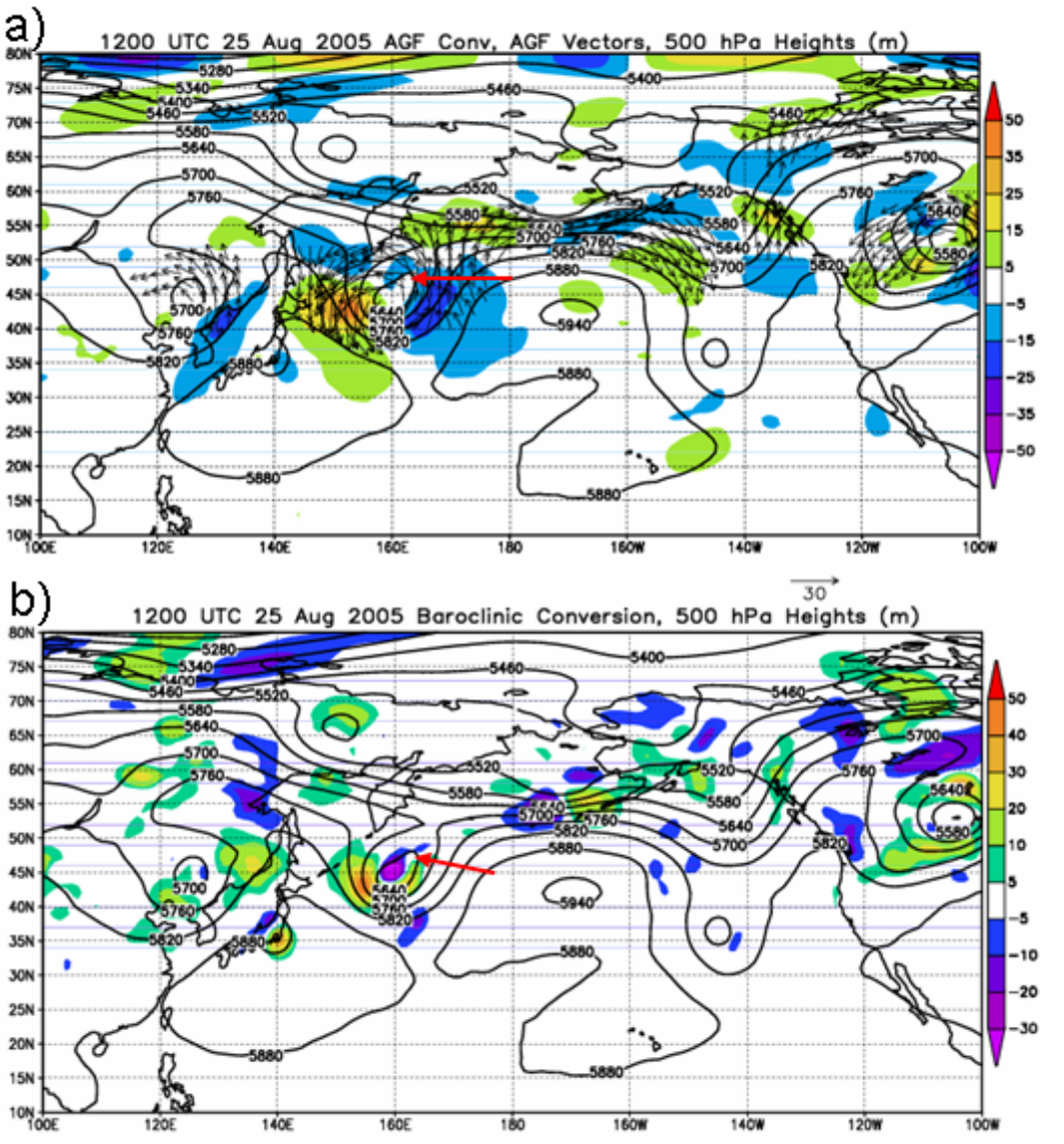

Figure 38. As in Fig. 36, except for 1200 UTC 25 August 2005.

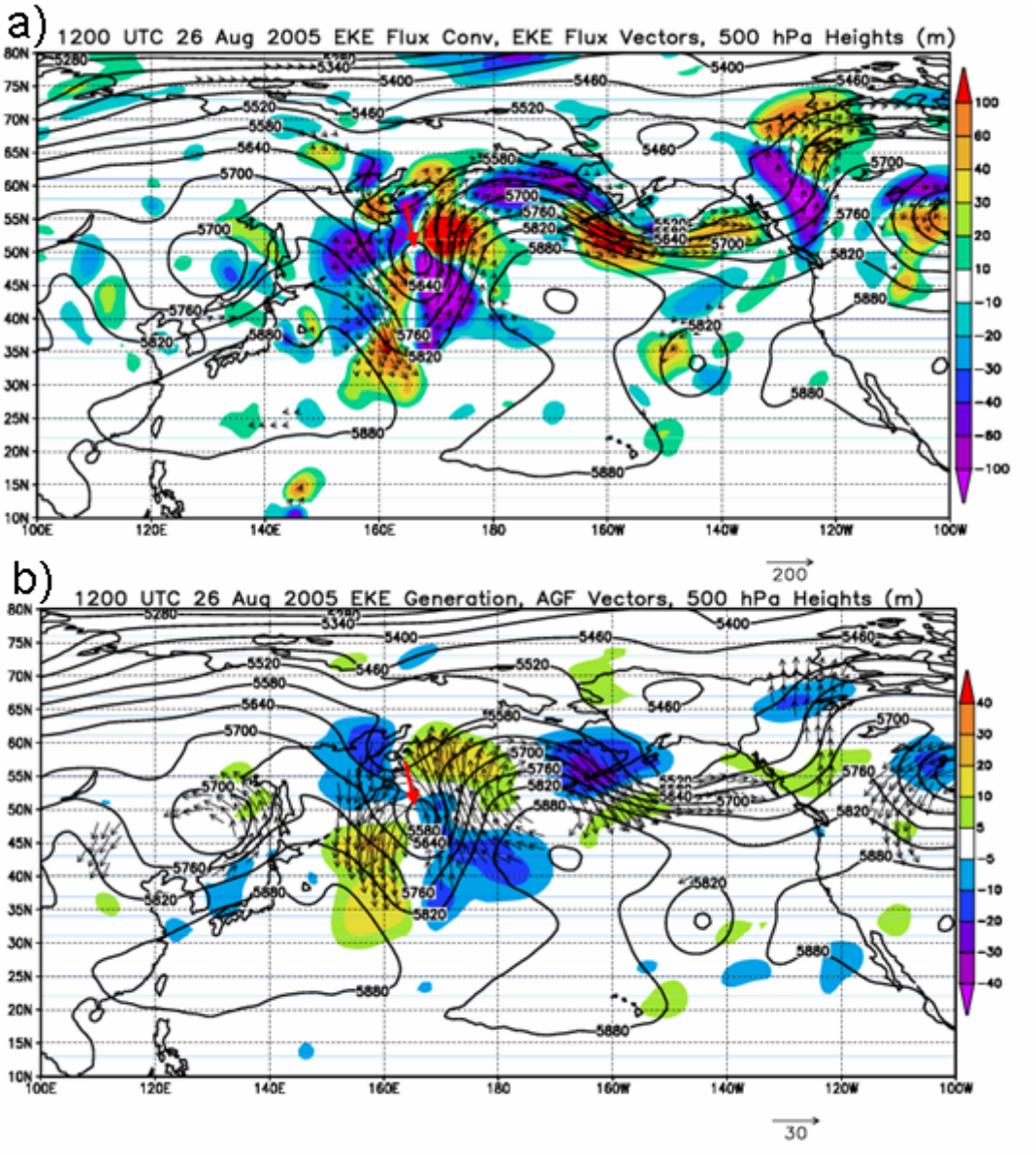

Figure 39. As in Fig. 35, except for 1200 UTC 26 August 2005.

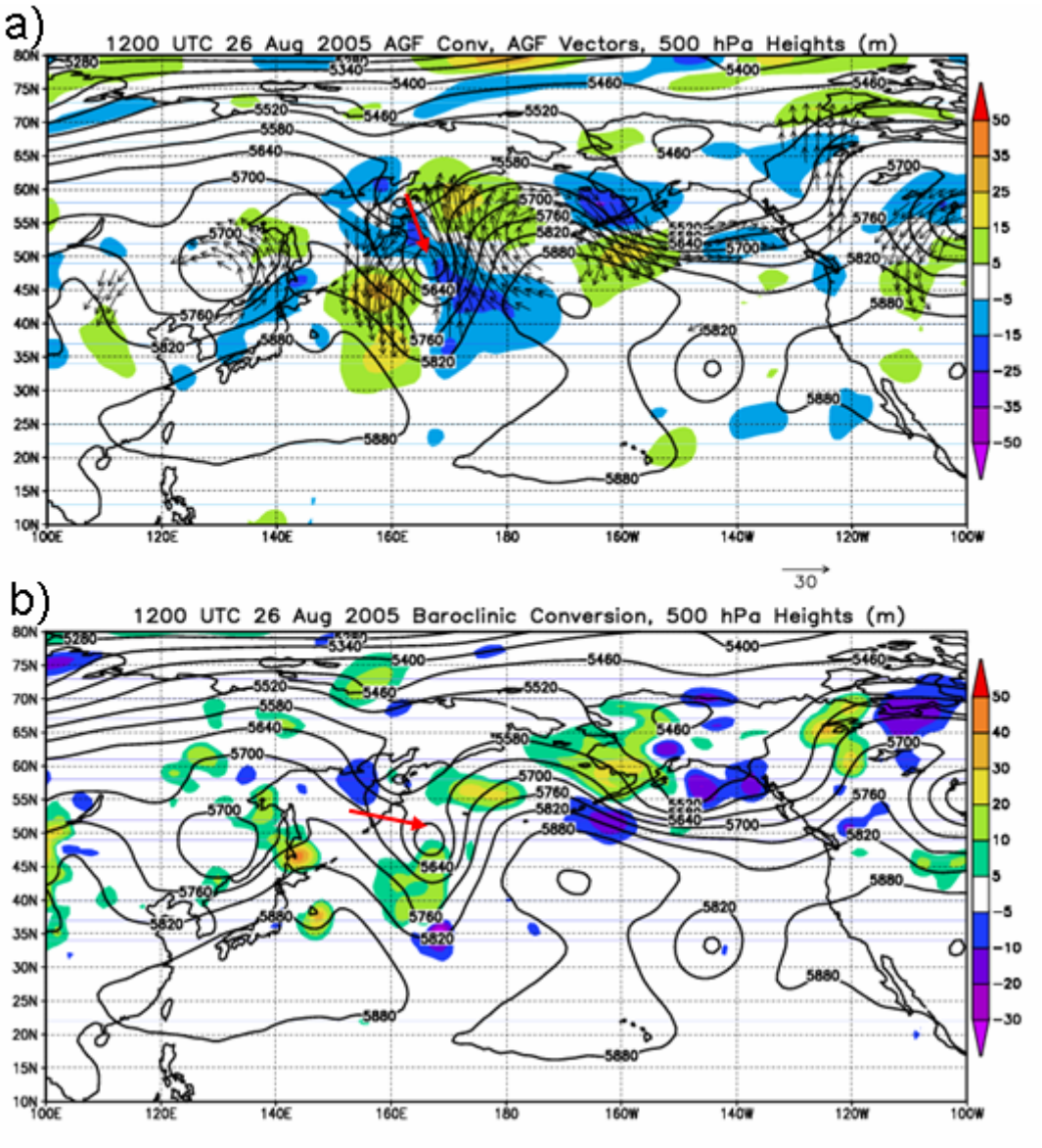

Figure 40. As in Fig. 36, except for 1200 UTC 26 August 2005.

3. Summary

It is clear in Figs. 34a-e that there was no direct impact on the downstream circulation from the ET of Guchol. However, the merger of Guchol with a developing midlatitude trough increased the generation of EKE in the upstream side of the trough through BC associated with sinking cold air. This generated EKE that was transported to the downstream side of the trough and

then dispersed downstream or recycled within the trough. Near the end of the analyzed sequence, a new energy center had formed downstream near the Aleutian Islands.

D. TY NABI

With maximum sustained 10-minute wind speeds of 95 knots (48.9 m s^{-1}) and a minimum central pressure of 925 hPa (Table 1), Nabi represents a case involving an international class 5 TC (from Digital Typhoon (2007): http://agora.ex.nii.ac.jp/digital-typhoon/summary/wnp/s/200514.html.en). The mid- and upper-tropospheric environment present during this case was in a highly zonal pattern before ET at 0600 UTC 8 September 2005 (Table 2).

1. Synoptic Evolution

At 0000 UTC 5 September 2005, Nabi was at 27.9° N, 130.7° E (Fig. 41a). A weak 500 hPa ridge in the midlatitudes was north of Nabi, and a weak trough was upstream of this ridge. Across the North Pacific downstream of Nabi, a mature low that previously existed west of the Kamchatka Peninsula was now near 170° E and a weak trough was south of Alaska. The trough over the Japan Sea that would influence the recurvature of Nabi was associated with a strong potential temperature gradient on the tropopause (Fig. 41b). Over the next 24 h, Nabi moved to 31.4° N, 130.0° E (Fig. 42a). Both the 500 hPa ridge and the upstream trough became slightly more pronounced. The mature cyclone previously east of the Kamchatka Peninsula moved north of the Aleutian Islands, and the trough over the eastern North Pacific began to dig southward. A distinct ridge developed on the dynamic tropopause over the Japan Sea poleward of Nabi (Fig. 42b).

Nabi moved northeastward to 37.5° N, 133.0° E by 0000 UTC 7 September 2005 (Fig. 43a). The 500 hPa ridge, which had been poleward of Nabi, moved slightly downstream of Nabi. Downstream of this ridge, a trough developed along 170° E. The amplitude of the ridge on the dynamic tropopause extended farther northward near Japan, while at the same time a deeper trough started to appear near 170° E (Fig. 43b).

By 0000 UTC 8 September 2005, Nabi had moved northeastward to 46.0° N, 145.0° E (Fig. 44a). The amplitude of the ridge immediately downstream of Nabi had increased, as had the amplitude of the trough that had developed near 170° E. The ridge in the dynamic tropopause continued to increase in amplitude, as did the downstream trough in the central North Pacific (Fig. 44b). Over the next 24 h, Nabi moved east-northeastward to 49.9° N, 157.6° E (Fig. 45a). The 500 hPa trough associated with the ex-Nabi extratropical cyclone became closed and was nearly vertically stacked with the surface circulation (Fig. 45a). The downstream ridge and trough couplet resulted in an extreme poleward displacement in the ridge on the dynamic tropopause and a corresponding large equatorward extension of high potential vorticity to 30° N along 170° W (Fig. 45b).

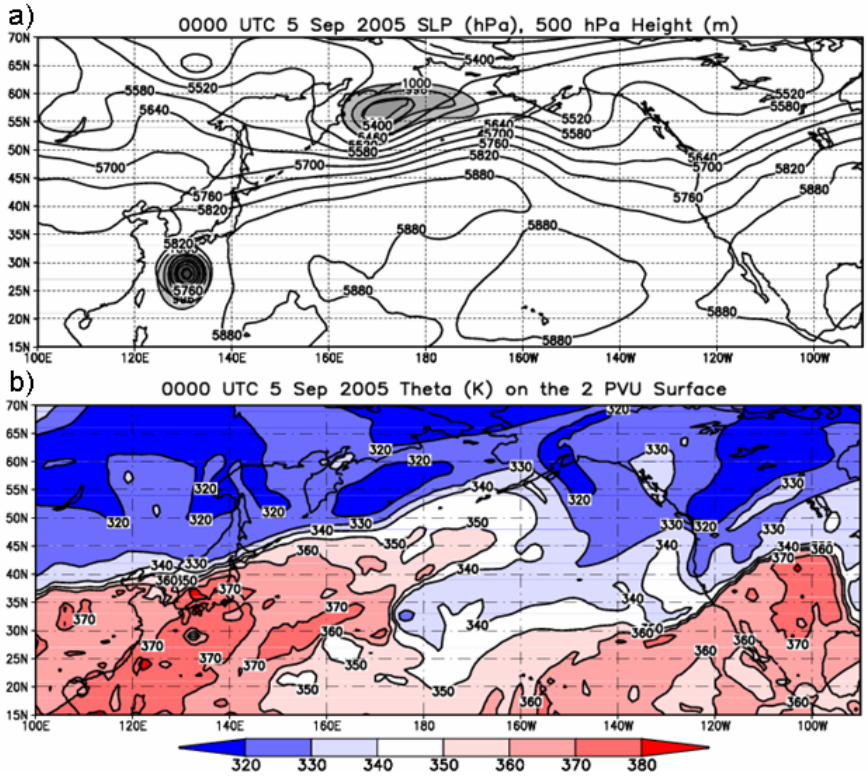

Figure 41. As in Fig. 5, except for 0000 UTC 5 September 2005.

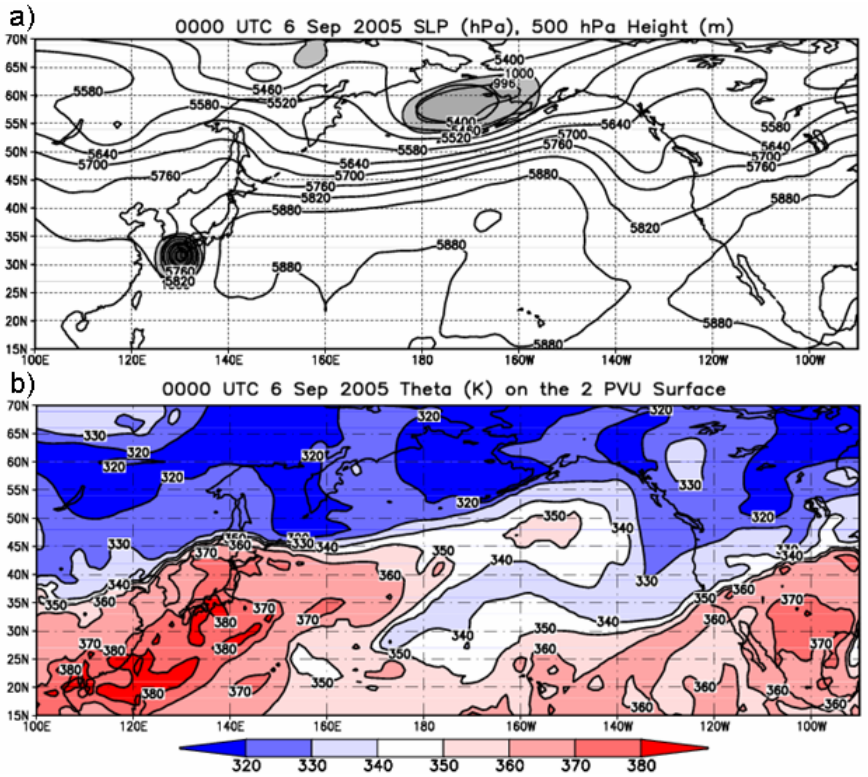

Figure 42. As in Fig. 5, except for 0000 UTC 6 September 2005.

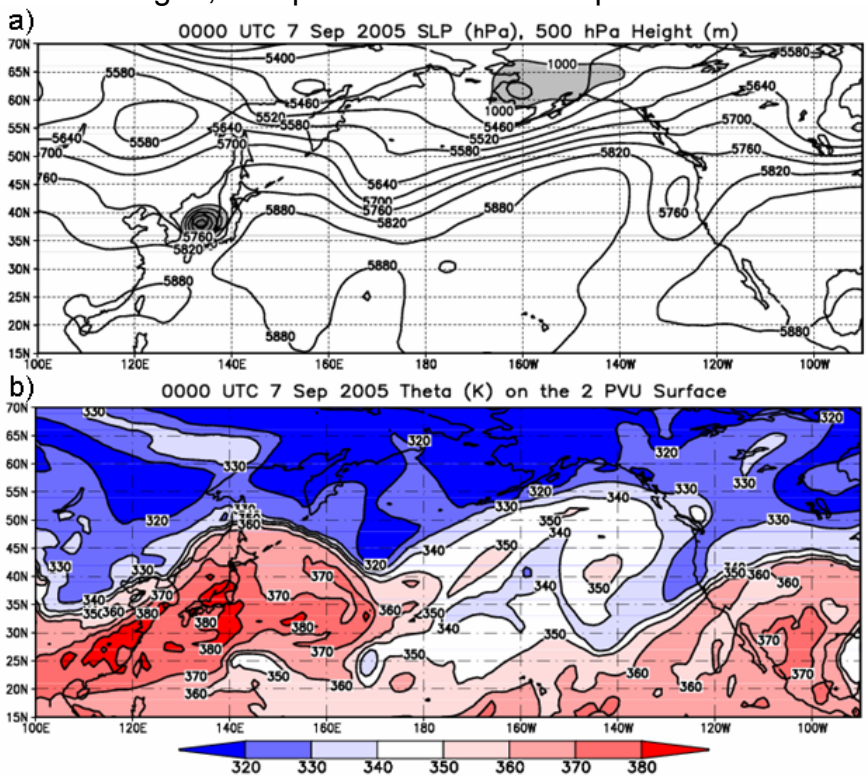

Figure 43. As in Fig. 5, except for 0000 UTC 7 September 2005.

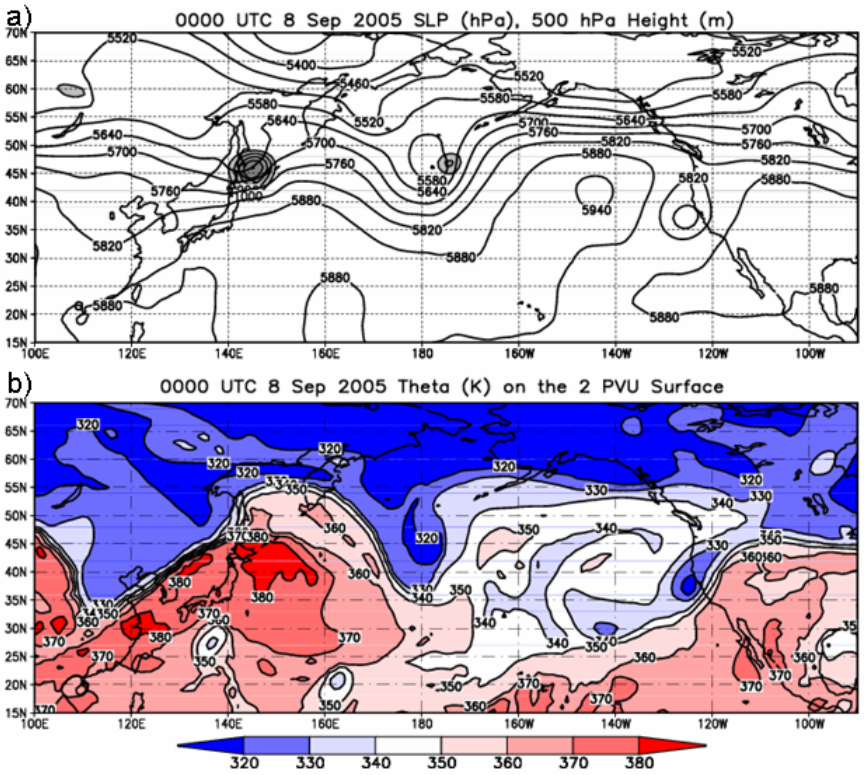

Figure 44. As in Fig. 5, except for 0000 UTC 8 September 2005.

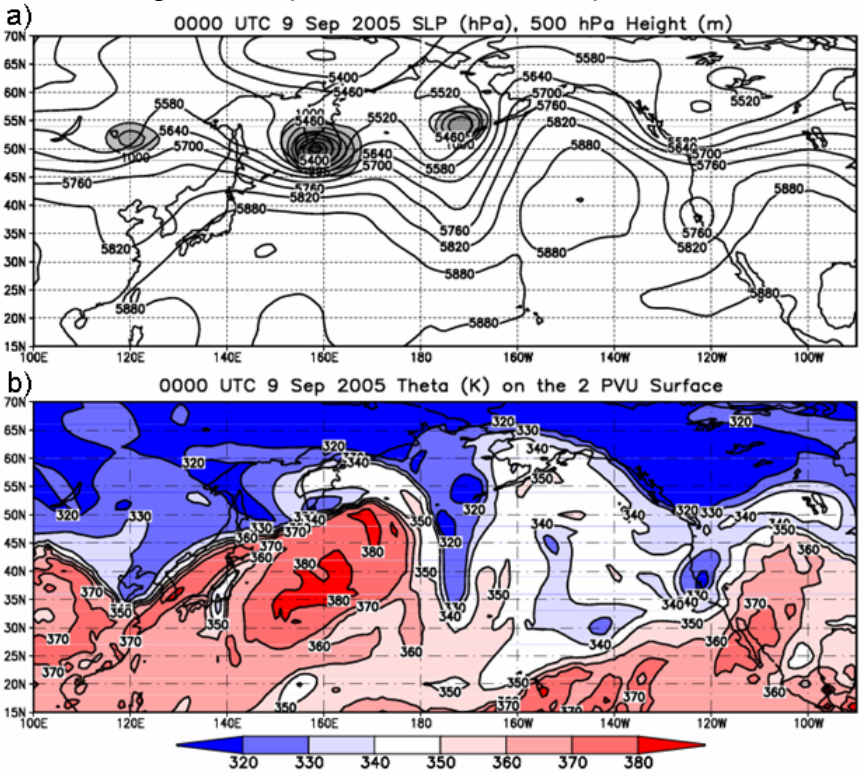

Figure 45. As in Fig. 5, except for 0000 UTC 9 September 2005.

Prior to the movement of Nabi into the midlatitudes, the North Pacific was dominated by the mature cyclone north of the Aleutian Islands and a strong ridge to its southeast (Fig. 41a). As the mature system moved eastward toward Alaska, a trough formed and moved southeastward over the eastern North Pacific. However, the western and central North Pacific was dominated by zonal flow.

The poleward motion of Nabi resulted in an amplifying ridge to its east. A trough then formed over the central Pacific to the east of this ridge that was associated with the northward movement of Nabi. A new ridge then formed east of the central Pacific trough (Figs. 41a – 45a). Therefore, the movement of Nabi into the midlatitudes changed a mostly zonal circulation to a high amplitude pattern of a series of ridges and troughs that extended to the west coast of North America.

2. EKE Budget

a. Vertically Averaged EKE and Total EKE Flux Vectors

The discussion of the EKE budget associated with the ET of Nabi begins at 0000 UTC 3 September 2005 to highlight that the EKE over the North Pacific was decreasing before the movement of Nabi into the midlatitudes. At 0000 UTC 3 September 2005, Nabi was associated with an asymmetric EKE center (Fig. 46a). The distribution of total EKE flux vectors indicated that Nabi was not yet connected to the distribution of EKE in the midlatitudes. The mid-tropospheric flow over the Sea of Okhotsk was dominated by the low and the EKE associated with the strong flow to the south (Fig. 46a). Over the next 12 h, EKE associated with the low over the Sea of Okhotsk and the trough now over the Aleutian Islands increased (Fig. 46b). The two energy centers were connected by total EKE flux vectors, which represented a flow of energy from the low over of the Sea of Okhotsk to the developing trough over the Aleutian Islands.

As the mid-tropospheric low moved closer to the Kamchatka Peninsula by 0000 UTC 4 September 2005 (Fig. 46c), its associated EKE center remained concentrated in the strong flow of the midlatitude circulation. Meanwhile, the trough over the Aleutian Islands had moved southwest of mainland Alaska and the magnitude of the EKE center had increased slightly (Fig. 46c). Eddy kinetic energy fluxes in the midlatitude flow continued to connect these two EKE centers across a weak ridge. Although Nabi continued to move northward, there was still no connection to the midlatitude circulation in terms of EKE fluxes. Twelve hours later at 1200 UTC 4 September 2005 (Fig. 46d), the fluxes of EKE continued to indicate that energy was flowing from the upstream EKE center over the Sea of Okhotsk to the downstream EKE center over the Aleutian Islands (Fig. 46d). However, the amplitudes of these midlatitude EKE centers were decreasing. The EKE flux vectors emanating from Nabi had started to make a connection with the midlatitudes by 0000 UTC 5 September 2005 (Fig. 46e). It was apparent that the EKE centers associated with the low east of the Kamchatka Peninsula and the trough in the Gulf of Alaska (Fig. 46e) had significantly weakened. Twelve hours later (Fig. 46f), the areal coverage of EKE fluxes from Nabi had expanded northward across the Japan Sea and the concentration of vertically integrated EKE associated with Nabi was larger than that with the mid-latitude flow across the North Pacific and eastern Asia.

At 0000 UTC 6 September 2005 (Fig. 46g), EKE flux vectors emanating from Nabi had made a stronger connection with the midlatitude flow. These EKE flux vectors had begun streaming away mainly north of the TC and were focused into the developing 500-hPa ridge north of Japan. At this time, Nabi was now the dominant EKE center over the North Pacific and eastern Asia.

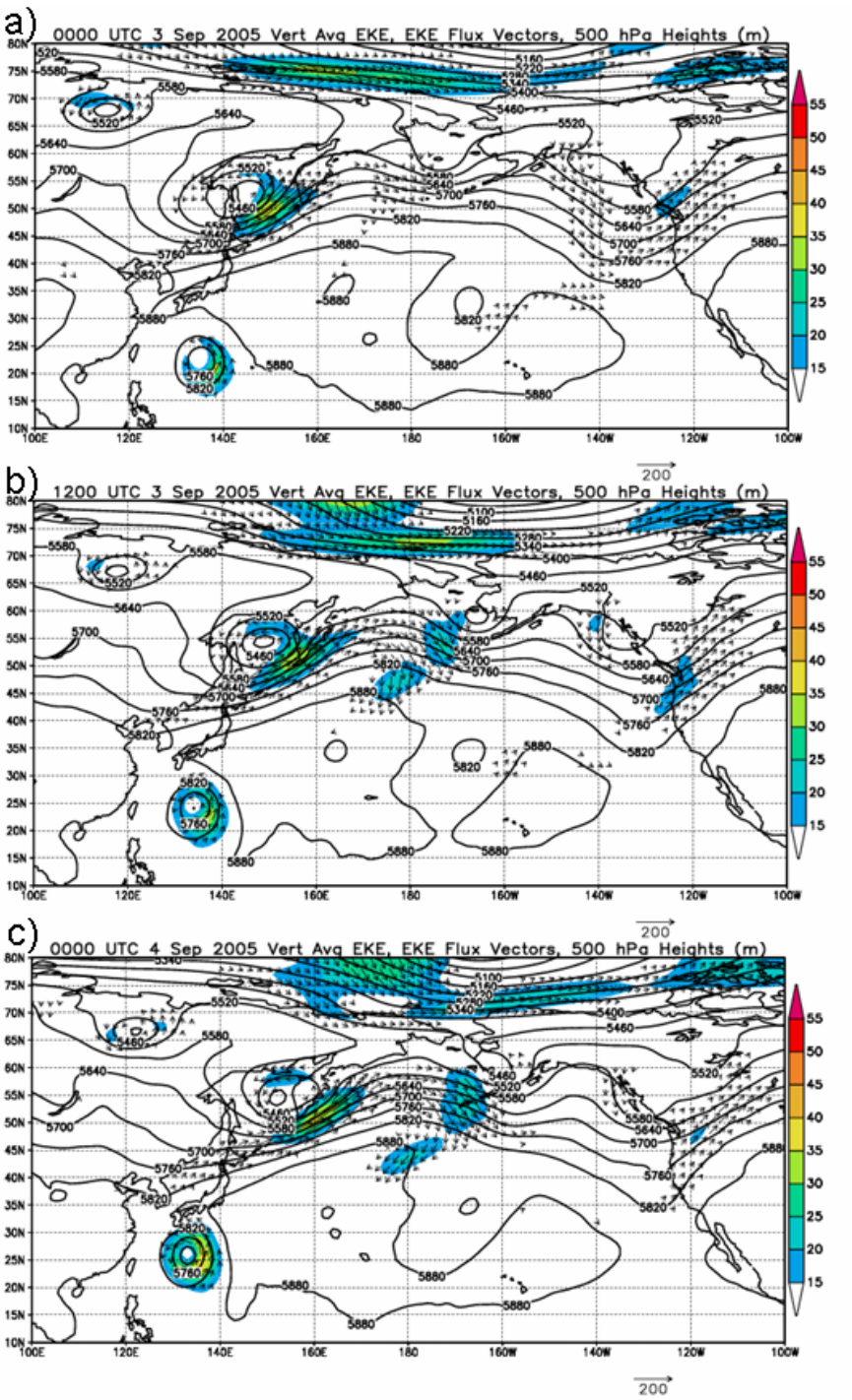

Figure 46. As in Fig. 10, except that the time period 0000 UTC 3 September 2005 through 0000 UTC 9 September 2005 is represented in panels (a) through (m).

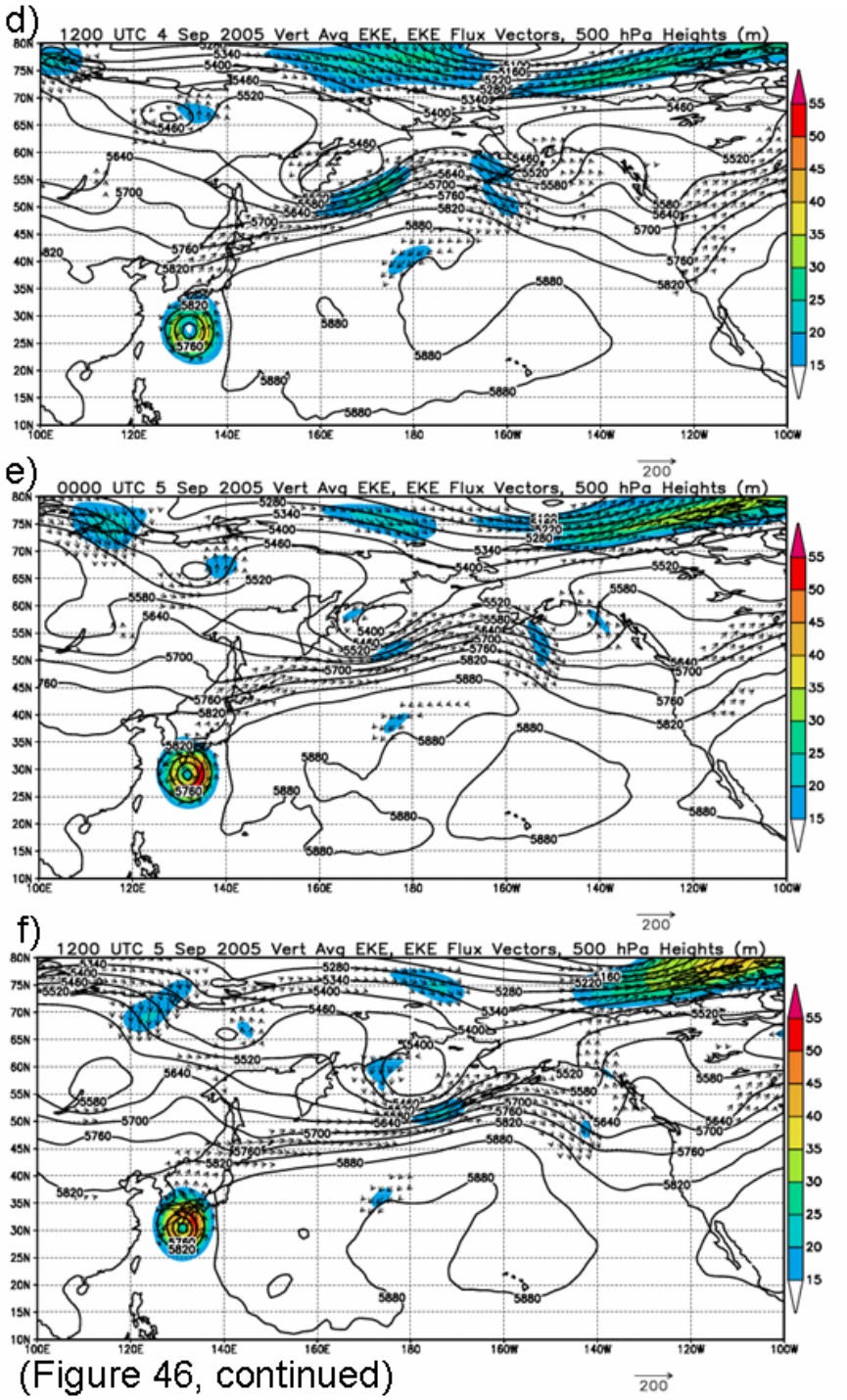

(Figure 46, continued)

Over the next 12 h (Fig. 46h), EKE fluxes from Nabi continued to stream into the 500-hPa ridge that had now moved over the Sea of Okhotsk. An EKE energy center had developed on the downstream side of this ridge in a shortwave trough that was beginning to amplify. At this time, EKE fluxes affecting this EKE center were from a midlatitude trough to the northwest as well as from Nabi (Fig. 46h). At 0000 UTC 7 September 2005 (Fig. 46i), the new downstream EKE center was now centered near 45° N, 165° E on the upstream side of the amplifying trough along 170° E. The EKE associated with Nabi had been decreasing and now the new energy center downstream had become a larger magnitude EKE center relative to Nabi. In addition, EKE fluxes were extending downstream of the EKE center associated with the central North Pacific trough.

Vertically averaged EKE associated with the ex-Nabi remnants had reached a minimum by 1200 UTC 7 September 2005 (Fig. 46j) as Nabi filled and EKE continued to be transported downstream. The downstream trough had continued to amplify. Some of the EKE on the downstream side of the central North Pacific trough was being recycled back into the EKE center on the upstream side of the trough (Fig. 46j). However, a portion of the EKE fluxes was also being transported downstream toward the Gulf of Alaska into an EKE center south of Alaska.

By 0000 UTC 8 September 2005 (Fig. 46k), the EKE center associated with the ex-Nabi remnants began to increase and continued to be a source of EKE fluxes downstream to the trough along 180° E. The downstream EKE center that developed on the east side of the trough near 50° N, 170° W (Fig. 46k) was now more intense than the upstream EKE center. At this time, the trough had developed into a closed cyclonic circulation and EKE continued to be recycled back into the EKE center east of 180° E from the center at 170° W. The EKE fluxes emanating from the EKE center at 170° W were also being directed downstream to the new trough developing southwest of Alaska (Fig. 46k).

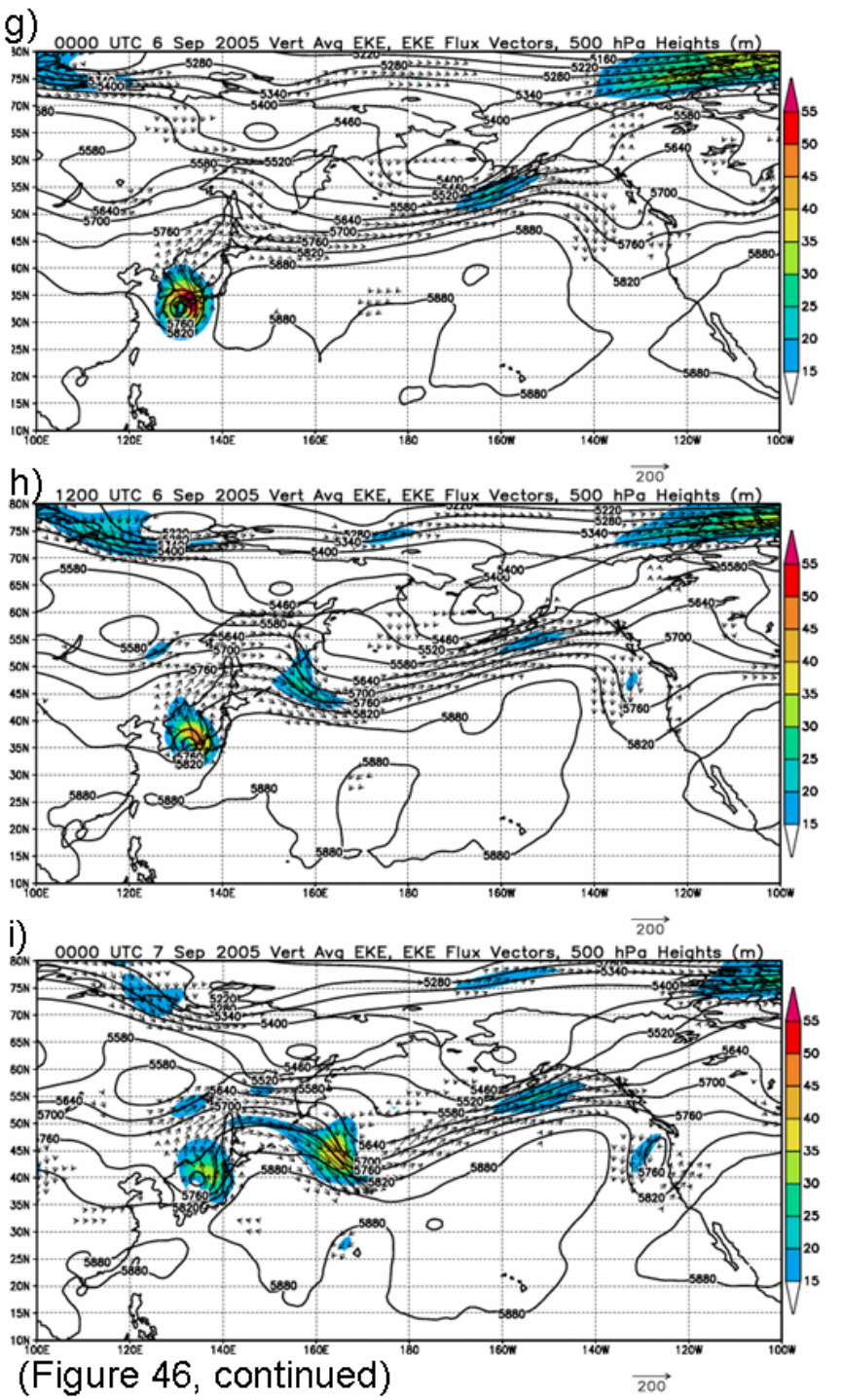

(Figure 46, continued)

Twelve-hours later at 1200 UTC 8 September 2005 (Fig. 46l), the remnants of ex-Nabi had re-intensified as an extratropical cyclone, and the associated EKE center had also re-intensified. In addition, EKE continued to be transported downstream to the trough over the central North Pacific. The EKE centers upstream and downstream of the trough along 170° W strengthened during the time period. The amount of EKE being recycled within the circulation appeared to be reduced, but fluxes from the EKE center along 165° W increased downstream of the trough into the new trough over the Gulf of Alaska (Fig. 46l).

The remnants of ex-Nabi had continued intensifying to 0000 UTC 9 September 2005 (Fig. 46m). The initial EKE center upstream of the trough over the central North Pacific had diminished in intensity, but the EKE fluxes continued to radiate from the EKE center along 165° W into the amplifying ridge and trough immediately downstream over southwestern Alaska.

Before the connection of Nabi to the midlatitude circulation, the distribution of EKE across the North Pacific was dominated by the low over the Sea of Okhotsk. Eddy kinetic energy was transferred downstream to a trough near southwestern Alaska through total EKE fluxes. However, both of these EKE centers had weakened by 0000 UTC 5 September 2005, which left a relatively zonal and relatively low-EKE midlatitude environment into which Nabi would enter.

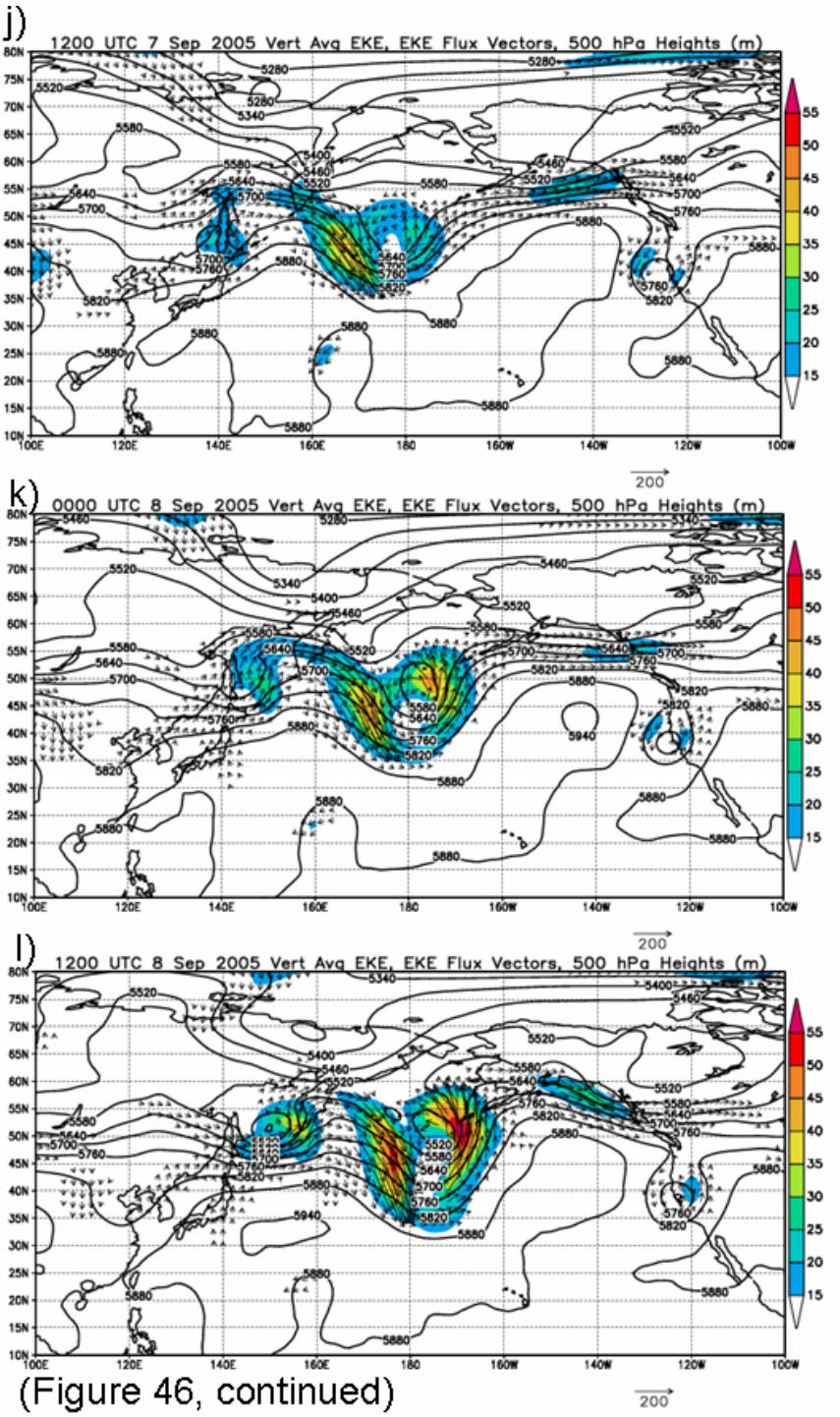

(Figure 46, continued)

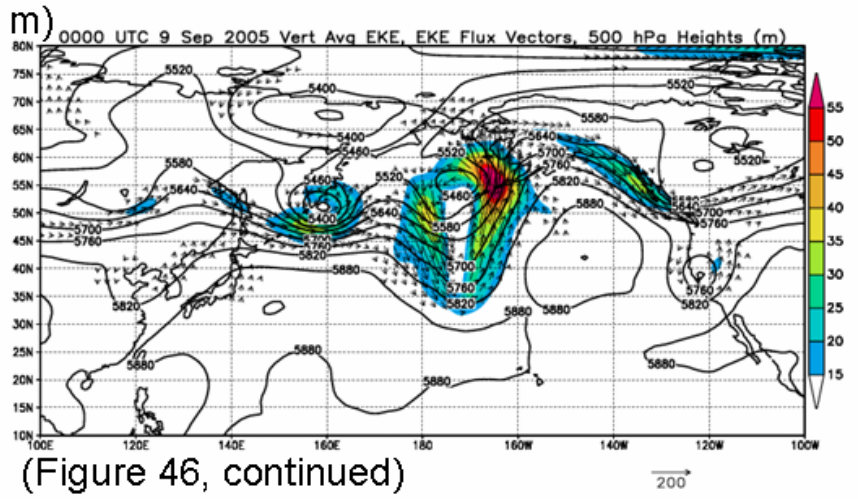

(Figure 46, continued)

As Nabi approached the midlatitudes, fluxes of EKE from Nabi began to contribute to a new EKE center downstream that was associated with a developing trough. This amplifying trough eventually gained a closed mid-tropospheric circulation and developed another EKE center on its downstream side. Furthermore, the re-intensification of ex-Nabi allowed continuation of downstream transport of EKE. The closed circulation associated with the central North Pacific trough led to a recycling of EKE within the circulation, but EKE was also transferred into another amplifying ridge over southwestern Alaska. This transfer of EKE that started during the ET of Nabi and continued through the re-intensification of ex-Nabi as an extratropical cyclone helped sustain the distribution of EKE across the North Pacific. This evolution is in contrast to the circulations previously decaying after an initial period of minor development. In the following section, the flux convergence of EKE and contributions to EKE generation are investigated for several key periods in this scenario.

b. Components of Total EKE

At 1200 UTC 3 September 2005, which was prior to the connection of Nabi with the midlatitude circulation, a strong positive/negative EKEFC couplet existed about the EKE centers associated with the Sea of Okhotsk cyclone and the trough near the Aleutian Islands (Fig. 47a). The generation of EKE (Fig. 47b) in the Sea of Okhotsk cyclone was supported by significant positive AGFC on the

east and south sides of the cyclone (Fig. 48a). Baroclinic processes (Fig. 48b) contributed EKE to regions just east of the cyclone center and this energy was dispersed into the western side of the ridge east of the Kamchatka Peninsula (Fig. 48a). This pattern of EKE generation and dispersion was contributing to the development of the trough over the Aleutians.

A strong EKEFC couplet remained about the EKE center east of the Kamchatka Peninsula 24 h later (Fig. 49a), while the prime generation region through AGFC was again to the northeast of this EKE center (Fig. 49b). Baroclinic conversion was still generating EKE east of the Kamchatka Peninsula, but was diminished in magnitude from the previous 24 h (Fig. 50b). Eddy kinetic energy dispersion through AGFC (Fig. 50a) continued downstream of the EKE center associated with the trough moving into the Gulf of Alaska (Fig. 50a).

By 1200 UTC 6 September 2005, the EKEFC directly north of Nabi was transporting EKE into the ridge that had built north and east of Nabi (Fig. 51a). Generation of EKE was occurring in the developing trough along 160° E (Fig. 51b). The generation of EKE via BC around Nabi (Fig. 52b) was being dispersed into the midlatitudes (Fig. 52a), but there was little connection downstream at that time. At that time, AGFC (Fig. 52a) from a region near the tip of Kamchatka seemed to dominate the region of the western North Pacific trough. Twelve hours later (Fig. 53), EKEFC continued to transport energy into the developing trough near 40° N, 170° E (Fig. 53a). The region of the trough was also a region of large EKE generation, as was the region directly north of Nabi (Fig. 53b). Eddy kinetic energy generation also increased through AGFC and BC in this same area (Figs. 54a,b). Baroclinic conversion had increased in the vicinity of Nabi as extratropical transition progressed, but EKE generation was offset by dispersion into the midlatitude flow, as indicated by negative AGFC (Fig. 54a,b).

By 1200 UTC 8 September 2005 (Fig. 55), the pattern of total EKE transferred (Fig. 55a) defined a general downstream flow of energy across the

western North Pacific. The generation of EKE (Fig. 55b) was concentrated in the region of the re-intensifying ex-Nabi and the trough near 180° E. The generation of EKE in both these regions was due to a maxima in BC (Fig. 56b). Ageostrophic fluxes were then responsible for the dispersion of this energy into the downstream region associated with the closed low over the Sea of Okhotsk and another closed low over the Aleutian Islands (Fig. 56a).

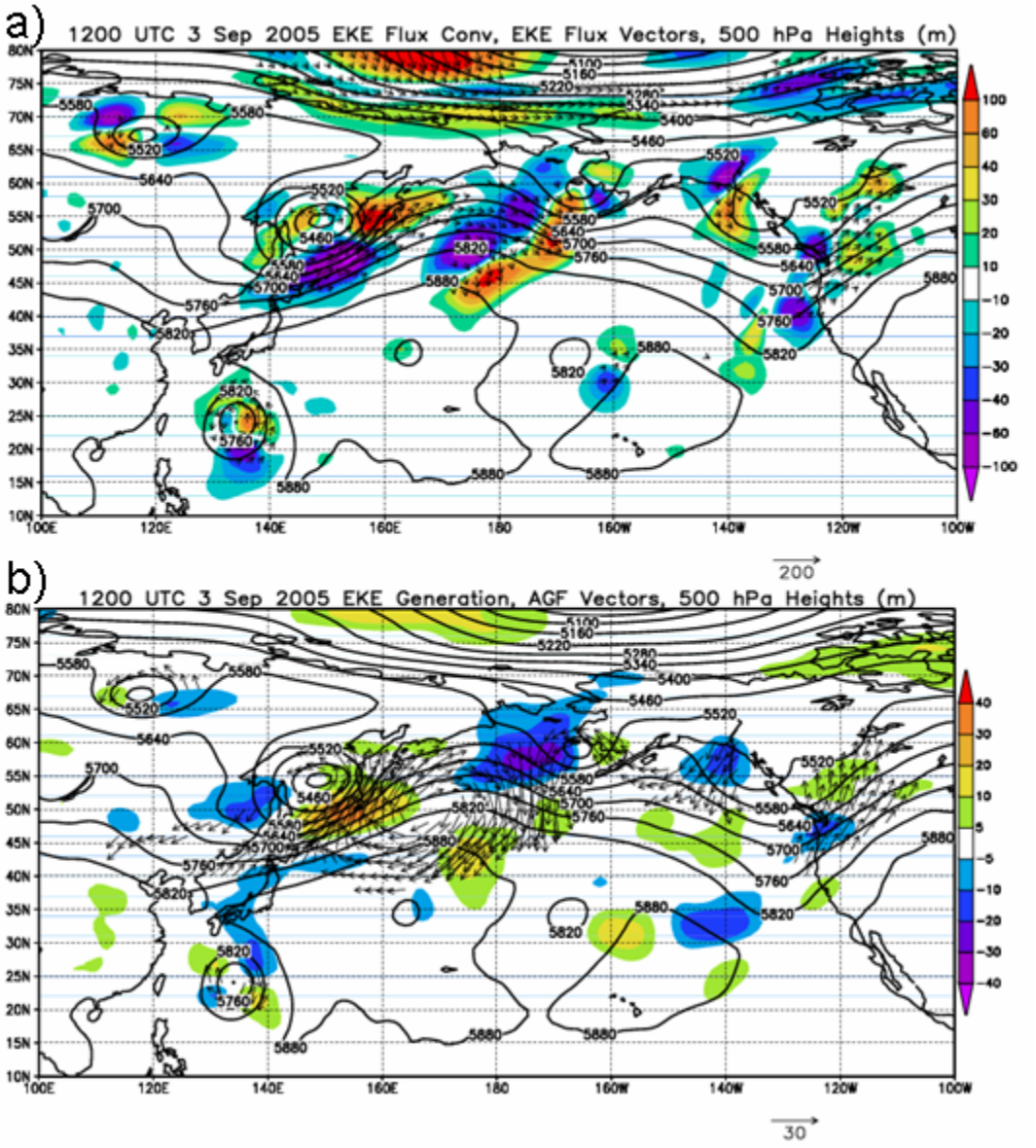

Figure 47. As in Fig. 11, except for 1200 UTC 3 September 2005.

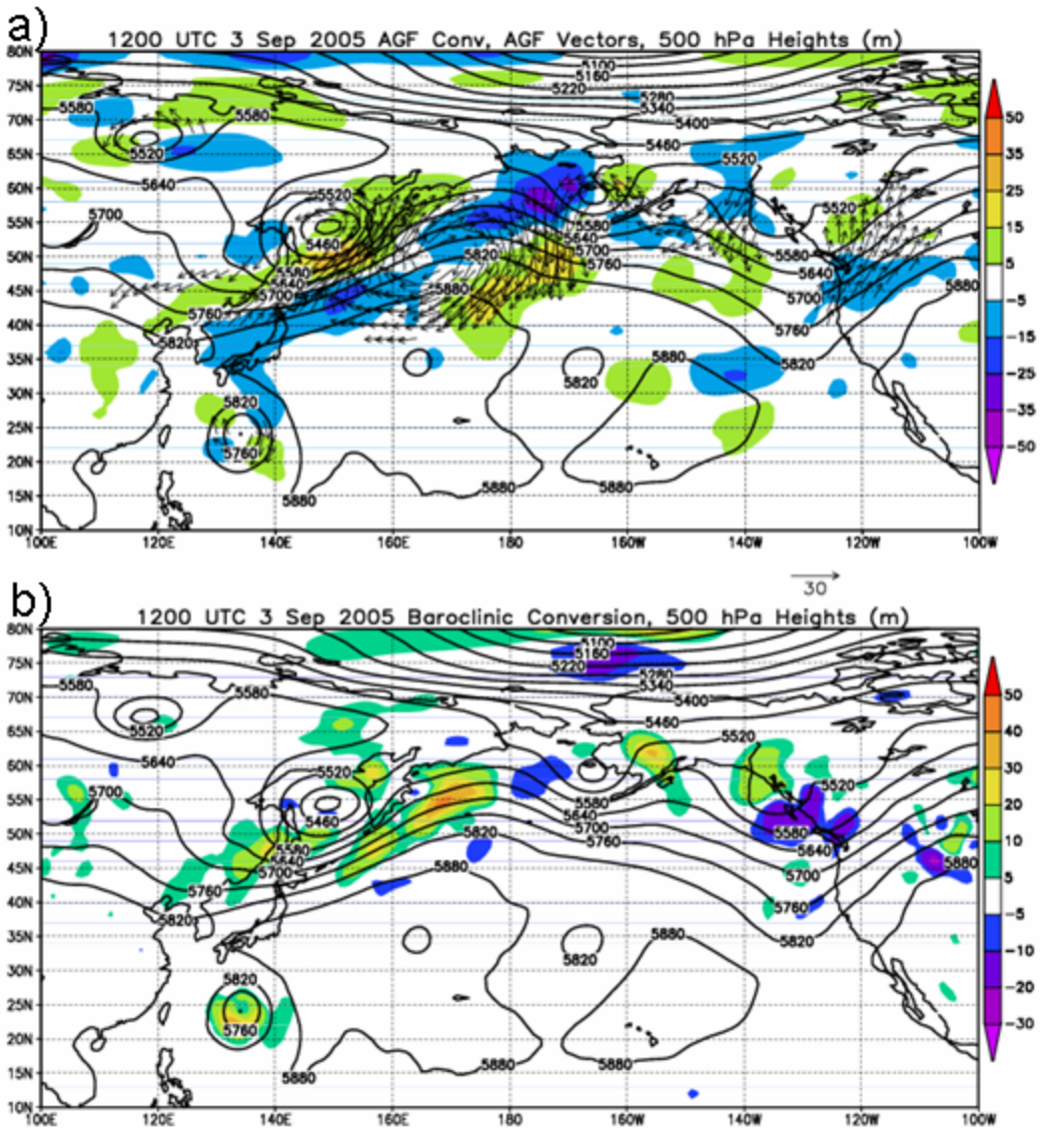

Figure 48. As in Fig. 12, except for 1200 UTC 3 September 2005.

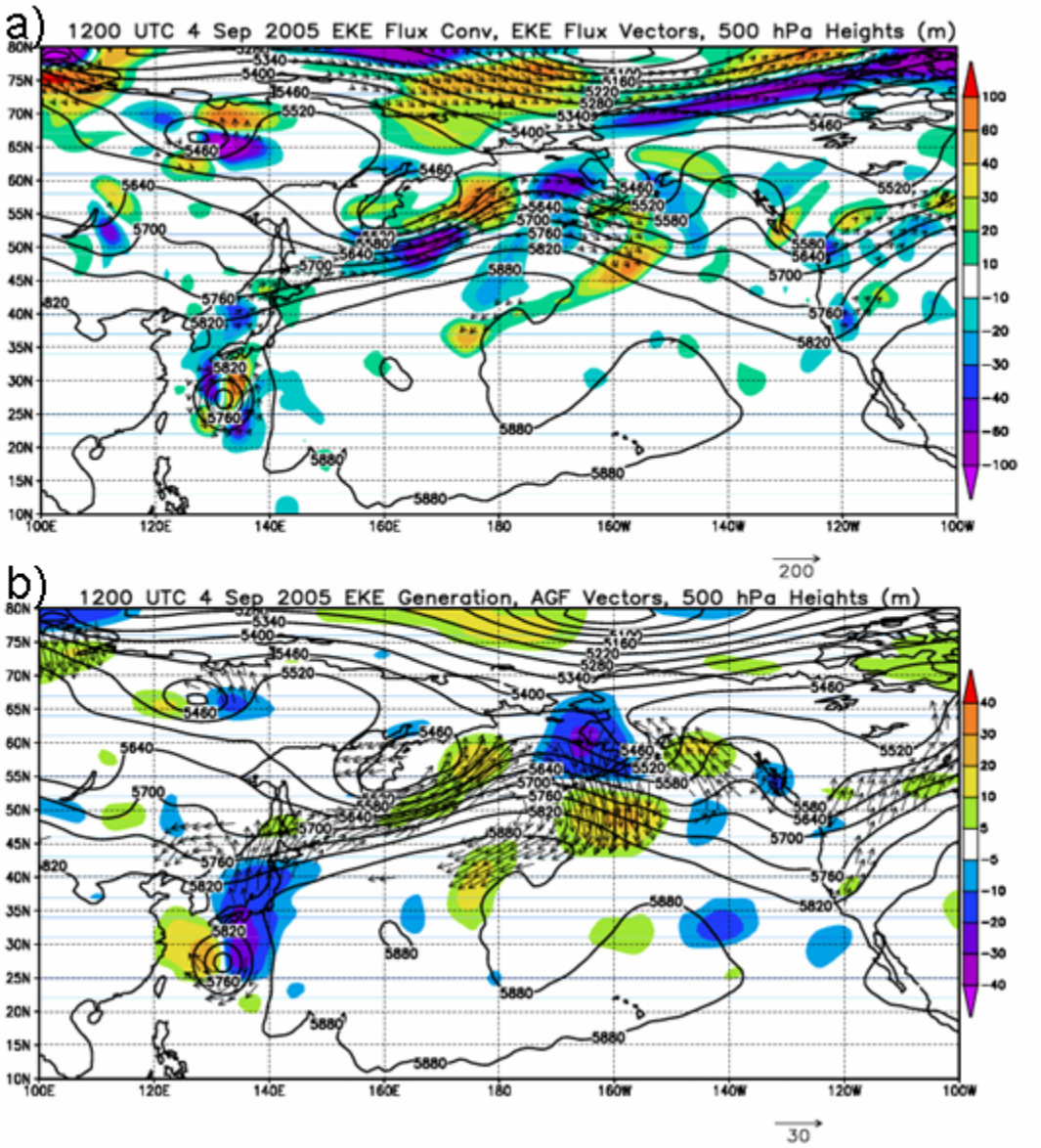

Figure 49. As in Fig. 11, except for 1200 UTC 4 September 2005.

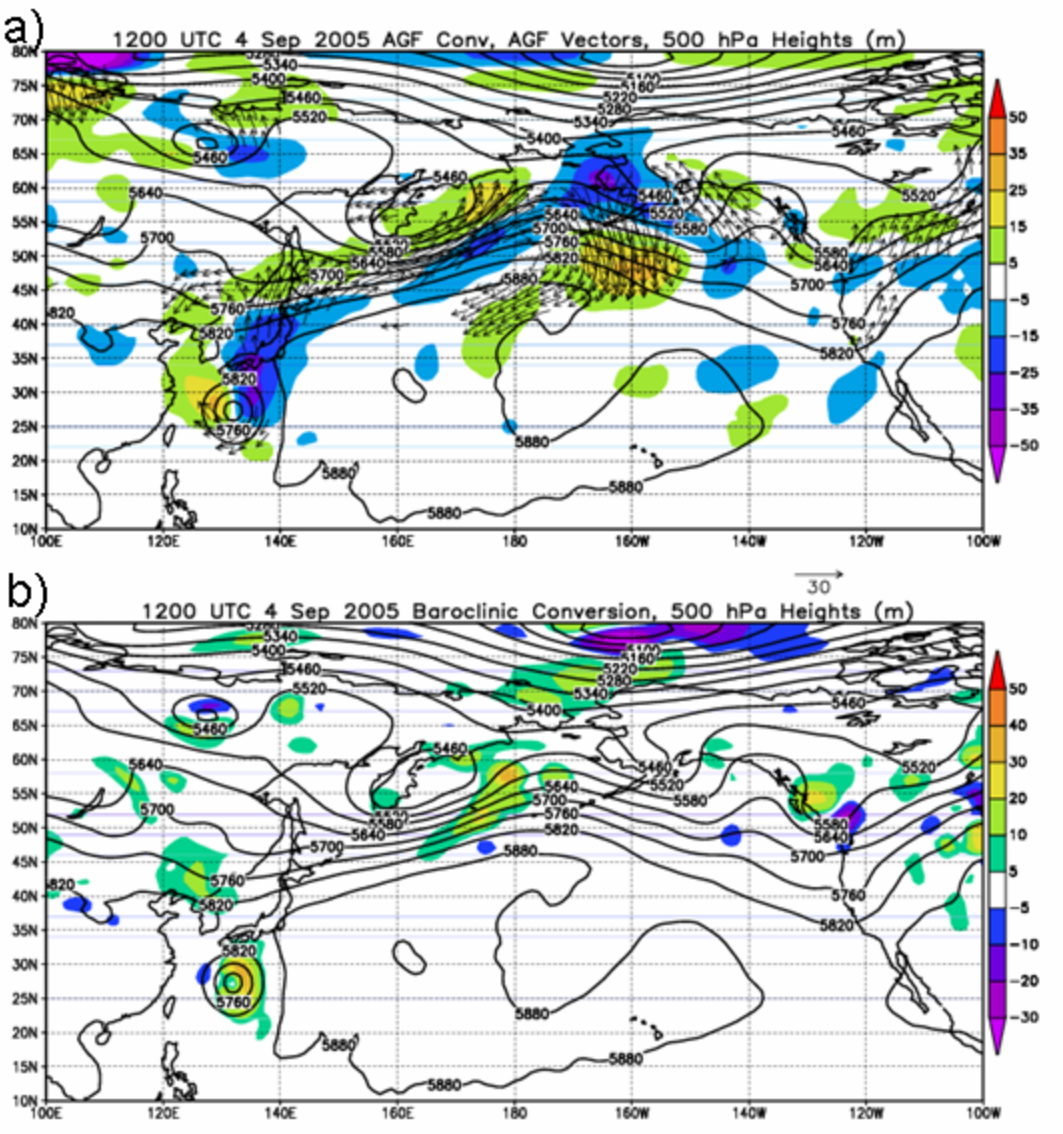

Figure 50. As in Fig. 12, except for 1200 UTC 4 September 2005.

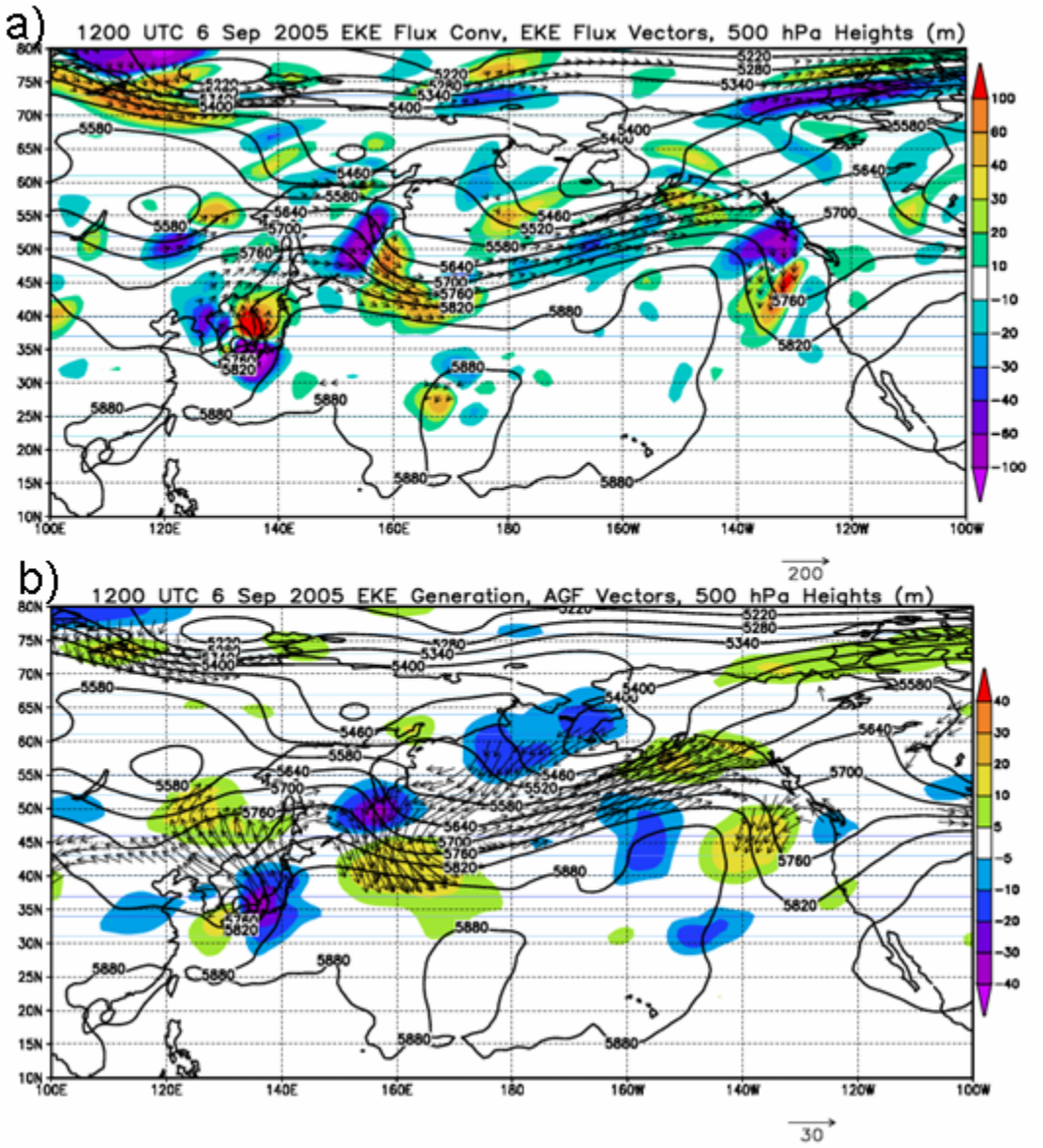

Figure 51. As in Fig. 11, except for 1200 UTC 6 September 2005.

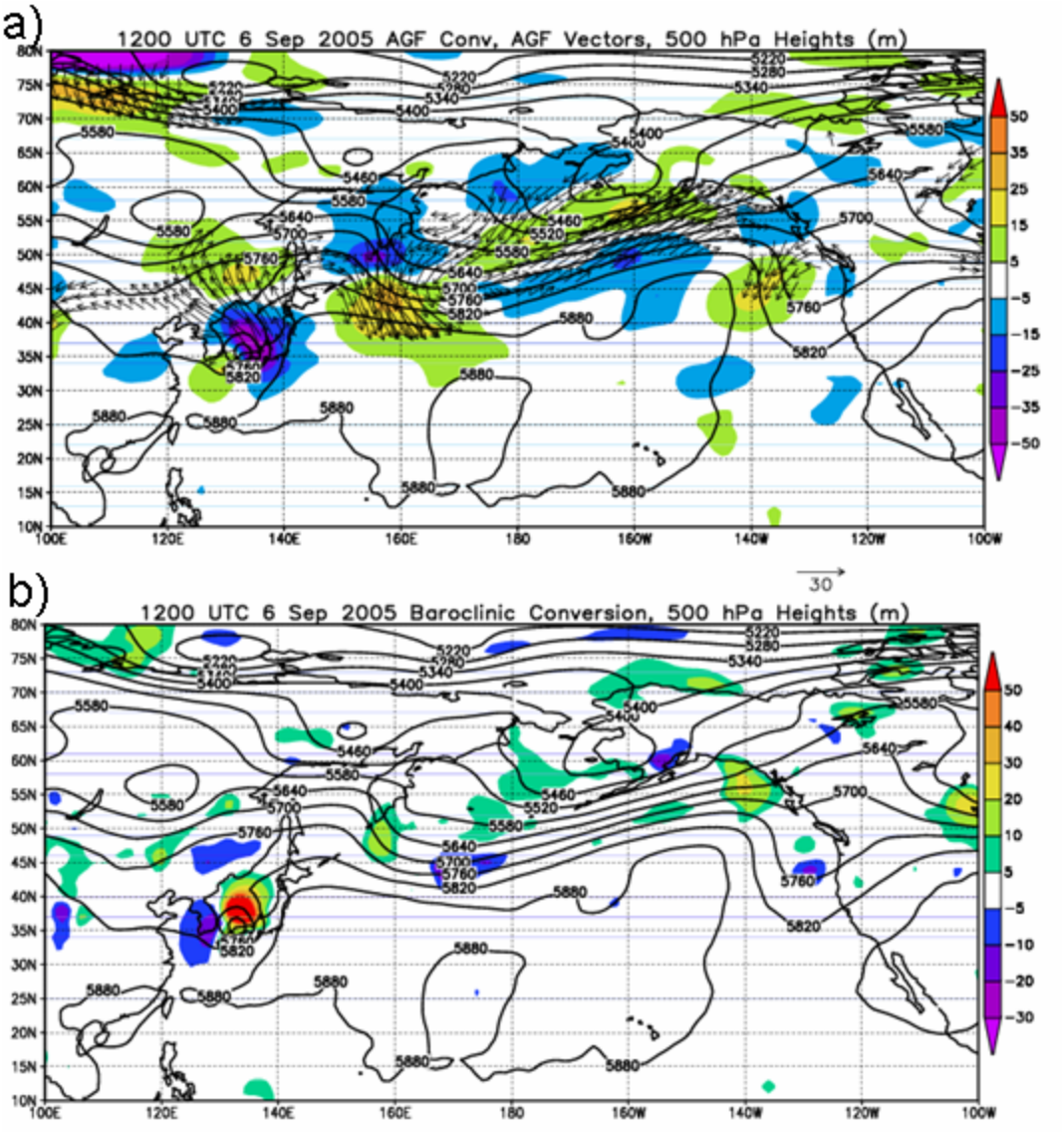

Figure 52. As in Fig. 12, except for 1200 UTC 6 September 2005.

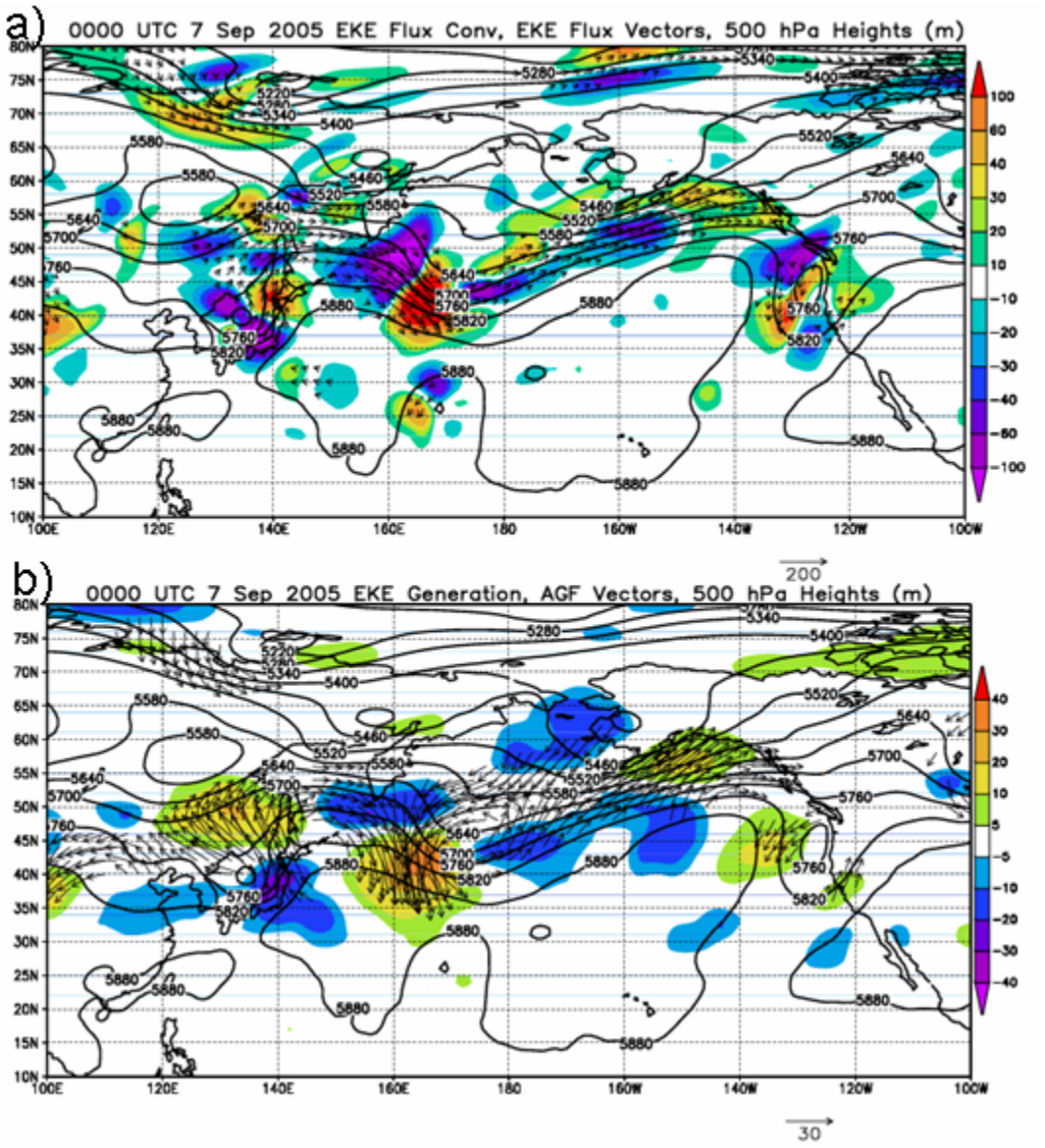

Figure 53. As in Fig. 11, except for 0000 UTC 7 September 2005.

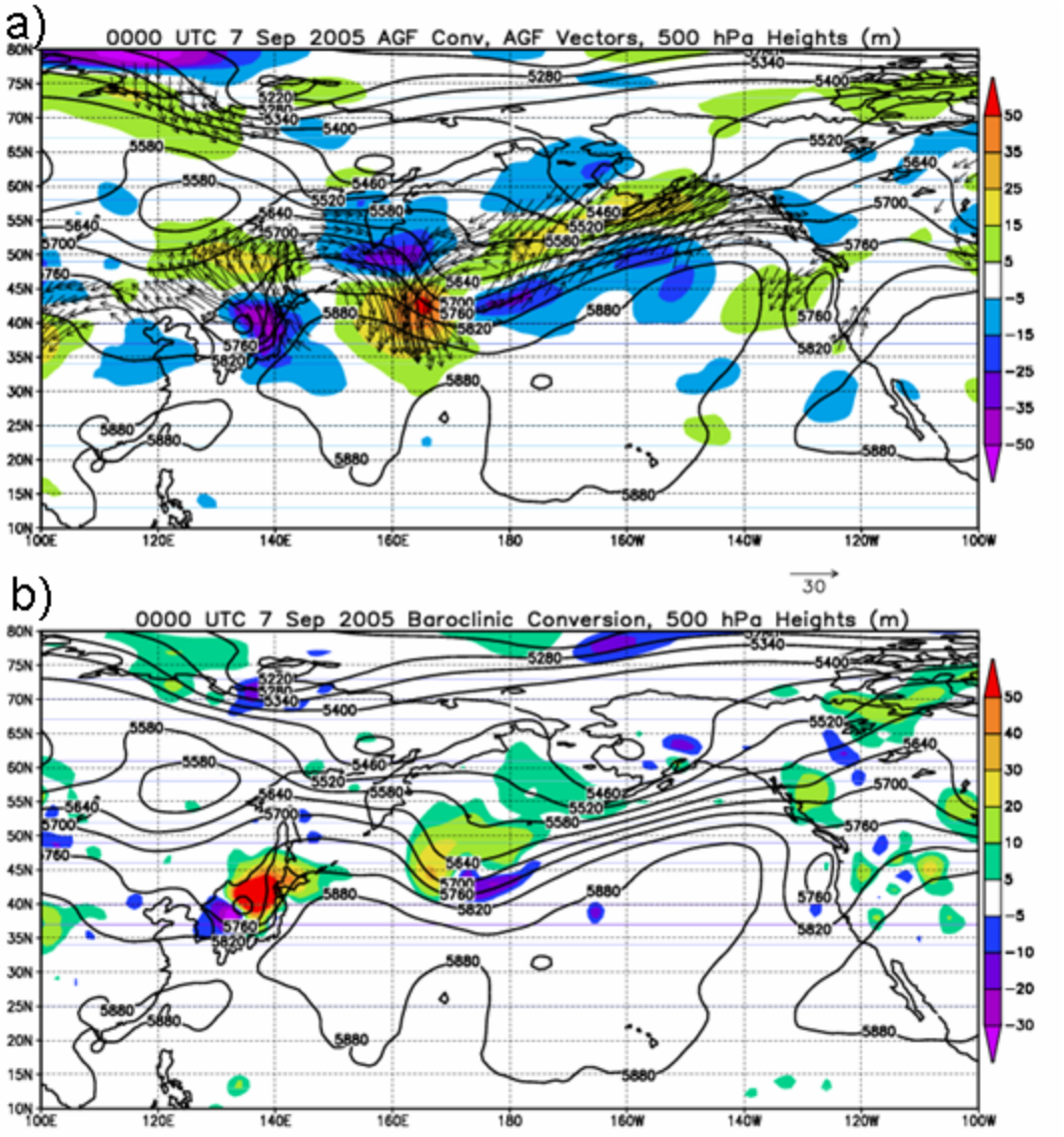

Figure 54. As in Fig. 12, except for 0000 UTC 7 September 2005.

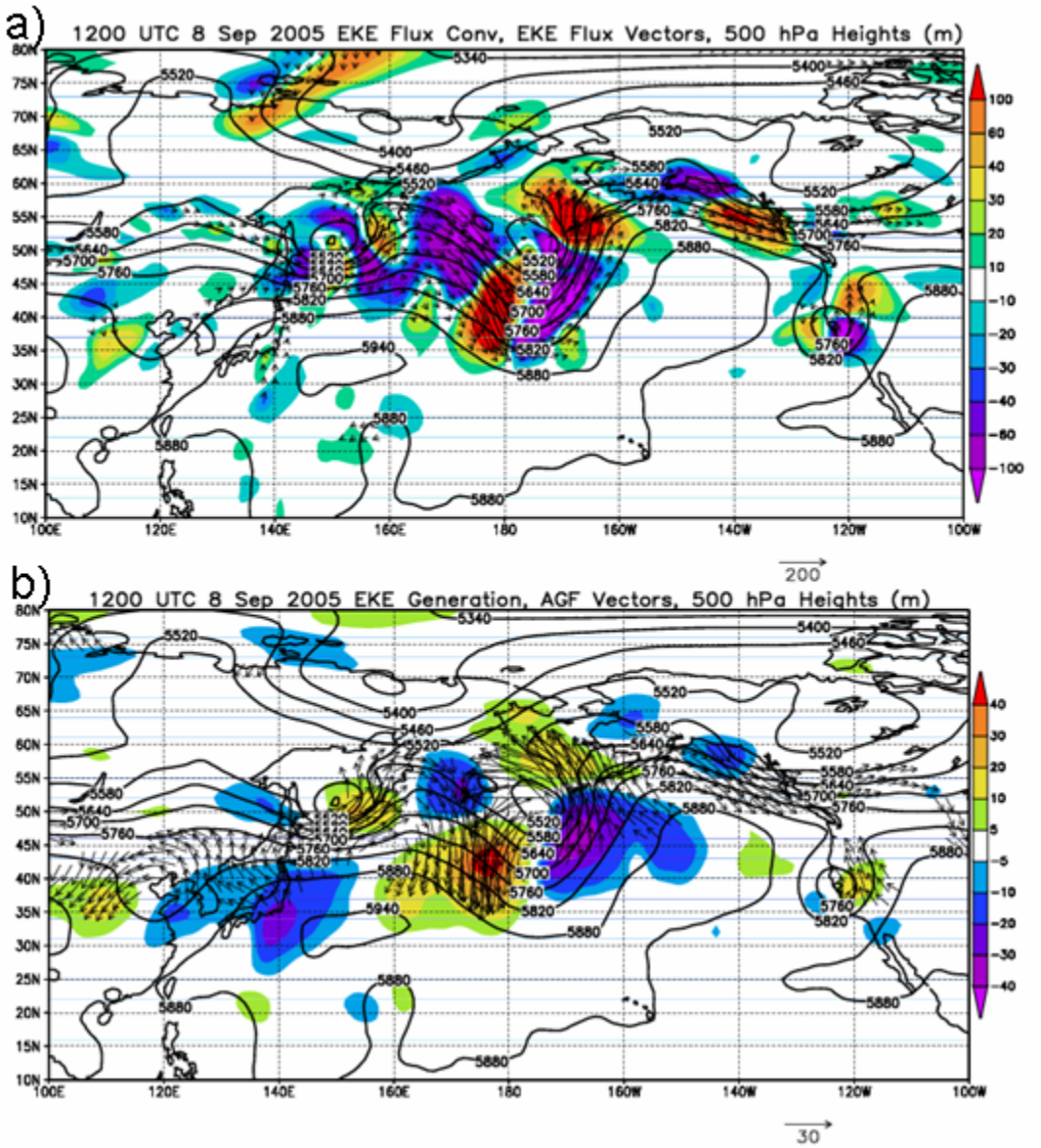

Figure 55. As in Fig. 11, except for 1200 UTC 8 September 2005.

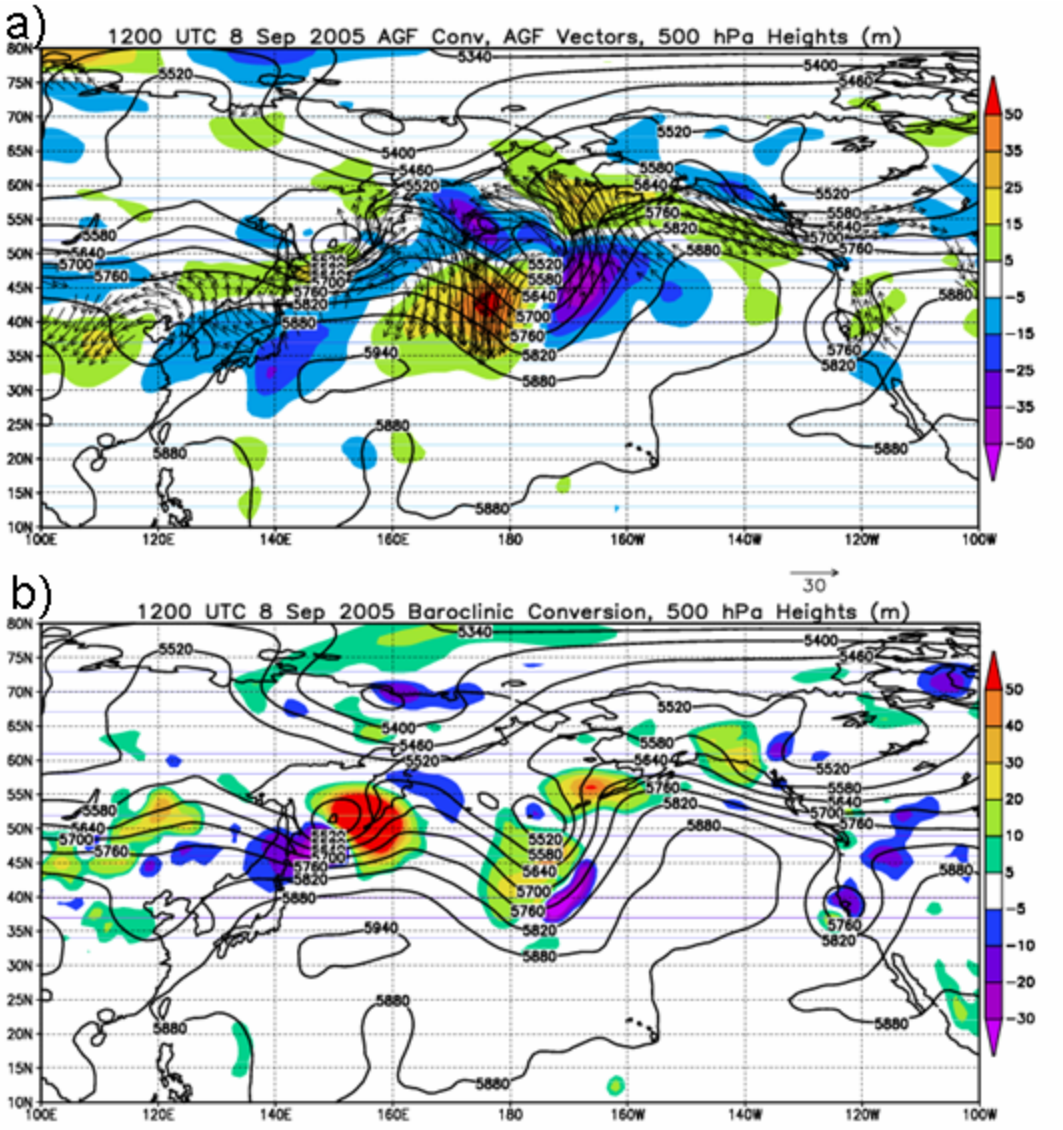

Figure 56. As in Fig. 12, except for 1200 UTC 8 September 2005.

3. Summary

Prior to the ET of Nabi, the EKE center associated with the cyclone near the Sea of Okhotsk was transferring EKE into the EKE center near the Aleutian Islands. Both features then began to deteriorate once AGFC weakened and moved farther east of the EKE center that was associated with the cyclone, and after passing the Kamchatka Peninsula, the BC weakened. As long as the EKE center remained intact, the EKEFC was tending to disperse the EKE center.

When the EKE center was no longer being replenished by BC or AGFC, then the EKEFC dominated and tended to weaken the EKE center around the cyclone near the Sea of Okhotsk and the Kamchatka Peninsula.

After Nabi had started moving into the midlatitudes, AGFC emanating from Nabi had deposited EKE into the ridge to its north, which initiated amplification in the ridge. On the downstream side of this ridge, AGFC was also present and generated more EKE in the already-developing EKE center on the upstream side of the trough in the central North Pacific.

Baroclinic conversion became important for EKE generation during the re-intensification of the ex-Nabi extratropical remnants, which dominated over the AGFC. Baroclinic conversion also contributed to, but did not dominate, the EKE generation in the EKE center in the upstream side of the trough over the central North Pacific. Finally, EKE helped to amplify the ridge over southwestern Alaska by 1200 UTC 8 September 2005.

IV. SUMMARY, CONCLUSIONS, AND RECOMMENDATIONS

A. SUMMARY

Prior to the ET of Tokage, a decrease in EKE occurred in the midlatitude circulation across the North Pacific. As Tokage moved into the midlatitudes, it contributed to an increase in EKE over the western North Pacific and to the development of a deep trough. Baroclinic processes due to the circulation of Tokage contributed to EKE generation, which was dispersed to the midlatitudes via ageostrophic fluxes. This EKE was dispersed downstream into a developing trough over the western North Pacific, but only for a short duration as the downstream trough extended equatorward and the poleward movement of the ex-Tokage remnants cut off the energy transport.

The case of Banyan represented a mid-summer, low-EKE midlatitude environment. Energy was transferred downstream through EKEFC and AGFs. This downstream flux of energy from Banyan into a shortwave trough contributed to re-intensification of the ex-Banyan remnants as an extratropical cyclone. Following re-intensification of the ex-Banyan remnants, EKE was directed downstream toward the eastern North Pacific in association with a developing shortwave trough.

Guchol was dominated in size and EKE by the midlatitude trough into which Guchol was absorbed. However, this event triggered EKE generation through BC of cold air sinking on the upstream side of the midlatitude trough and this EKE was transported to the downstream side of the trough and then farther dispersed downstream or recycled within the trough. A new EKE center associated with a shortwave trough then developed near the Aleutian Islands.

TY Nabi is a case in which a significant impact on downstream development was made by the ET of the TC as it re-intensified into a deep extratropical cyclone. It was shown that prior to the ET of Nabi, the midlatitude circulation contained weakening EKE centers associated with weakening

baroclinic midlatitude features. Following this evolution, a low-energy, highly zonal circulation pattern became established across the western North Pacific. Ageostrophic geopotential flux convergence deposited EKE poleward of Nabi as it began to move out of the tropics, which initiated amplification of a ridge north of Nabi. Eddy kinetic energy was also transported by AGFC into a developing energy center immediately downstream of the ridge. Baroclinic conversion of available potential energy into EKE became more significant during ET for the remnants of Nabi and also played a part in enhancing the EKE center downstream of the ridge amplified by Nabi.

B. CONCLUSIONS

The four cases selected for this thesis represented a variety of TC characteristics and midlatitude flow patterns in which energetics analyses have been used to describe the characteristics of downstream development due to the ET of TCs. Analyses of these four cases in this thesis revealed that the ET of TCs can affect downstream development in varying degrees. Tokage was a more intense TC that did not re-intensify strongly after ET, and was accompanied by a weakening high-amplitude, high-EKE midlatitude circulation. A limited time was available to initiate significant downstream development in a subtropical central North Pacific trough as the two features moved away from each other. Banyan was a stronger TC that moved into a weak midlatitude circulation typical of a mid-summer case. Banyan influenced downstream development through EKEFC and AGFs to a downstream shortwave trough, which assisted in its re-intensification, and later to an EKE center downstream associated with a developing shortwave trough near the Aleutian Islands.

The Guchol case involved interaction between a weaker TC and a stronger midlatitude circulation. Through an increase in EKE generation through BC after Guchol's absorption into a midlatitude trough, Guchol appeared to be able to influence downstream development in spite of being a weaker TC. Nabi

was a classic case of an intense TC experiencing ET that emerged from the tropics into a zonal midlatitude circulation and caused significant midlatitude flow amplification.

C. RECOMMENDATIONS FOR FUTURE RESEARCH

Forty-five percent of Atlantic Ocean TCs experience ET, as determined by Jones et al. (2003). It would be beneficial to perform a similar examination, as in this thesis, on cases in the Atlantic basin, or in other TC basins around the world to determine similarities and differences.

Another avenue of research should be focused on the sensitivities on downstream development in light of different midlatitude circulation types, following the lead of similar research done for ET of TCs by Harr et al. (2000).

Based on the energetics analysis and the significant downstream impact, even through Guchol was weak, analysis of the sensitivity to the merger of the TC and the midlatitude trough could be done using a numerical model simulation.

Future research could be focused on EKE wave packet analysis on TCs experiencing ET. Work done by Decker and Martin (2005) indicated that midlatitude cyclones that had associated EKE wave packets decayed at differing rates depending upon the position of the cyclone relative to its wave packet. Such a technique applied to re-intensifying remnants of former TCs could provide insight into the amount of downstream development that is experienced from a single ET event, considering how long EKE would be supplied by the TC remnants to downstream energy centers.

THIS PAGE INTENTIONALLY LEFT BLANK

LIST OF REFERENCES

Browning, K. A., G. Vaughan, and P. Panagi, 1998: Analysis of an ex-tropical cyclone after reintensifying as a warm-core extra-tropical cyclone. *Quart. J. Roy. Meteor. Soc.,* **124,** 2329-2356.

Chang, E. K. M., 1993: Downstream development of baroclinic waves as inferred by regression analysis. *J. Atmos. Sci.,* **50,** 2038-2053.

——, 1999: Characteristics of wave packets in the upper troposphere. Part II: Seasonal and hemispheric variations. *J. Atmos. Sci.,* **56,** 1729-1747.

—— and I. Orlanski, 1993: On the dynamics of a storm track. *J. Atmos. Sci.,* **50,** 999-1015.

—— and D. B. Yu, 1999: Characteristics of wave packets in the upper troposphere. Part I: Northern Hemisphere winter. *J. Atmos. Sci.,* **56,** 1708-1728.

Computational and Information Systems Laboratory (CISL), The National Center For Atmospheric Research: Dataset ds083.2 documentation page, cited 2007: CISL Research Data Archive: ds083.2. [http://dss.ucar.edu/datasets/ds083.2/docs/more.summary.html]

Decker, S., and Martin, J., 2005: A local energetics analysis of the life cycle differences between consecutive, explosively deepening, continental cyclones. *Mon. Wea. Rev.,* **133**, 295-316.

DiMego, G. J., and L. F. Bosart, 1982: The transformation of tropical storm Agnes into an extratropical cyclone. Part I: The observed fields and vertical motion computations. *Mon. Wea. Rev.,* **110,** 385–411.

Foley, G. R., and B. N. Hanstrum, 1994: The capture of tropical cyclones by cold fronts off the west coast of Australia. *Wea. Forecasting,* **9,** 577-592.

Harr, P.A., and R. L. Elsberry, 2000: Extratropical transition of tropical cyclones over the western North Pacific. Part I: Evolution of structural characteristics during the transition process. *Mon. Wea. Rev.,* **128,** 2613-2633.

——, ——, and T. F. Hogan, 2000: Extratropical transition of tropical cyclones over the western North Pacific. Part II: The impact of midlatitude circulation characteristics. *Mon.Wea. Rev.,* **128,** 2634-2653.

Hart, R. E., and J. L. Evans, 2001: A climatology of extratropical transition of Atlantic tropical cyclones. *J. Climate,* **14,** 546-564.

Iredell, M.: About the global parallel system, cited 2007: About the global forecast system. [http://wwwt.emc.ncep.noaa.gov/gmb/para/parabout.html]

Jones, S. C., P. A. Harr, J. Abraham, L. F. Bosart, P. J. Bowyer, J. L. Evans, D. E. Hanley, B. N. Hanstrum, R. E. Hart, F. Lalaurette, M. R. Sinclair, R. K. Smith, and C. Thorncroft, 2003: The extratropical transition of tropical cyclones: Forecast challenges, current understanding, and future directions. *Weather and Forecasting*, **18**, 1052-1092.

Keyser, D., M. J. Reeder, and R. J. Reed, 1988: A generalization of Petterssen's frontogenesis function and its relation to the forcing of vertical motion. *Mon. Wea. Rev.,* **116,** 762–780.

Klein, P. M., P. A. Harr, and R. L. Elsberry, 2000: Extratropical transition of western North Pacific tropical cyclones: An overview and conceptual model of the transformation stage. *Weather and Forecasting*, **15**, 373–396.

Lee, S., and I. M. Held, 1993: Baroclinic wave packets in models and observations. *J. Atmos. Sci.,* **50,** 1413-1428.

Orlanski, I., and E. K. M. Chang, 1993: Ageostrophic geopotential fluxes in downstream and upstream development of baroclinic waves. *J. Atmos. Sci.,* **48,** 1972-1998.

——, and J. Katzfey, 1991: The life cycle of a cyclone wave in the Southern Hemisphere. Part I: Eddy energy budget. *J. Atmos. Sci.,* **48**, 1972-1998.

——, and Sheldon, J., 1993: A case of downstream baroclinic development over western North America. *Mon. Wea. Rev.,* **121**, 2929-2950.

——, and ——, 1995: Stages in the energetics of baroclinic systems. *Tellus,* **47A,** 605-628.

Petterssen, S., 1955: A general survey of factors influencing development at sea level. *J. Meteor.,* **12,** 36–42.

——, and S. J. Smebye, 1971: On the development of extratropical cyclones. *Quart. J. Roy. Meteor. Soc.,* **97**, 457–482.

Rabier, F., E. Klinker, P. Courtier, and A. Hollingsworth, 1996: Sensitivity of forecast errors to initial conditions. *Quart. J. Roy. Meteor. Soc.,* **122,** 121-150.

Sinclair, M. R., 2002: Extratropical transition of southwest Pacific tropical cyclones. *Mon. Wea. Rev.,* **130,** 590–609.

Sutcliffe, R. C., and A. G. Forsdyke, 1950: The theory and use of upper air thickness patterns in forecasting. *Quart. J. Roy. Meteor. Soc.,* **76,** 189–217.

Thorncroft, C. D., B.J. Hoskins, and M. E. McIntyre, 1993: Two paradigms of baroclinic-wave life-cycle behavior. *Quart. J. Roy. Meteor. Soc.,* **119,** 17-55.

THIS PAGE INTENTIONALLY LEFT BLANK

INITIAL DISTRIBUTION LIST

1. Defense Technical Information Center
   Ft. Belvoir, Virginia

2. Dudley Knox Library
   Naval Postgraduate School
   Monterey, California

3. Air Force Weather Technical Library
   Air Force Combat Climatology Center
   Asheville, North Carolina

4. Air Force Institute of Technology
   Wright-Patterson Air Force Base, Ohio

5. Professor Philip Durkee
   Naval Postgraduate School
   Monterey, California

6. Professor Patrick Harr
   Naval Postgraduate School
   Monterey, California

7. Professor Russell Elsberry
   Naval Postgraduate School
   Monterey, California

8. Jonathan M. Dea, Capt, USAF
   Air Force Technical Applications Center
   Patrick Air Force Base, Florida